Clemson University
TigerPrints

All Dissertations | Dissertations

8-2018

Particle Manipulation in Viscous Flows: Singularity Models and Phase Space Boundaries

Senbagaraman Sudarsanam
Clemson University, ssudars@g.clemson.edu

Follow this and additional works at: https://tigerprints.clemson.edu/all_dissertations

Recommended Citation
Sudarsanam, Senbagaraman, "Particle Manipulation in Viscous Flows: Singularity Models and Phase Space Boundaries" (2018). *All Dissertations*. 2181.
https://tigerprints.clemson.edu/all_dissertations/2181

This Dissertation is brought to you for free and open access by the Dissertations at TigerPrints. It has been accepted for inclusion in All Dissertations by an authorized administrator of TigerPrints. For more information, please contact kokeefe@clemson.edu.

Particle Manipulation in Viscous Flows: Singularity Models and Phase Space Boundaries

---

A Dissertation
Presented to
the Graduate School of
Clemson University

In Partial Fulfillment
of the Requirements for the Degree
Doctor of Philosophy
Mechanical Engineering

---

by
Senbagaraman Sudarsanam
August 2018

Accepted by:
Dr. Phanindra Tallapragada, Committee Chair
Dr. Joshua Bostwick
Dr. Ethan Kung
Dr. Xiangchun Xuan

Abstract

Particle Manipulation in Viscous Flows:
Singularity Models and Phase Space Boundaries

Senbagaraman Sudarsanam

This dissertation develops a modeling framework to address the problem of particle manipulation in low Reynolds number fluid flows. This framework combines singularity methods in low Reynolds number fluid dynamics with the theory of transport in phase space of dynamical systems. While dynamical systems theory offers tools to study the properties of geometric features in systems such as fluid flows, singularity methods enable the construction of models for low Reynolds number flows that are simple to work with and yet, preserve the essential geometric features of the flow. Hence, the combination of these techniques offers a natural framework for the study of particle transport in varied problems of the viscous/low Reynolds number flow regime. The first problem studied is that of inertial particle manipulation in microfluidic channels integrated with acoustically excited micro-bubbles. The Lagrangian Coherent Structures(LCS) of micro-bubble streaming flows serve as a guideline for placement of micro-bubbles within the channel in a manner that enhances focusing and size based separation of inertial particles. Second, the dynamics of viscous micro-rotors within a bounded domain is modeled. The influence of viscous

boundary effects on the dynamics is assessed. The application of micro-rotors for the purpose of chaotic micro-mixing is explored using numerical simulations.

Dedication

I dedicate this dissertation to all of humanity. The many stories of humanity's resilience in the face of overwhelming strife inspire me everyday.

Acknowledgments

First, I would like to express my deepest gratitude to my advisor Dr. Phanindra Tallapragada. Over the past five years he has served as my advisor, critic, mentor and a friend. His consistent support and encouragement over the years have been crucial to my experience as a graduate student. There exists no doubt in my mind that he has been the single biggest influence in my development as a researcher.

I would like to thank Dr.Joshua Bostwick for serving on my dissertation committee as well as for organizing the graduate student seminar series which helped me hone my skills in presenting my research to a diverse audience. I would also like to extend my gratitude to Dr. Ethan Kung and Dr. Xiangchun Xuan for serving on my doctoral dissertation committee.

A sincere note of appreciation to Clemson University for generous allotment of compute time on Palmetto Cluster. I would also like to thank Ashwin Srinath for helping me improve my skills in scientific computing.

I am very thankful for the many friendships that I have found over the years in Clemson. In particular, I would like to thank my flatmates Kaushik, Vishal, Mohan, Rama, Venky and Akash. Prakash deserves a special mention for being a trusted friend over the past two years. I have been fortunate to have been surrounded by smart and accommodating colleagues at the department of mechanical engineering. I would like to thank Beau, Vitaliy, Arnab and Rucha for being colleagues whom I

could look forward to meeting in office every day. I owe my gratitude to Jake for being a great friend and for being supportive over the past few months.

I thank Pranaya, for helping me sail past life's most difficult storms.

Most importantly, I would like to thank my parents, Sudarsanam and Sumathi, for their unconditional love and their unwavering faith in me. I thank god for everything.

Table of Contents

Title Page . . . . . **i**

Abstract . . . . . **ii**

Dedication . . . . . **iv**

Acknowledgments . . . . . **v**

List of Figures . . . . . **ix**

1 Introduction **1**
1.1 Particle dynamics and manipulation in microfluidics 1
1.2 Organization of the dissertation 4
1.3 Key Contributions 5

2 Review of Singularity Methods **6**
2.1 Fundamental solution of the Stokes equation 6
2.2 Derivatives of the Stokeslet solution 8
2.3 The method of images 10
2.4 Collocation schemes for singularity driven flows 18

3 Review of Geometric Methods for Phase Space Transport **20**
3.1 Geometric methods in the study of dynamical systems 20
3.2 Lyapunov exponents of a dynamical system 23
3.3 Stability measures for time dependent systems 25
3.4 Definition and computational method for FTLE 26

4 Review of Micro-Bubble Streaming Flow Theory and Inertial Particle Dynamics **30**
4.1 Overview of the development of steady streaming flow theory 30
4.2 Micro-bubble streaming flows 31
4.3 Governing equations and solution 32
4.4 Maxey-Riley Equation 37
4.5 Inertial particle manipulation in micro-bubble streaming flows 42

4.6 Singularity model of wall bounded micro-bubble streaming 43

5 Particle Dynamics in Simple Models of Ideal Flows 45
5.1 Potential flow models 45
5.2 Global stability of inertial particle trajectories within domains of instability 47
5.3 Particle manipulation in viscous flows 53

6 Particle Dynamics in Micro-Bubble Streaming Flows 55
6.1 Singularity model of micro-bubble streaming flows 55
6.2 Stability of micro-bubble streaming for inertial particle dynamics . . 61
6.3 Dynamical boundaries in micro-bubble streaming flows 65
6.4 Inertial particle manipulation 69
6.5 Comparison of modeling results to experimental results 73

7 Chaotic Transport of Tracer Particles by Micro-rotors 77
7.1 Review of microfluidic mixing 77
7.2 Micro-rotor dynamics and confinement 80
7.3 Regular and chaotic dynamics of micro-rotors 83
7.4 Chaotic advection of tracers: Numerical experiments 86
7.5 Lagrangian Coherent Structures in micro-rotor induced mixing 90
7.6 Quantifying mixing 92

8 Conclusion 95
8.1 Summary 95
8.2 Closing remarks 96

Bibliography 97

List of Figures

2.1 Vertically oriented singularity solutions of the 2D Stokes equation . . 7
2.2 Streamlines of flow due to a rotlet. 11
2.3 Streamlines of flow due to a vertically oriented stokeslet in the presence of a viscous wall boundary 13
2.4 Streamlines of flow due to a vertically oriented potential dipole in the presence of a viscous wall boundary 14
2.5 Singularity representations inside a circular cylinder 16
2.6 Reflection of singularities and images enables us to construct the flow due to a singularity between parallel walls. 17
2.7 (a)$2N$ stokeslets(blue bubbles) inside a circular cylinder of unit radius, imposing $2N$ velocity boundary conditions at N boundary locations(black bubbles).(b)Velocity field due to a pair of translating circular cylinders inside a circular domain. 18

3.1 Stability of equilibrium points of a 2D system 23
3.2 Continuous and Discrete Time Representation of Dynamical Systems 24
3.3 Flow map. 28
3.4 Flows driven by various Stokeslet configurations 29
3.5 Forward time FTLE field for Stokeslets switching between blinking configuations 1 and 2. 29

4.1 Oscillating bubbles next to a no-slip wall produces steady streaming vortices. 32
4.2 Steady streaming flow due to wall bounded micro-bubble 35
4.3 Stable(D_s) and unstable(D_u) sub-domains of a flow domain. 39
4.4 The magnitude of deflection near the bubble surface is proportional to particle size. 41
4.5 Singularity model of oscillating bubble next to a no-slip wall constructed using a stokeslet and potential dipole. The no penetration boundary condition is satisfied on the instantaneous radius of the oscillating bubble surface while the mean bubble surface is shown here. 44

5.1 Streamlines are shown in blue for (a)Point vortex and (b) Cell flow. . 46

5.2 (a)The trajectory of an inertial particle(black) inside the unstable subset(H_u) of a gaussian vortex flow(b) The net relative velocity of the inertial particle decaying despite never leaving the unstable region(c) Projections α and β over time (d) Eigen vectors at various positions of the inertial particle. 48
5.3 Various stages in the decay of relative velocity in the unstable subset of Gaussian vortex flow domain. 50
5.4 (a)Inertial particle trajectory in a cell flow(b)Decay of relative velocity w with time. 51
5.5 Various stages in the decay of relative velocity in the unstable subset of cell flow domain. 52
5.6 A framework to study particle transport in viscous fluid flows. 54

6.1 The method of reflections used to model the presence of a parallel wall. 58
6.2 Singularity model of micro-bubble streaming 60
6.3 Binary plots showing the stable(gray) and unstable(black) subsets of the flow domain. 63
6.4 Magnitude of relative velocity $|w|$ along the trajectory of a $10\mu m$ inertial particle exaggerated to show the spatial variation. 64
6.5 Sizes $10\mu m$(red),$7.5\mu m$(green),$5\mu m$(magenta) and $2.5\mu m$(cyan) . . . 64
6.6 Repelling Lagrangian Coherent Structures in one bubble configuration. 67
6.7 Attracting Lagrangian Coherent Structures in one bubble configuration. 68
6.8 Inertial particle attraction towards attracting fluid LCS. 69
6.9 Two bubble flow-Configuration 1 71
6.10 Two bubble flow-Configuration 2 72
6.11 Two bubble flow with bubble on opposing walls. 73
6.12 LCS determines particle focusing behavior 74
6.13 Focusing behavior harnessed for particle separation 75

7.1 Flow has to be stretched and folded into filaments to accelerate viscous diffusion. 80
7.2 Two and three rotlet trajectories in an un-bounded domain 81
7.3 N- rotlet configurations in a circular-bounded domain of unit radius . 83
7.4 (Left most)The trajectories of three rotlets started at different distances $r = 0.2$(cyan),$r = 0.4$(green) and $r = 0.6$(blue) from the center of the domain.(Figures 2-4) Trajectories of a fluid tracer gives rise to significant unmixed regions when stirred using each of the three rotlet configurations. 84
7.5 Dynamics of the bounded 2 rotlet configuration 85
7.6 Rotlets not initially collinear with the center of the domain 87
7.7 Poincaré maps corresponding to the two rotor configurations in Figs. 7.5a-7.5u. Different colored bands are maps of initial conditions started off in different regions that do not mix with each other. 88

7.8 Poincaré map for rotors close to the boundaries. 88
7.9 Mixing of fluid tracers using the bounded 2 rotor configuration at various intervals of time in the stirring process 89
7.10 Mixing mechanism in the bounded 2 rotor configuration with corresponding streamlines of flow which are imaterial lines of the flow field. 91
7.11 Repelling LCS induces stretching about itself. 92
7.12 Forward time FTLE and the associated LCS for micro-rotor mixing. . 93
7.13 Mixing configurations in Fig.7.5 and the associated variance 94

Chapter 1

Introduction

1.1 Particle dynamics and manipulation in microfluidics

Particles of various sizes are often encountered in applications of microfluidic Lab on a chip devices such as in cell separation [1, 2], encapsulation [3] and microorganism manipulation [4, 5] among others. To be able to predictably manipulate these particles is an important problem with a wide range of application in physical and life sciences. In the case of finite sized inertial particles, the encountered particles could either be undesirable inclusions which need to be filtered out altogether from the underlying fluid or they could be a mixture of desirable and undesirable types of particles which need to be selectively sorted before the undesirable particles are filtered out. Also of interest are infinitesimal fluid tracer particles which serve as an effective model as well as a visualization tool to study the Lagrangian flow behavior in microfluidic mixing studies motivated by applications such as sample preparation in analytical chemistry [6].

We use two theoretical frameworks to address the problem of microfluidic particle manipulation. First is the framework of singularity methods in low Reynolds number fluid dynamics [7]. The singularity method provides a means to create simple models of microfluidic flows without having to resort to detailed analytic solutions or involved computational models of the full governing equations. In this framework, fluid flows are modeled as a combination of singularity solutions of the Stokes equation. Boundary conditions can then be easily satisfied by selecting appropriately chosen image singularities at strategic positions relative to the original singularities or by using numerical collocation schemes.

Second, we use the framework of phase space transport in dynamical systems [8] to uncover the underlying geometric structure of the fluid flow. The phase space of several dynamical systems of interest often possess long lived geometric features which influence the time evolution of the dynamical system due to their stability properties.

In this dissertation, we apply the aforementioned techniques to study two problems in microfluidic particle manipulation. In particular, we study flows that can be reliably approximated as being two dimensional. Examples of situations where the 2D approximation of the flow field is justified include [9], flows where the third spatial dimension is very small relative to the other two dimensions such as in several geophysical flows, flows where the dynamics is confined to two dimensions such as flows on thin soap films and third, in flows where the dynamics are identical at every plane and studying the dynamics at one such plane is representative of the entire domain. The dynamics of neutrally buoyant particles could be considered an example of the third kind of situation. The 2D approximation can simplify complex flow models while still yielding useful insights.

The first problem studied is that of finite sized particle manipulation in micro-

channels using steady streaming flows generated by acoustically excited micro-bubbles. Micro-bubble streaming in microfluidic channels is now a well studied fluid flow phenomenon with the full fluid flow problem well understood [10, 11]. The problem of particle manipulation using micro-bubble streaming is now gaining interest [12, 13, 14]. We show that finite time Lyapunov exponent calculations serve as a guide to bubble placement within the channel so as to enhance desired inertial particle behavior.

The second problem studied is the mixing of passive tracer particles by magnetically actuated viscous micro-rollers. The ability of passive tracer particles to exhibit chaotic trajectories even when the underlying time dependent Eulerian flow field is orderly is called chaotic advection and was first demonstrated by Hassan Aref [15] by using the now classic blinking vortex model. The classic blinking vortex model utilizes singularities of potential flow called point vortices as a simplified model of stirrers that are switched 'on' and 'off' alternatively. No-penetration boundary conditions are usually imposed on a circular bounding contour surrounding the blinking vortex system to approximate a stirred container of fluid. While these simplified models have yielded deep insights into the problem of fluid mixing, the all important viscous effects are ignored. The viscous boundary effects are particularly important in microfluidic mixing studies where fluids are forced to flow through minute geometries and consequently the influence of interfaces are felt throughout the flow field [16]. We use a singularity model to demonstrate chaotic mixing in bounded-viscous flows by free moving magnetic micro-rollers.

While a few works in the past have used a combination of singularity methods and tools from dynamical systems theory [17, 18], the potential of this framework for addressing problems in particle manipulation is immense.

1.2 Organization of the dissertation

The fundamental singularity of stokes flow and it's higher order multi-poles are derived in chapter 2. The method of images used for modeling of low Reynolds number flow phenomenon is reviewed. Chapter 3 focuses on reviewing the theoretical ideas and computational schemes that enable the study of geometric phase space transport in dynamical systems. Particularly, the computation of finite time lyapunov exponent(FTLE) fields and the significance of high FTLE ridges in the scalar FTLE field called Lagrangian Coherent Structures (LCS) is discussed.

Chapter 4 is used to review the physics of micro-bubble generated steady streaming flows while also reviewing the governing equation of motion for finite sized particles. Chapter 5 presents the results of a dynamical systems analysis of inertial particle motion near simple singularity models of vortex driven ideal flows. The insights gained from this study motivates us to extend this study to more realistic viscous flow scenarios.

Chapter 6 covers the study of particle laden micro-bubble streaming flows and strategies for micro-particle manipulator design based on insights gained from LCS of the fluid flow.

Chapter 7 presents a brief review of the immense mathematical field of chaotic mixing followed by a study of the complex dynamics exhibited by viscous micro-rotors when confined inside a circular domain. We demonstrate the ability of free moving micro-rotors to induce chaotic mixing in low Reynolds number flows. We conclude with a summary of the conducted work and some closing remarks in chapter 8.

1.3 Key Contributions

- We present a framework for studying the broad problem of particle manipulation in viscous flows by combining the analytical techniques of singularity modeling and tools from dynamical systems theory.

- We study the properties of micro-bubble streaming flows from the dynamical systems perspective and use the insights gained to make suggestions about micro-bubble placement within microfluidic channels.

- We identify the existence of complex behavior in small assemblies of viscous micro-rotors when confined inside a finite region. We demonstrate chaotic mixing of fluid tracers using small assemblies of such micro-rotors.

Chapter 2

Review of Singularity Methods

2.1 Fundamental solution of the Stokes equation

2.1.1 Linearized viscous flows

The incompressible Navier-Stokes equation can be written in the non-dimensional form as [7]

$$\beta\frac{\partial u}{\partial t} + Re(u\cdot\nabla u) = -\nabla P + \mu^2\Delta u \qquad (2.1)$$
$$\nabla\cdot u = 0$$

β is used to denote the frequency parameter which can be broken down into a product of the Reynolds number $Re = \frac{UL}{\nu}$ and the Strouhal number $Sl = \frac{L}{U\tau}$. Here, U, L and τ are characteristic velocity, length and time scales of the flow while ν is the kinematic viscosity of the fluid. For flows with $Re \to 0$, the contribution of the inertial terms in the Navier-Stokes equations become very small relative to that of the viscous terms and can be neglected. As long as Sl does not grow arbitrarily large as $Re \to 0$,

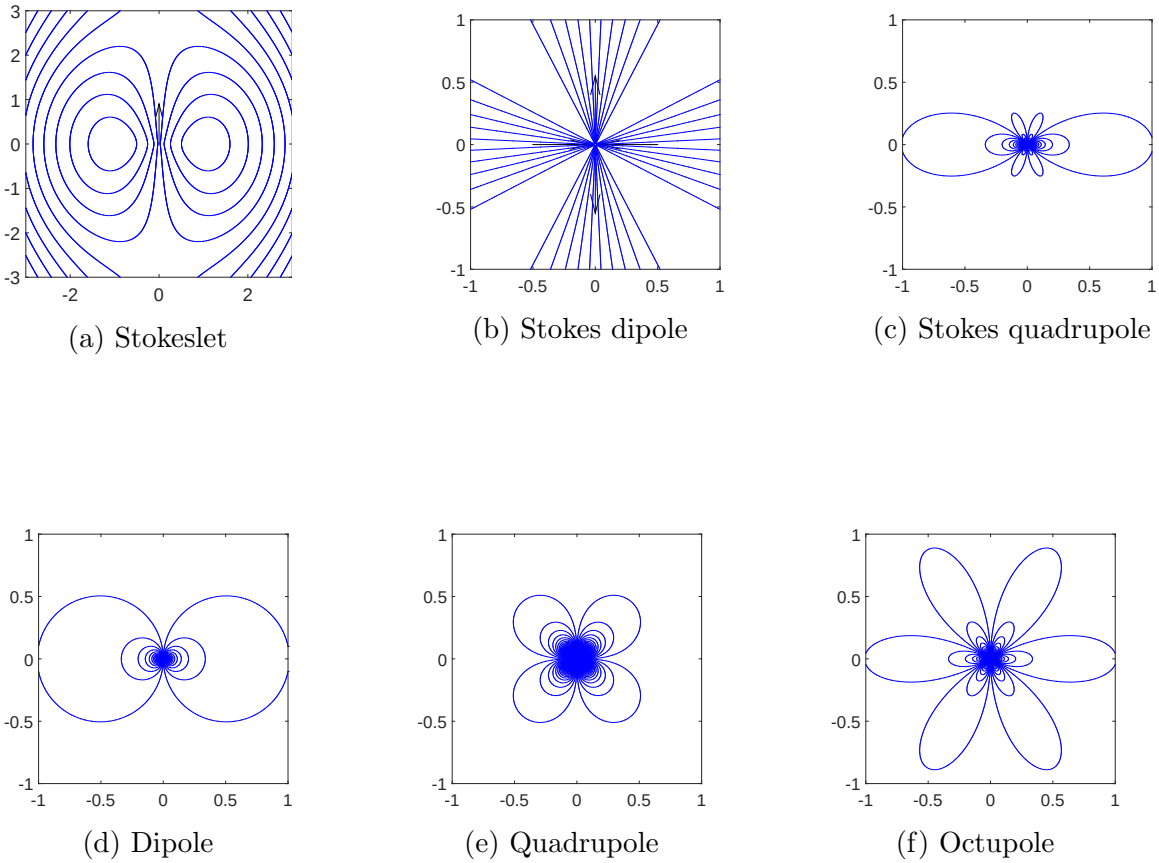

(a) Stokeslet (b) Stokes dipole (c) Stokes quadrupole

(d) Dipole (e) Quadrupole (f) Octupole

Figure 2.1: Vertically oriented singularity solutions of the 2D Stokes equation

the governing equations can be re-written without the non-linear advection and time dependent terms resulting in the steady Stokes equation [7].

$$\mu^2 \Delta u = \nabla P \tag{2.2}$$

$$\nabla \cdot u = 0$$

2.1.2 Singularity Solutions of the 2D Stokes Equation

The linearity of the Stokes equations implies that their solutions can be superimposed to obtain new solutions for the same governing equations and this forms

the basis of the singularity method in low Reynolds number flow modeling [19].

The fundamental solution of the 2D Stokes equations is the solution of the 2D version of (2.1) with a point force inhomogeneity,

$$\mu^2 \Delta u - \nabla P = F\delta(x, x_0) \tag{2.3}$$
$$\nabla \cdot u = 0$$

where $\delta(x, x_0)$ is a dirac delta function centered at x_0. The solution of this set of equations can be expressed in terms of a free space Green's function in 2D as,

$$(u_s)_i = \frac{1}{4\pi\mu} G_{ij}(x, x_0) F_j \tag{2.4}$$
$$\text{with, } G_{ij}(x, x_0) = -\delta_{ij} ln(r) + \frac{(x_i - x_{0_i})(x_j - x_{0_j})}{r^2}$$
$$\text{and, } r = \sqrt{\left((x_i - x_{0_i})^2 + (x_j - x_{0_j})^2\right)}$$

This is the fundamental solution of the Stokes equations called a *Stokeslet* [7]. The singularity method is reviewed next based on [7, 20] and others.

2.2 Derivatives of the Stokeslet solution

To study the flow field in the vicinity of a Stokeslet, the stokeslet velocity can be expanded in a Taylor series about a point ξ very close to the stokeslet center x_0 so that for velocities at points $x >> \xi$ we have that $(x - \xi) \approxeq (x - x_0)$ [20](i.e)

$$u_s(x - x_0) = u_s(x) - (x_0 \cdot \nabla) u_s(x) + \frac{1}{2}(x_0 \cdot \nabla)^2 u_s(x) + ... \tag{2.5}$$

where the first term on the right hand side is the usual Stokeslet, the second term is the first derivative of the Stokeslet and represents a Stokes doublet, the third term is

the Stokes quadruplet and so on. The Stokes doublet is an order 2 tensor and can be thought of as the velocity due to a force dipole and warrants special attention,

$$u_{sd_i} = \frac{G^{sd}_{ijk} D_{jk}}{4\pi\mu} \tag{2.6}$$
$$\text{with, } G^{sd}_{ijk}(x, x_0) = \frac{\delta_{ij}\hat{x_l} - \delta_{il}\hat{x_j} - \delta_{jl}\hat{x_i}}{r^2} + \frac{2\hat{x_i}\hat{x_j}\hat{x_l}}{r^4}$$

where $\hat{x_i} = x_i - (x_0)_i$. The stokes doublet can be decomposed into symmetric and anti-symmetric components which have physical significance and are fundamental solutions of the stokes equations in their own right.

The symmetric component represents the straining motion due to the doublet and is called a stresslet denoted by u_{ss}. The stresslet is identical to an axis-symmetric stokes dipole seen in Fig. 2.1b. The anti-symmetric component represents the torque due to the doublet and it is derived as the velocity due to a point torque in the fluid and is called a rotlet denoted by u_r and shown in Fig. 2.2.

$$(u_r)_i = \frac{G^r_{im} c_m}{4\pi\mu} \text{ where, } G^r_{im} = \epsilon_{imk}\frac{\hat{x_k}}{r^2} \tag{2.7}$$

The next higher derivative is the stokes quadruplet,

$$(u_{sq})_i = \frac{G^{sq}_{ijlm} Q_{jlm}}{4\pi\mu} \tag{2.8}$$
$$G^{sq}_{ijlm}(x, x_0) = \frac{-\delta_{ij}\delta_{lm} + \delta_{il}\delta_{jm} + \delta_{jl}\delta_{im}}{r^2} \tag{2.9}$$
$$-2[\frac{(-\delta_{ij}\hat{x_l} + \delta_{il}\hat{x_j} + \delta_{jl}\hat{x_i})\hat{x_m} + \delta_{im}\hat{x_j}\hat{x_l} + \delta_{jm}\hat{x_i}\hat{x_l} + \delta_{lm}\hat{x_i}\hat{x_j}]}{r^4} + 8\frac{\hat{x_i}\hat{x_j}\hat{x_l}\hat{x_m}}{r^6}$$

For the symmetric case with $l = m$, the quadruplet green's function reduces to,

$$(u_{pd})_i = \frac{G_{ij}^{pd} pd_j}{4\pi\mu} \tag{2.10}$$

$$G_{ij}^{pd}(x, x_0) = -(\frac{\delta_{ij}}{r^2} - \frac{2x_i x_j}{r^4}) \tag{2.11}$$

Which is the familiar first derivative of a potential source monopole, called the potential dipole. Thus the potential dipole and hence all of its higher derivatives such as the potential quadrupole, octupole, hexadecapole and so on are also solutions to the linear viscous flow equation (2.3).

2.3 The method of images

A powerful idea that makes singularity methods attractive is the ability to combine individual singularities in such a way as to satisfy no-slip boundary conditions typically encountered in viscous flows. Singularities modeling fluid flows of interest can be superimposed with complementary singularities called mirror images in such a manner as to cancel their velocities on a particular geometry while also incorporating the boundary's effects on the rest of the flow field. Examples of typical boundaries encountered in two dimensional flows include, flat walls such a microfluidic channel walls or circular bounding contours such as petri dishes or other containers often used in lab settings.

2.3.1 Singularity representations near a no-slip wall

Blake [21] studied the problem of flow due a stokeslet in the presence of a wall by using tools from Fourier analysis to construct an analytic solution. The solution was found to be a combination of elementary and higher order solutions of the stokes

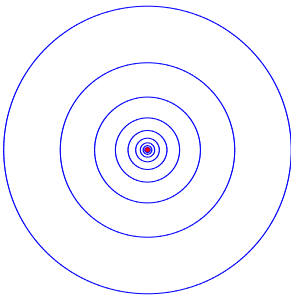

Figure 2.2: Streamlines of flow due to a rotlet.

equation (2.1). Motivated by this, Blake and Chwang [22], used similar techniques to derive image systems for various other singularity solutions such as a rotlet, a potential source and potential source dipole.

In particular, the image of system for a stokeslet next to a wall was found to be a stokeslet of equal strength but opposite sign, a stokes dipole and a potential dipole with the strengths of the stokes dipole and potential dipoles varying in a linear fashion with the distance of the original stokeslet from the wall. All images are placed at an identical distance from the wall as the original singularity on the other side of the wall.

For 2D singularities pointed in the vertical direction which is of interest to us in the subsequent applications, the image system can be compactly written down as two expressions based on [7, 23],

$$\begin{aligned} S^n(x_o)_{wall} = S^n(x_o) + (-1)^{n+1}(2n-3)S^n(x_i) + 2h(-1)^n S^{n+1}(x_i) \\ + 2(-1)^{n+1}(n-1)(n-2)M^{n-2}(x_i) + 4h(-1)^n(n-1)M^{n-1}(x_i) \\ + 2h^2(-1)^{n+1}M^n(x_i) \end{aligned} \quad (2.12)$$

$$M^n(x_o)_{wall} = M^n(x_o) + (-1)^n(2n+1)M^n(x_i) + 2h(-1)^{n+1}M^{n+1}(x_i) + 2(-1)^n S^{n+2}(x_i) \quad (2.13)$$

Where, S^n represents that "n"th stokes singularity at x_0 starting with the stokeslet for $n = 1$ and stokes doublet for $n = 2$ and so on for higher order multiplets. Similarly, M^1 is the potential-dipole and $n = 2$ and greater are higher order potential multipole singularities obtained by differentiating the potential dipole. x_o has been used to denote the position of the original singularity at a height 'h' above the wall, while x_i is used to denote the mirror image position below the wall.

For more general image systems for singularities oriented in any arbitrary directions, the reader is directed to [7, 23].

2.3.2 Singularity driven flows inside a bounded domain

Chaotic advection inside a circular bounding contour is a canonical problem in theoretical fluid dynamics starting with the pioneering works by Hassan Aref [15, 24]. Several practical problems in low Reynolds number fluid dynamics, in particular, fluid mixing problems would benefit immensely by having a simple yet effective method to model the viscous influence of a bounding contour. Early investigations into the problem of singularity driven stokes flow inside a circular bounding contour were motivated by the problem of rotating annular cylinders in viscous fluids [25]. Ranger [26] derived the solution for the problem of a rotlet singularity inside a circular cylinder, while Smith [27] extended these results to arrays of rotlets inside a circular cylinder. The more contemporary work by Meleshko and Aref [28] served to popularize

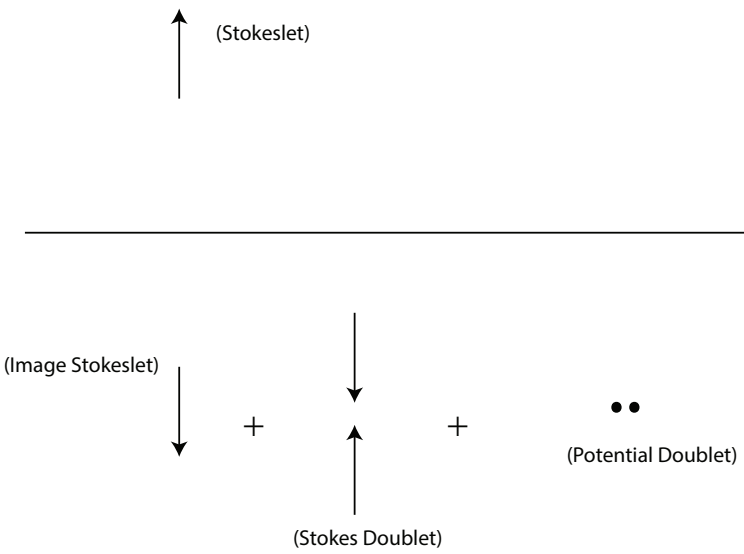

(a) Image system.

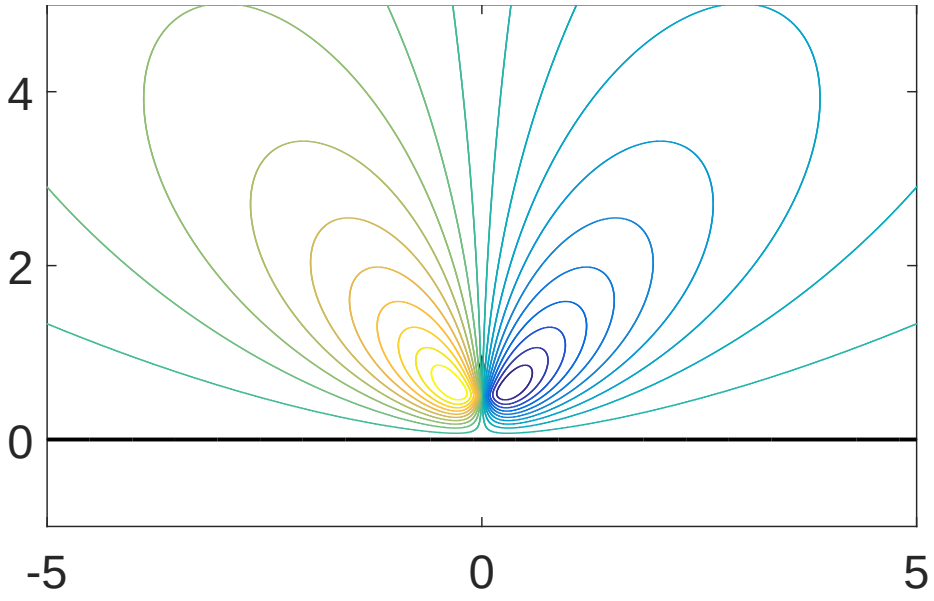

(b) Streamlines of flow.

Figure 2.3: Streamlines of flow due to a vertically oriented stokeslet in the presence of a viscous wall boundary

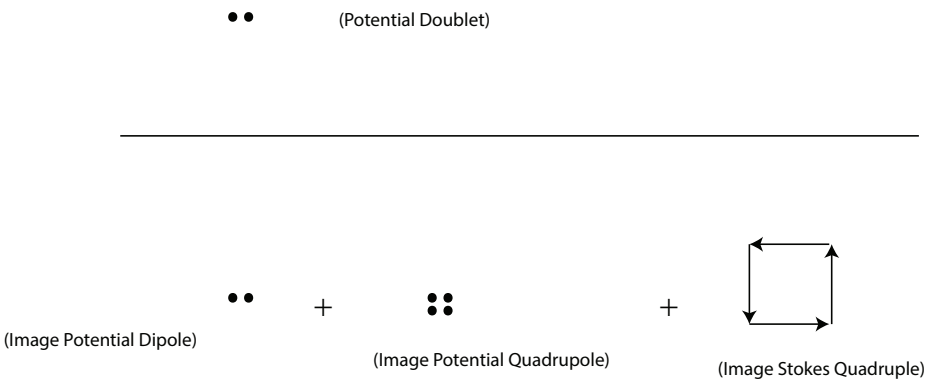

(a) Image system.

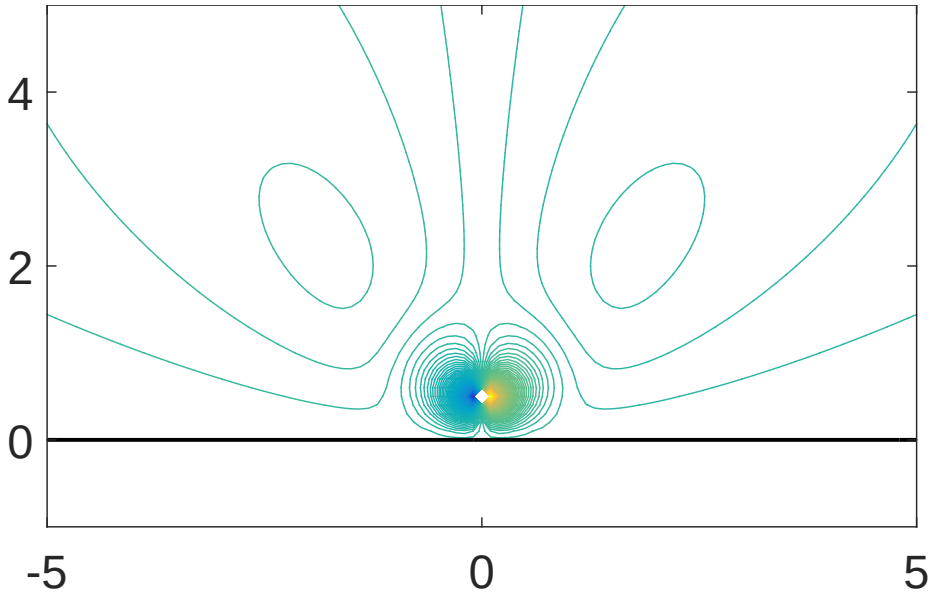

(b) Streamlines of flow.

Figure 2.4: Streamlines of flow due to a vertically oriented potential dipole in the presence of a viscous wall boundary

the use of singularity driven stokes flows inside a circular contour for the studying problems in microfluidic mixing. A comprehensive investigation of singularity driven two dimensional stokes flows inside a circular boundary was conducted in a series of papers by Prabir Daripa and D.Palaniappan [29, 30, 31], where a library of analytic solutions for singularity driven stokes flows in the interior and exterior of a circular cylinder are derived. It is notable that these solutions were derived for a general case of stick-slip boundary conditions on the cylinder with the degree of slip as an adjustable parameter.

For two dimensional flows with velocities u_x in the x-direction and u_y in the y-direction, the stream function of flow denoted by ψ is a function such that [32],

$$\begin{aligned} u_x &= \frac{\partial \psi}{\partial y} \\ \text{and, } u_y &= -\frac{\partial \psi}{\partial x}. \end{aligned} \tag{2.14}$$

Some of the analytical expressions for singularities inside circular cylinders for the no-slip case are given here in stream function formulation from [29]:

- The stream function of flow due to a 2D rotlet singularity of strength σ located at position $(b, 0)$, inside a circular cylinder of radius a is given as,

$$\psi(r,\theta) = \sigma\big[log\frac{R}{\frac{bR_1}{a}} + (1 - \frac{r^2}{a^2})\frac{a^4 - b^2r^2}{2b^2R_1^2}\big] \tag{2.15}$$

  where, $R = \sqrt{(r^2 - 2brcos\theta + b^2)}$ and $R_1 = \sqrt{\big(r^2 - 2\frac{a^2}{b}rcos\theta + \frac{a^4}{b^2}\big)}$ are the distance of the rotlet inside the circle at position $(b, 0)$ and that of an image rotlet at position $(\frac{b^2}{a}, 0)$ outside the circular domain respectively from a field point (r, θ).

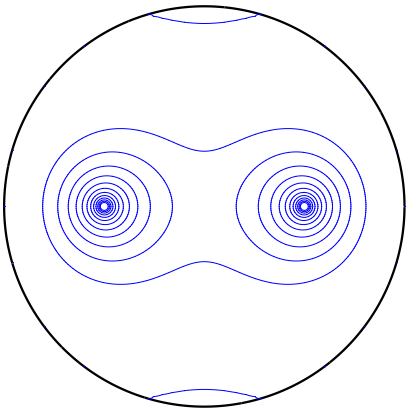

(a) Two rotlets inside a unit circle.

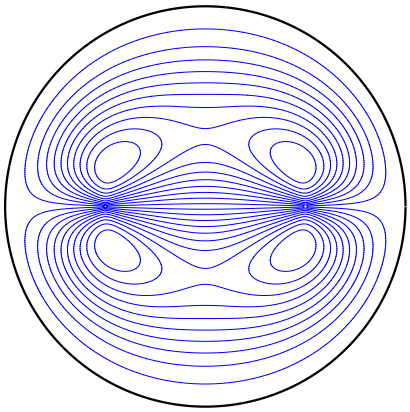

(b) Two stokeslets inside a unit circle.

Figure 2.5: Singularity representations inside a circular cylinder

- The case of a horizontally oriented stokeslet of strength σ located at position $(b, 0)$, inside a circular cylinder of radius a is given as,

$$\psi(r,\theta) = \sigma r \sin\theta \Big[log \frac{R}{\frac{bR_1}{a}} + (r^2 - a^2)\frac{b^2 - a^2}{2b^2 R_1^2} \Big] \tag{2.16}$$

- The case of a vertically oriented stokeslet of strength σ located at position $(b, 0)$, inside a circular cylinder of radius a is given as,

$$\psi(r,\theta) = \sigma \Big[\frac{rb\cos\theta - a^2}{b^2 - a^2} log \frac{bR_1}{a} - (r\cos\theta - b) log R + \frac{(b^2 - a^2)(\frac{r^2}{a^2} - 1)}{2b} \frac{r(r - \frac{a^2}{b}\cos\theta)}{R_1^2} \Big] \tag{2.17}$$

The linearity of stokes flow solutions lets us superimpose these stream functions to study stokes flows of varied nature. Rotlets for instance, can be thought of as a model for rotating stirrers [28] Fig.2.5a, while a stokeslet can be used to model the flow due to translating stirring rods Fig. 2.5b.

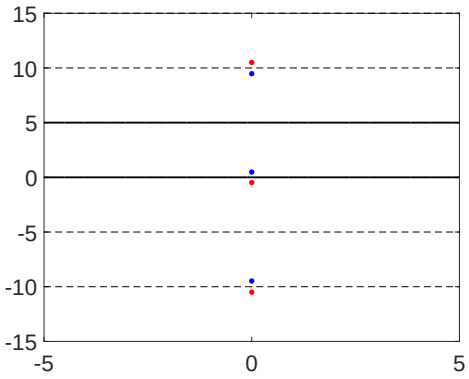

(a) Original singularity between the plates is indicated by a blue dot. The images are represented by a red dot.

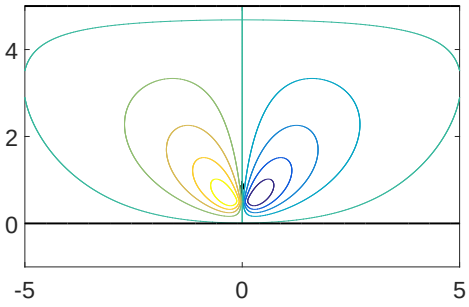

(b) Streamlines of flow due to a vertically oriented stokeslet between parallel walls.

Figure 2.6: Reflection of singularities and images enables us to construct the flow due to a singularity between parallel walls.

2.3.3 Reflection of image singularities

Very often, the effect of confinement plays an important role in microfluidic flows. One of the most important situations where such a flow occurs is the flow through microfluidic channels. In such a situation, the use of method of images to construct the solution for flow in the half plane is insufficient. To construct the flow bounded between parallel planes, the original singularities along with their images can be reflected about a second wall as shown in Fig. 2.6a. However, such a reflection procedure while satisfying the no penetration boundary condition on the second wall, will now violate the no-penetration boundary condition on the first wall. This can be remedied by a second reflection about the first wall which violates the boundary condition on the second wall. However, repeating this procedure over several reflections successively improves the no-penetration boundary condition on both walls [23] Fig. 2.6b. This procedure provides us a with a simple numerical alternative to using analytically involved expressions for singularities of bounded stokes flows [7].

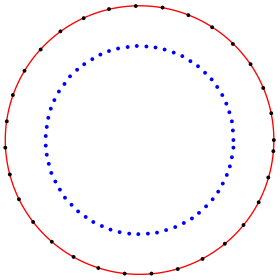

(a) Collocation of singularities inside a circle imposes boundary conditions on the circle's periphery.

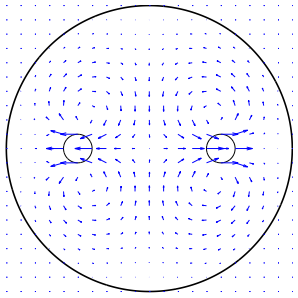

(b) Velocity field.

Figure 2.7: (a)$2N$ stokeslets(blue bubbles) inside a circular cylinder of unit radius, imposing $2N$ velocity boundary conditions at N boundary locations(black bubbles).(b)Velocity field due to a pair of translating circular cylinders inside a circular domain.

2.4 Collocation schemes for singularity driven flows

While several interesting boundary geometries can be modeled using the method of images, the more complex geometries are not easy to model. In addition, the analytic solutions for complex geometries are usually involved and the solution procedure can often be tedious [33]. One way to overcome this is to use the so called method of fundamental solutions [34] which is a numerical collocation scheme involving the placing of stokes flow singularity solutions in the vicinity of boundaries with their strengths chosen so as to obtain the prescribed conditions on boundaries of the flow domain. An effective way to determine the singularity strengths for non-trivial geometries involves solving a system of linear algebraic equations with the singularity strengths as variables.

To illustrate this procedure, let us consider the example of a two dimensional cylinder translating with a velocity $V = \sqrt{v_x^2 + v_y^2}$. We pick N points on the circular cylinder's periphery and impose $2N$ boundary conditions(N each for the velocities in the x and y directions in two dimensional Cartesian-coordinates). We then determine

the velocities at these points due to $2N$ stokeslets placed inside the circle Fig. 2.7a. This gives us a set of $2N$ linear equations with $2N$ unknowns which can then be solved to determine the strengths $s_i, i = 1..2N$of the stokeslets.

$$V_{(2N,1)} = \begin{bmatrix} v_{N1,s1} + v_{N1,s2} + ... + v_{N1,s_{2N}} \\ v_{N2,s1} + v_{N2,s2} + ... + v_{N2,s_{2N}} \\ . \\ . \\ . \\ v_{Nn,s1} + v_{Nn,s2} + ... + v_{Nn,s_{2N}} \end{bmatrix} \begin{bmatrix} s_1 \\ s_2 \\ . \\ . \\ . \\ s_{2N} \end{bmatrix} \tag{2.18}$$

We can use the the GMRES function with restarts of MATLAB(R) to get the best solution for the given set of equations. The usefulness of such a scheme is apparent in more complex geometries such as the one shown in Fig. 2.7b where the inner circles representing a pair of circular rods moving apart, are obtained by collocation of singularities placed on their periphery. The outer bounding contour is obtained using the method of images where each singularity in the collocation scheme has its own set of images outside the circular domain.

Chapter 3

Review of Geometric Methods for Phase Space Transport

3.1 Geometric methods in the study of dynamical systems

The dynamics of innumerable complex phenomenon arising out of nature and engineering has been fruitfully studied from the dynamical systems perspective [35, 36, 37]. The mathematical field of dynamical systems theory provides us with tools to gain insight into the long time behavior of differential or difference equations that model time evolution of physical or engineering systems. These equations are often difficult or impossible to solve analytically and one of the leading reasons for this is the nonlinearity of the phenomenon that is being modeled. Fluid dynamics is an important source of nonlinear problems in physics and the Lagrangian specification of fluid flow has fascinated dynamical systems theorists for several decades[15, 38, 39]. In this chapter, we shall review some basic ideas from the geometric approach to

dynamical systems based on [40] and[41].

For continuous time situations, dynamical systems studied usually take the form,

$$\dot{X}(t) = f(X,t) \tag{3.1}$$

$$\text{with, } X = \begin{bmatrix} x_1 \\ \vdots \\ x_n \end{bmatrix} \textbf{ and, } X(t_0) = \begin{bmatrix} (x_1)_0 \\ \vdots \\ (x_n)_0 \end{bmatrix}$$

In such a system, $X \in \Re^n$ is a vector space representing the space of all possible values that the system's n state variables can take as the system evolves in time from time t_0 to time t. This vector space is called the phase space of the dynamical system at hand. The phase space of a dynamical system is often endowed with geometric features which persist with time. The central theme in phase space transport in dynamical systems involves the study of sets of initial conditions for the system as they evolve relative to these invariant structures in the n dimensional phase space[42].

The invariant objects of interest in phase space include fixed points, periodic orbits or other analogous coherent structures and the stable and unstable manifolds associated with them. In the case of autonomous dynamical systems, one can identify geometric features in phase space by a linearized stability analysis around the fixed points or equilibrium points of the system (i.e) around phase space co-ordinates $X^\star$ such that $f(X^\star, t) = 0$. The stability analysis involves a study of the eigen values of its jacobian $J = Df(X,t)$ of the system (3.1)at $X^\star$. Re-writing the autonomous version of the n dimensional system (3.1) as "n" $1D$ equations,

$$\dot{x_1}(t) = f_1(X) \tag{3.2}$$
$$\dot{x_2}(t) = f_2(X)$$
$$\vdots$$
$$\dot{x_n}(t) = f_n(X)$$

the Jacobian of the system can now be written as,

$$J = \begin{bmatrix} \frac{\partial f_1(x_1 \ldots x_n)}{\partial x_1} & \frac{\partial f_1(x_1 \ldots x_n)}{\partial x_n} \\ \vdots & \vdots \\ \frac{\partial f_n(x_1 \ldots x_n)}{\partial x_1} & \frac{\partial f_n(x_1 \ldots x_n)}{\partial x_n} \end{bmatrix}. \tag{3.3}$$

(3.4)

At an equilibrium point $X^\star$, the eigenvalues of the Jacobian $J^\star$ are,

$$det(J^\star - \lambda I) = 0 \tag{3.5}$$
$$\lambda = \lambda_1, \lambda_2, \ldots, \lambda_n \tag{3.6}$$

Depending on the eigenvalues of the system at the equilibrium point, the equilibrium point can be classified broadly into (1) Hyperbolic equilibrium point if $|Re(\lambda_1, \lambda_2, \ldots, \lambda_n)| > 0$ (2) Non-hyperbolic equilibrium point if at-least one of the eigen values have a zero real part. There can be multiple fixed points for a system that influence the flow topology in phase space.

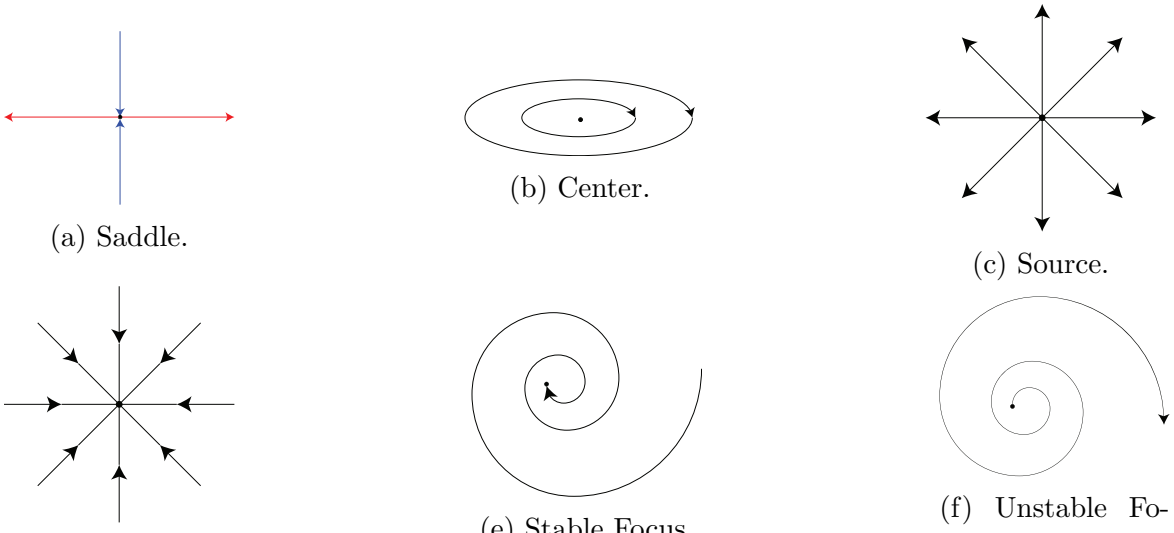

(a) Saddle.

(b) Center.

(c) Source.

(d) Sink.

(e) Stable Focus.

(f) Unstable Focus.

Figure 3.1: Stability of equilibrium points of a 2D system

Some major types of fixed points include,

- **Saddle:** Is a type of hyperbolic fixed point where some of the associated eigen values have a positive real part while others have a negative real part.
- **Source:** Is a type of hyperbolic fixed point where all the associated eigen values are positive and real.
- **Sink:** Is a type of hyperbolic fixed point where all the associated eigen values are negative and real.
- **Center:** Is a type of non-hyperbolic fixed point where the associated eigen values have a zero real part.

3.2 Lyapunov exponents of a dynamical system

One way to describe the flow when not in the vicinity of hyperbolic fixed points involves the calculation of the lyapunov exponent Λ which in some sense convey

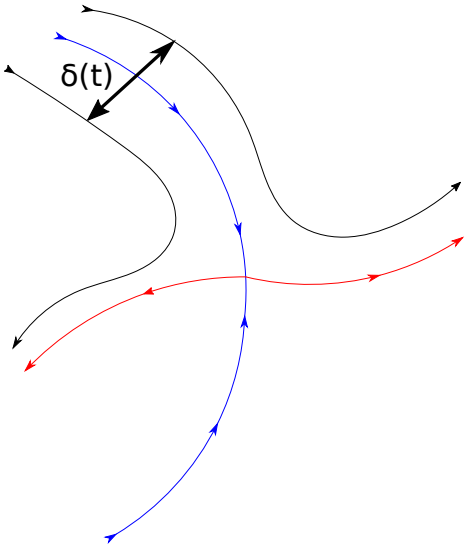

(a) Stretching of trajectories.

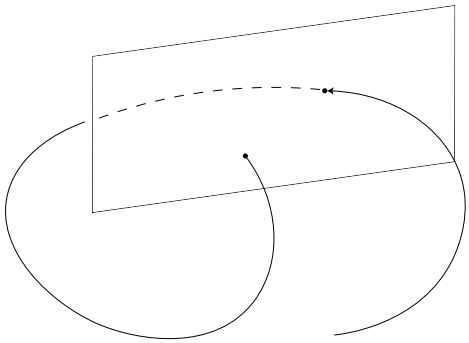

(b) 2D Poincaré map.

Figure 3.2: Continuous and Discrete Time Representation of Dynamical Systems

information about how fast two neighboring trajectories diverge away from each other and are defined as [40],

$$||\delta(t)|| \cong |||\delta_0|| \exp(\Lambda t) \textbf{ with, } t \to \infty \tag{3.7}$$

where δ_0 and $\delta(t)$ are the distance between two initially nearby trajectories at $t = 0$ and some later time 't'. This can be re-written as,

$$\Lambda = \lim_{t\to\infty} \frac{1}{t} \log \frac{||\delta(t)||}{||\delta_0||} \tag{3.8}$$

Lyapunov exponents measure the sensitivity of the system to the initial conditions and is hence a measure of chaos in the dynamics of the system. The eigen values associated with the Jacobian of a system at an equilibrium point can be considered a local lypaunov exponent that tells us about the local stability properties of the system in that neighborhood [41].

3.3 Stability measures for time dependent systems

For systems such as (3.1) with explicit time dependence, a linearized analysis of the system's behavior around fixed points is not possible owing to the fact that the flow field is now unsteady and the solution trajectories are constantly re-orienting in phase space. If the time dependence is periodic, one way to analyze such a system is by studying a discrete map associated with the system in a lower dimensional space [43]. Such a map called a Poincaré map or a first return map represents the intersection of a trajectory in n-dimensional phase space with an $(n-1)$-dimensional surface. Thus, for the case of 3D phase space, the the associated map includes successive return orbits to a 2D plane as seen in Fig.3.2b where periodic orbits are fixed points of the associated poincaré map. In the case of maps, the associated stability can be calculated using an analogous idea as used for the continuous time version in (3.7),

$$||\delta(t)|| \approxeq |||\delta_0|| \exp(\Lambda n) \text{ with, } n \to \infty \tag{3.9}$$

where, n is the number of iterations of the map [40].

However, if the time dependence is arbitrary, one way to identify invariant manifold like geometric structures is to calculate a finite time analogue of the lyapunov exponents Λ, called finite time lypaunov exponents or FTLE and the ridges of high FTLE in a scalar FTLE field can now be considered separatrices in unsteady phase space [44, 45]. These ridges enclose coherent structures in the flow, that persist even if they get advected along by the flow and are hence called Lagrangian Coherent Structures(LCS)[38]. If calculated for a time independent system, the LCS would identify the invariant manifolds in phase space and can be called steady largangian coherent structures (sLCS) [46].

3.4 Definition and computational method for FTLE

Here, we review in brief the definition and a numerical scheme to compute FTLE based on [45]. Considering the evolution of an initial condition X in phase space expressed as $f(X, 0)$, relative to the time evolution of a neighboring initial condition $X+\delta X$ (The perturbation δX is infinitesimal and oriented in some arbitrary direction) expressed as $f(X+\delta X, 0)$, the final separation after a finite time T, between the two initially close phase space points can be expressed as,

$$\delta X(T) = \frac{df}{dX}\delta X(0). \tag{3.10}$$

The magnitude of this growth can be written using the vector L_2 norm as,

$$||\delta X(T)|| = \sqrt{< X(0), \frac{df}{dX}\frac{^*df}{dX}\delta X(0) >} \tag{3.11}$$

$$\tag{3.12}$$

Here,

$$C = \frac{df}{dX}\frac{^*df}{dX} \tag{3.13}$$

is the Cauchy-Green deformation tensor.

If the perturbation δX is not arbitrary in its orientation, and is to be chosen to be in the direction of maximal stretching around the two initial points, the direction of perturbation would have to be along the eigen vector associated with the maximum eigen value of the Cauchy-Green strain tensor C. The magnitude of the perturbation growth in this case would be,

$$||\delta X(T)|| = \sqrt{\lambda_{max} C}||\delta X(0)||$$

with T=t-0

Being interested in exponential stretching that is typical of initial conditions chosen in the vicinity of attracting and repelling invariant manifolds in phase space, we can write the ratio of initial and final magnitudes of the perturbation as

$$\begin{aligned} ||\delta X(T)|| &= ||\delta X(0)|| \exp(\sigma)|T| \\ \text{where, } \sigma &= \frac{1}{|T|} \log \sqrt{\lambda_{max} C} \end{aligned} \tag{3.14}$$

Here, σ is the FTLE at the location X after time T.

Using this definition of the FTLE, a scalar field of local stretching ratios can be constructed for the instantaneous flow field which allows us to identify Lagrangian coherent structures of the flow.

To compute the FTLE at a point in the flow field at a time t over a finite time interval T, we need information about the gradient of the flow map between the initial time $t = 0$ and final time $t = T$. This can be done by choosing grid of densely packed tracers and advecting them under the influence of the flow for the prescribed time. Using the information about the initial and final position of tracers about a point in the flow field, we can compute the gradient of the flow at that point using a finite difference scheme. For a 2D flow, this can be written down as,

$$\frac{df}{dX} = \begin{bmatrix} \frac{x_{(i+1,j)}(T) - x_{(i-1,j)}(T)}{x_{(i+1,j)}(0) - x_{(i-1,j)}(0)} & \frac{x_{(i,j+1)}(T) - x_{(i,j-1)}(T)}{x_{(i,j+1)}(0) - x_{(i,j-1)}(0)} \\ \frac{y_{(i+1,j)}(T) - y_{(i-1,j)}(T)}{y_{(i+1,j)}(0) - y_{(i-1,j)}(0)} & \frac{y_{(i,j+1)}(T) - y_{(i,j-1)}(T)}{y_{(i,j+1)}(0) - y_{(i,j-1)}(0)} \end{bmatrix}. \tag{3.15}$$

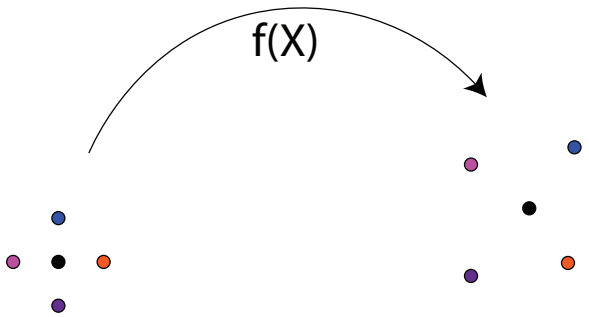

Figure 3.3: Flow map.

With this information, the Cauchy Green deformation tensor can be obtained as (3.13) and the required FTLE associated with that point at a time t and can be obtained.

Let us consider the illustrative example of a Stokeslet induced flow. The fixed points of flow due a single vertically oriented Stokeslet is easy to compute analytically. The governing dynamical system for the motion of a tracer in the vicinity of a Stokeslet driven flow is,

$$\begin{aligned} \dot{x} &= \frac{xy}{r^2} \\ \dot{y} &= -0.5\log(r^2) + \frac{y^2}{r^2}. \end{aligned} \tag{3.16}$$

By setting $\dot{x} = 0$ and $\dot{y} = 0$ in (3.16), the fixed points of this system can be easily seen to be $(1, 0)$,$(-1, 0)$,$(0, 2.7183)$ and $(0, -2.7183)$ as shown in Fig.3.4a. Identifying these fixed points as one of the several major types of fixed points discussed in 3.1 helps us understand the long term behavior of fluid tracer trajectories around these fixed points.

However, consider the case of a stokeslet inside a unit circle as shown in Fig.3.4b. Finding the fixed points analytically is still possible albeit more cumber-

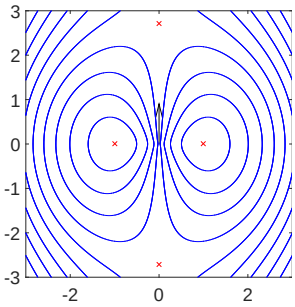

(a) Fixed points in a 2D Stokeslet driven flow .

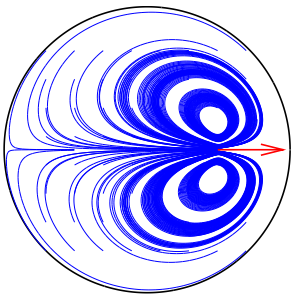

(b) Blinking Stokeslet configuration 1.

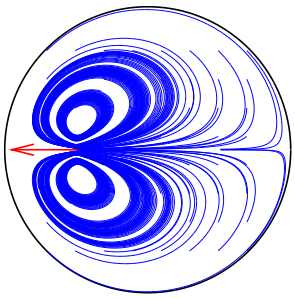

(c) Blinking Stokeslet configuration 2.

Figure 3.4: Flows driven by various Stokeslet configurations

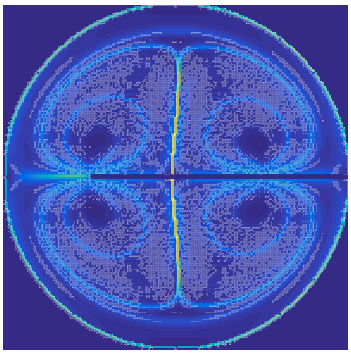

Figure 3.5: Forward time FTLE field for Stokeslets switching between blinking configuations 1 and 2.

some.

If the stokeslet now switched position and orientation periodically in time between the configurations shown in Fig.3.4b and Fig.3.4c, finding fixed points of the flow and thus, the invariant structures associated with them is not possible using the techniques used above. One way of identifying flow structures that lets us predict the dynamics of tracers over finite time intervals is to compute the FTLE field of the time time dependent flows. The ridges of the forward time FTLE field shown in Fig.3.5, in addition to acting as separatrices of the flow, also having the property of being structures that stretch apart fluid flow on either side.

Chapter 4

Review of Micro-Bubble Streaming Flow Theory and Inertial Particle Dynamics

4.1 Overview of the development of steady streaming flow theory

The presence of a net steady flow in oscillatory fluid flows has come to be known as steady streaming [47]. While steady streaming like phenomenon were observed in experiments as far back as the 19th century [48, 49, 50], notable early work on theoretical analysis of the steady streaming flow phenomenon was performed by Lord Rayleigh [51], Nyborg[52] and Westervelt[53]. These early contributions were recognized by Sir James Lighthill in his review of acoustic streaming [54] by calling the case of steady streaming in cases of negligible fluid inertia as RNW streaming, after names of the pioneering authors. In the years that followed, the steady stream-

ing problem was further studied by several people [55, 56, 57]. The use of steady streaming to manipulate particles suspended in fluid has been studied experimentally [58, 59] and using theoretical/computational methods [60].

4.2 Micro-bubble streaming flows

The motivation to study steady streaming flows in the vicinity of oscillating micro-drops or micro-bubbles emerged from the study of phenomenon such as cavitation and sonoluminescence [61, 62]. A notable work in this direction was the derivation of an analytical approximation of the flow due to a bubble undergoing volumetric and translational vibration next to a wall [63]. The usefulness of micro-bubble streaming as particle manipulation elements in microfluidic flows were realized with the works of Mormottant and Hilgenfeldt [64, 65, 66]. In the rest of this chapter, we review some of the results from [67, 10, 11, 68] that clarify the nature of micro-bubble steady streaming flows in microfluidic channel flows .

The problem being reviewed is that of a micro-bubble of radius a trapped at the side wall of a microfluidic channel and oscillating at angular frequency ω and amplitude A in a fluid with dynamic viscosity μ. The typical set up of microfluidic lab on a chip device with integrated micro-bubble streaming involves fabricating a PDMS channel with a side channel at right angle to one or both of the main channel's side walls Fig. 4.1. The hydrophobic nature of the PDMS causes any aqueous solution introduced into the main channel to not enter the side channel, thus creating an air-liquid interface shaped as a hemispherical bubble as a result. Piezo transducers are then used to generate ultrasonic waves that sets the air liquid interface into high frequency oscillation. Such devices are also called Lateral Cavity Acoustic Transducers or LCATs for short [69].

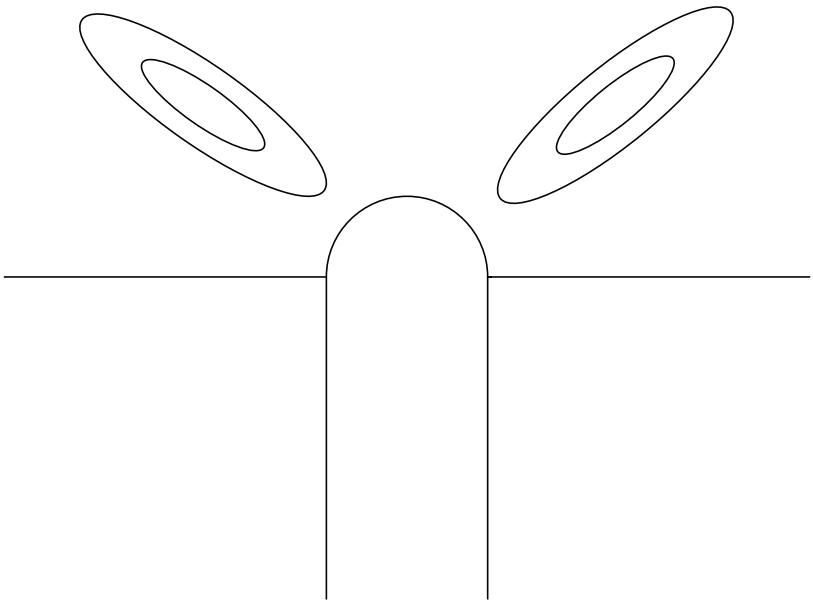

Figure 4.1: Oscillating bubbles next to a no-slip wall produces steady streaming vortices.

4.3 Governing equations and solution

Starting with the 2D-incompressible Navier-Stokes equations in non-dimensional form [68],

$$\frac{\partial u}{\partial t} + \epsilon(u \cdot \nabla)u = -\nabla p + \frac{\delta^2}{2}\mu\nabla^2 u$$
$$\nabla \cdot u = 0 \tag{4.1}$$

where, $\delta = \sqrt{\frac{2\nu}{a^2\omega}}$ is a dimensionless boundary layer thickness and $\epsilon = \frac{U_0}{a\omega}$ is a dimensionless small parameter which is the ratio of bubble oscillation amplitude A to bubble's characteristic length scale a.

Defining vorticity as $\zeta = \nabla \times u$ and taking the curl of (4.1) eliminates the

gradient of pressure and the vorticity equation is obtained,

$$\frac{\partial \zeta}{\partial t} + \epsilon(u \cdot \nabla)\zeta = \frac{\delta^2}{2}\mu\nabla^2\zeta$$

For the two-dimensional case considered here, the vorticity equation can be re-written in terms of the stream function $-\zeta = \nabla^2\psi$. Since the bubble streaming problem is best studied in the cylindrical polar co-ordinates, the governing equation in cylindrical coordinates is,

$$\frac{\partial}{\partial t}(\nabla^2\psi) - \frac{\epsilon}{r}(\frac{\partial \psi}{\partial r}\frac{\partial(\nabla^2\psi)}{\partial \theta} - \frac{\partial \psi}{\partial \theta}\frac{\partial(\nabla^2\psi)}{\partial r}) = \frac{\delta^2}{2}\mu\nabla^4\psi \tag{4.2}$$

Over the years, work on the analytical solutions of steady streaming flow problems have often adopted the approach of writing the stream function for the flow ψ in an asymptotic form in terms of a small parameter such that the leading order time dependent terms and the smaller in magnitude steady streaming flow terms are separated out [55, 57]. Here, the expansion is in terms of ϵ,

$$\psi = \psi_1(r, \theta, t) + \epsilon\psi_2(r, \theta) + O(\epsilon^2) \tag{4.3}$$

This allows the separation of the governing equation into separate equations for the leading order time dependent and higher order steady streaming flows which can then be solved separately.

4.3.1 Unsteady flow solution

The leading order flow solution ψ_1 is governed by an equation comprising terms of order $O(1)$ in (4.2),

$$(\frac{2}{\delta^2}\frac{\partial}{\partial t} - \nabla^2)\nabla^2\psi_1 = 0. \tag{4.4}$$

Assuming that the bubble surface with the mean radius R_1 undergoes undulations that are captured by the shape function, $R(\theta, t) = \left[R_1 - iS(\theta)e^{it}\right]$ the boundary conditions on the mean bubble surface are a no-penetration and a no-stress condition,

$$\begin{aligned} \frac{1}{r}\frac{\partial\psi_1}{\partial\theta} &= S(\theta)e^{it} \\ &\text{on r} = 1 \\ \frac{\partial^2\psi_1}{\partial r^2} - \frac{1}{r}\frac{\partial\psi_1}{\partial r} - \frac{1}{r^2}\frac{\partial^2\psi_1}{\partial\theta^2} &= 0 \\ &\text{on r} = 1 \end{aligned} \tag{4.5}$$

as well as no-slip boundary conditions on the bounding wall,

$$\frac{\partial\psi_0}{\partial r} = \frac{1}{r}\frac{\partial\psi_0}{\partial\theta} = 0 \text{ for, } \theta = 0 \text{ and, } \theta = \pi \tag{4.6}$$

The solution to (4.4) in separable variables $\boldsymbol{\psi(r)} = \bar{\psi}$,$\boldsymbol{\psi(\theta)} = e^{k\theta}$ and $\boldsymbol{\psi(t)} = e^{it}$ is of the form [10],

$$\psi_u = \big(\frac{C_k}{r^k} + D_k K_k(\alpha r)\big)e^{k\theta}e^{it}. \tag{4.7}$$

The boundary conditions can be incorporated by expanding out (4.7) in a Fourier sine series whose coefficients can be determined to satisfy the boundary con-

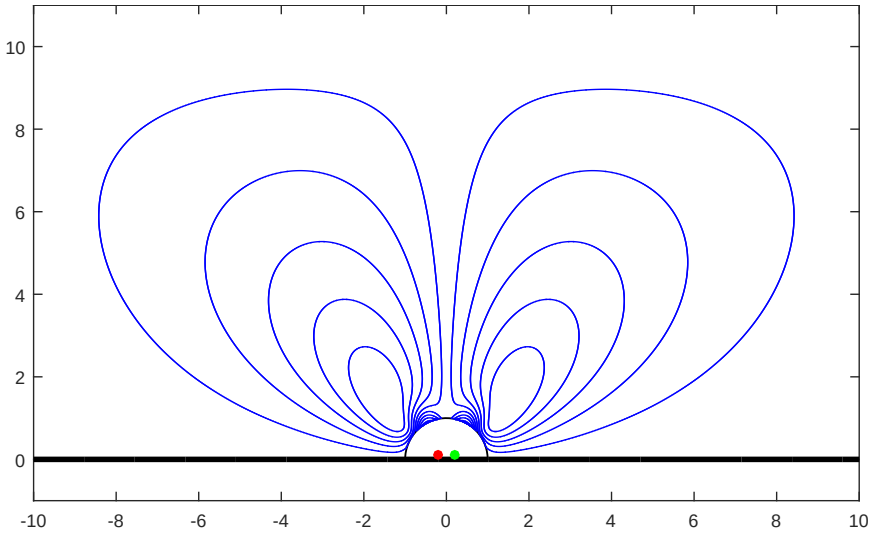

Figure 4.2: Steady streaming flow due to wall bounded micro-bubble

ditions on the bubble interface. The first term of the unsteady flow solution (4.7) is the algebraically decaying term which represents an oscillatory potential flow and can be modeled as the sum of oscillatory potential multipoles.

$$\psi_u = \sum_{k=0}^{\infty} \frac{C_k}{r^k} e^{k\theta} e^{it}. \tag{4.8}$$

This is the dominant part of the flow outside the bubble boundary layer and of interest to us while the second term is a modified bessel function of the second kind which is valid only inside the boundary layer adjacent to the bubble.

4.3.2 Steady streaming flow solution

The higher order terms of (4.2) constitute an in-homogeneous bi-harmonic equation,

$$\nabla^4 \psi_2 = \frac{-2}{\delta} \frac{1}{r} \frac{\partial(\psi_1, \nabla^2 \psi_1)}{\partial(r, \theta)} \tag{4.9}$$

This equation models the slower steady streaming components of the flow. The forcing term on the right hand side arises out of interactions between the first order solution's various shape modes of oscillation and the volume mode of oscillation as well as between various shape modes.

The boundary conditions to be satisfied are similar to that of the unsteady flow (4.5) however, the no-penetration condition is on the mean position of the bubble wall ,

$$\frac{1}{r}\frac{\partial \psi_1}{\partial \theta} = 0. \tag{4.10}$$

The solution to (4.9) is derived in [11], where the general solution is a series in singularity solutions of stokes flow such that the no-slip boundary condition at the wall (4.6) is satisfied,

$$\begin{aligned} \psi_{2S} = \sum_{n=1}^{\infty} \frac{a_n}{r^{2n-1}}[\cos(2n-1)\theta - \cos(2n+1)\theta)] \\ + \sum_{n=1}^{\infty} \frac{b_n}{r^{2n}}[\frac{1}{2n}\sin(2n)\theta - \frac{1}{2(n+1)}\sin 2(n+1)\theta)]. \end{aligned} \tag{4.11}$$

and the sum of the particular solution ψ_p and stokes drift terms ψ_d is given as,

$$\psi_p + \psi_d = \psi_{mn} = \rho_{mn} \sin 2(m-n)\theta \tag{4.12}$$

where, ρ_{mn} is the product of the normalized oscillation amplitude of the $m'th$ and $n'th$ modes.

The co-efficients a_n and b_n are chosen to satisfy the bubble boundary condi-

tions. This can be done numerically as it has been done in Fig. 4.2, or analytically as shown in [11] while matching the streamfunction ψ_{mn} on the bubble surface.

The combined second order solution is called the steady streaming flow solution ψ_{SS} and can is seen in experiments as steady vortex like closed streamlines in the vicinity of the oscillating bubbles.

4.3.3 Three dimensional effects in micro-bubble streaming flows

The typical microfluidic devices with integrated micro-bubble streaming used in particle manipulation experiments have an axial dimension which is a little over the diameter of the micro-bubble being used [12, 13]. This tight confinement in the axial direction has been found to damp out the three dimensional features of the flow, thus making the steady streaming phenomenon qualitatively approximately same at every cross section of the flow [10].

4.4 Maxey-Riley Equation

We take a detour from the review of micro-bubble streaming flows to review the equation of motion for finite sized particles, called the Maxey-Riley Equation [70] which is applicable for a small but finite sized, spherical and rigid particle.

$$\rho_p \frac{d\mathbf{v}}{dt} = \rho_f \frac{D\mathbf{u}}{Dt} + (\rho_p - \rho_f)g - \frac{9\nu\rho_f}{2a_p^2}(\mathbf{v} - \mathbf{u} - \frac{a_p^2\nabla^2\mathbf{u}}{6}) - \frac{\rho_f}{2}(\frac{d\mathbf{v}}{dt} - \frac{D}{Dt}[\mathbf{u} + \frac{\mathbf{a_p}^2}{10}\nabla^2\mathbf{u}]) - \frac{9\rho_f}{2a_p}\sqrt{\frac{\nu}{\pi}}\int_0^t \frac{1}{\sqrt{t-\tau}}\frac{d}{d\tau}(\mathbf{v} - \mathbf{u} - \frac{a_p^2\nabla^2\mathbf{u}}{6})\partial\tau. \quad (4.13)$$

The symbols ρ_f and ρ_p represent the density of the fluid and the particle respectively, while $\mathbf{v}$ is the velocity of the particle and $\mathbf{u}$ is the velocity of a fluid tracer at the same location as that of the particle. The other quantities are the acceleration due to gravity g, the kinematic viscosity ν and the particle radius a_p. The various forces that act on the particle can be identified on the right hand side of the (4.13) going from the left most term to the right as, the force exerted on the particle due to the undisturbed flow, the buoyancy force, the Stokes drag, the added mass correction and finally the Basset-Boussinesq history force.

The Maxey-Riley equation is valid for small particles quantified as $\frac{a_p}{L} << 1$, where L is the characteristic length scale of the flow and the particle Reynolds number is small (i.e) $\frac{a_p^2}{\mu}\frac{U}{L} << 1$, where U is a characteristic velocity scale of the flow. For many flow situations of interest, the Maxey-Riley equation can be simplified to yield a form of governing equation that is very easy to work with. Restricting the investigation to neutrally buoyant particles ($\rho_p = \rho_f$) with radius a_p which is non-negligible but small enough that a_p^2 is negligible, the buoyancy forces and Faxén correction ($a_p^2\nabla^2 u$) terms drop out. The Basset history term which represents the net diffusion of vorticity from the particle over the entire duration of its motion. It has been commonly accepted to neglect this term in simulations owing to its relative lack of importance in low Reynolds number flows with small relative velocities and considering the difficulty in its numerical implementation and the associated computational cost [71].

Considering these simplifications, and re-writing the material derivative along a tracer's path $\frac{D\mathbf{u}}{Dt} = \frac{\partial \mathbf{u}}{\partial t} + \mathbf{u}\cdot\nabla\mathbf{u}$ in terms of the material derivative along an inertial particle's path $\frac{d\mathbf{u}}{dt} = \frac{\partial \mathbf{u}}{\partial t} + \mathbf{v}\cdot\nabla\mathbf{u}$, the reduced form of Maxey-Riley equation can be written down as [72],

$$\frac{d(\mathbf{v}-\mathbf{u})}{dt} = -[(\mathbf{v}-\mathbf{u})\cdot\nabla]\mathbf{u} - \frac{2}{3}St^{-1}(\mathbf{v}-\mathbf{u}) \tag{4.14}$$

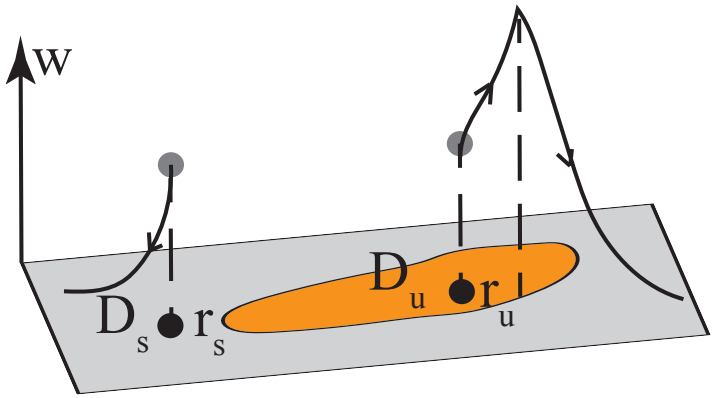

Figure 4.3: Stable(D_s) and unstable(D_u) sub-domains of a flow domain.

(or)

$$\frac{d\mathbf{w}}{dt} = -(J + \mu I) \cdot \mathbf{w} \tag{4.15}$$

where J is the gradient of undisturbed velocity field, $\mathbf{w} = \mathbf{v} - \mathbf{u}$ is the velocity of the particle relative to an underlying fluid tracer and $\mu = \frac{2}{3}St^{-1}$ with the Stokes number $St = \frac{2a_p^2 U}{9\nu L}$.

The evolution of the position of the inertial particle in the domain $r(x, y)$ is governed by the equation,

$$\frac{dr}{dt} = w + \mathbf{u}. \tag{4.16}$$

This equation along with equation (4.15) forms a four dimensional dynamical system which can be compactly represented as,

$$\frac{d\xi}{dt} = f(\xi) \tag{4.17}$$

where, $\xi = (x, y, w_x, w_y)$.

4.4.1 Stable and unstable sets for inertial particle dynamics

It has been found that fluid flows possess distinct subsets where the inertial particle lose any velocity they might have relative to that of an underlying passive tracer particle and settle down onto the streamlines of the flow while some other regions are such that the relative velocity does not decay, but instead it grows [72]. The unstable subset of the flow domain can thus be considered a repeller to inertial particle dynamics while the stable subset can be considered an attractor. Analytical criteria to identify these stable and unstable regions of any arbitrary flow field has been the subject of several investigations. An Eulerian criteria was given by Babiano [72], where it was proposed that for a conservative flow, every point of the flow field (x, y) that has the associated Okubo-Weiss criterion($Q(x, y) = \lambda^2$) greater than the square of the quantity $\mu = \frac{2}{3St}$ belongs to the unstable subset D_u of the flow. The eigen value λ of the Jacobian of system (4.17) is evaluated at every field point (x, y) to identify its stability. All points of the flow field that do not satisfy this criterion can be classified as being part of the stable subset of the flow D_s. This can be compactly stated as,

$$D_s = \{(x, y) : Q(x, y) < \mu^2\} \tag{4.18}$$
$$D_u = \{(x, y) : Q(x, y) > \mu^2\}.$$

This can be seen readily if one considers the equation (4.15) where the eigen values of $-(J + \mu I)$ govern the growth of the relative velocity w.

Sapsis and Haller [73] noted that the Eulerian criteria described in [72] does not take into account the fact that the inertial particles visit several points of the flow

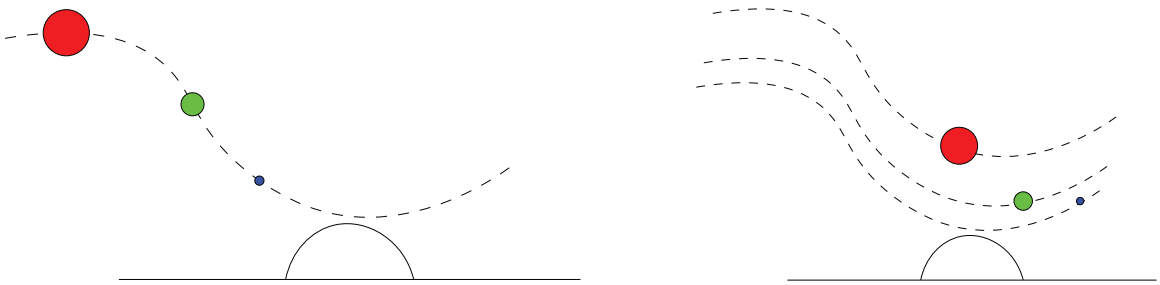

(a) Before deflection. (b) After deflection.

Figure 4.4: The magnitude of deflection near the bubble surface is proportional to particle size.

domain with differing stability properties and can thus possess enough relative velocity to get repelled from certain regions which are stable by the Eulerian criteria. The new criteria proposed in [73] is obtained by calculating the instantaneous deformation of a blob of initial conditions along the inertial particle's trajectory. Doing this calculation led them to the conclusion that the new Eulerian criteria that captured the full stable(H_s) and unstable sets (H_u) is,

$$H_s = \{(x, y) : \lambda_{min}(S(x, y)) < -\mu\} \tag{4.19}$$

$$H_u = \{(x, y) : \lambda_{min}(S(x, y)) > -\mu\} \tag{4.20}$$

.

where, $S = \nabla u + \nabla u^T$ and λ_{min} its minimum eigen value at that location. It is also proved in [73] that D_u is always a subset of H_u.

4.5 Inertial particle manipulation in micro-bubble streaming flows

The early works by Marmottant and Hilgenfeldt [64, 65] demonstrated the utility of micro-bubble streaming flows inside microfluidic channels for purposes of microparticle manipulation. Hilgenfeldt and co-workers have since studied the problem of particle manipulation in micro-bubble streaming flows in greater detail [12, 13, 14, 74]. where various particle manipulation schemes including particle trapping, sorting, switching and focusing have been experimentally demonstrated.

While initially, the mechanism that causes size dependent behavior in inertial particles in the presence of micro-bubble streaming was believed [14] to be direct interactions of the micro bubble with the particle which caused different sized particles to be displaced to different extents in the direction normal to the bubble as shown in Fig.4.4, it was later realized that the nature of the bubble's contribution to particle deflection was indirect and through the effect of a lubrication layer around the bubble and the associated disturbance force of the form $F_{lub} = -6\pi\rho\mu a_p^2 e_r \frac{v\cdot e_r - U_b}{4h}$ (where h is the distance of the particle from the bubble surface and U_b is the bubble's surface velocity) that it causes the inertial particle's trajectory to exhibit sized based different behavior near the bubble [74].

While the Saffman lift [75] has been found to be of importance in previous computational investigations of steady streaming flows near oscillating circular cylinders [60], the importance of the Saffman lift has been found to be extremely small and negligible in micro-bubble streaming flows [76, 74].

4.6 Singularity model of wall bounded micro-bubble streaming

The steady streaming flow due to an oscillating micro-bubble next to a wall was studied by Longuet-Higgins [63], where the flow due leading order volumetric and translational oscillations were found to be of the form,

$$\psi = \sin(\phi)[-\frac{r}{2} + \frac{1}{4r} + \frac{1}{4r^4}](1 - \cos^2\theta) \tag{4.21}$$

the terms of which are, from left to right, the stream function of a vertically oriented stokeslet followed by a potential dipole and finally a hexadecapole. The angle ϕ here denotes the phase difference between the oscillatory and translational motion. It was shown by Marmottant and Hilgenfeldt [65], that when not very close to the surface of the the bubble(outside the bubble-boundary layer), this solution was in good agreement with experimentally observed steady streaming flows set up due to acoustically excited oscillating bubbles on a flat surface. These micro-bubbles undergo only volumetric oscillations, however they are bounded by a wall from below, thus constraining them in the direction of vertical motion and causing the bubble's center of mass to translate up and down to accommodate the volumetric expansion and contraction [63]. Thus the flow due a wall bounded micro-bubble can be modeled using only the leading two terms of the solution (the hexadecapole velocity decays very fast away from the bubble) in conjunction with the image system for wall bounded singularities (2.12),(2.13) as shown in Fig.4.5 where the steady streaming flows do not penetrate the bubble surface, while the bubble surface itself is oscillating about a mean position.

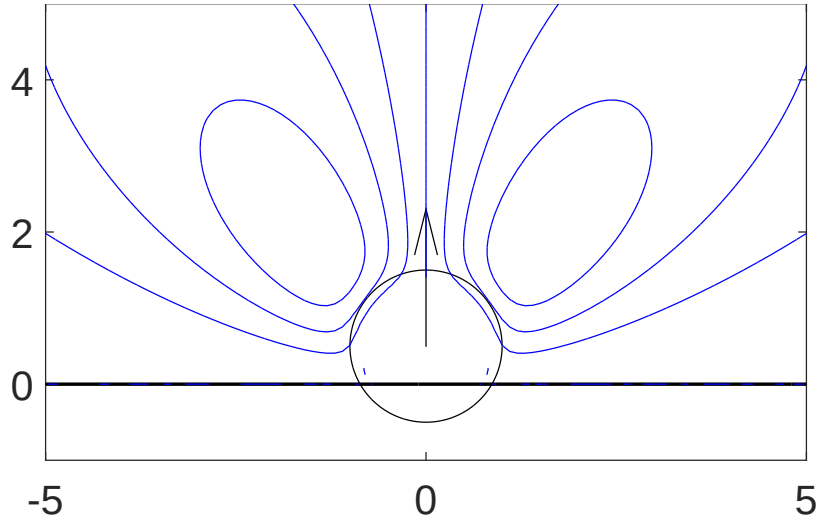

Figure 4.5: Singularity model of oscillating bubble next to a no-slip wall constructed using a stokeslet and potential dipole. The no penetration boundary condition is satisfied on the instantaneous radius of the oscillating bubble surface while the mean bubble surface is shown here.

Chapter 5

Particle Dynamics in Simple Models of Ideal Flows

In this chapter we use tools from dynamical systems theory to analyze the motion of inertial particles in simple potential flow models. We find that our investigations offer crucial insight into the nonlinear dynamics of inertial particles in such flows. Our success with simple models of ideal flows motivates us to study the dynamical boundaries of similarly simple models of more realistic viscous flows. The content of this chapter has been published as a paper by us [77].

5.1 Potential flow models

A better understanding of the dynamics of finite sized inertial particles in the vicinity of vortex flows helps further our ability to harness vortical flows encountered in several engineering applications such as Dean vortices in curved microfluidic channels [78] and steady streaming vortices in flows with high frequency fluid structure interactions for the purposes of non-contact manipulation of inertial particles. A

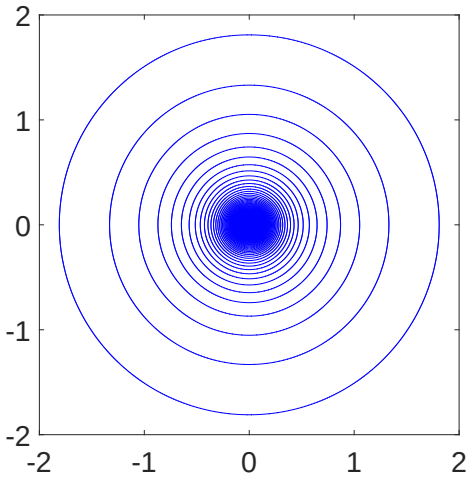

(a) Streamlines of flow due to a point vortex.

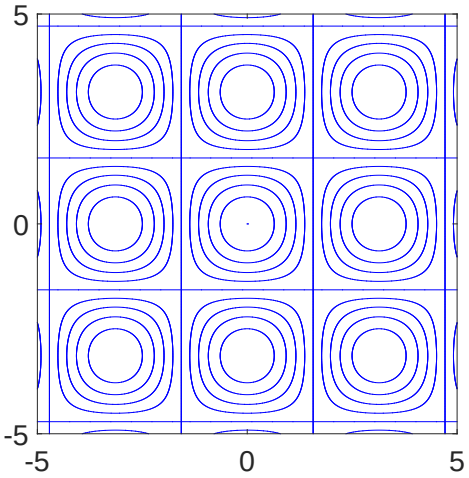

(b) Streamlines of a cell flow.

Figure 5.1: Streamlines are shown in blue for (a)Point vortex and (b) Cell flow.

highly idealized yet simple model of a vortex driven flow is the flow due to a point vortex. The point vortex model is a classical model introduced in 1858 by Helmholtz [79] and has since been extensively studied for its interesting properties [80] as well as for its effectiveness as a model for several realistic flows of interest [15, 81]. The point vortex is a Dirac delta function of vorticity embedded in an otherwise ir-rotational flow and the velocity field due to a point vortex of strength Γ centered at position (x_c, y_c) can be expressed as [82],

$$u_x(x,y) = -\frac{\Gamma}{2\pi}\frac{(y-y_c)}{[(x-x_c)^2+(y-y_c)^2]} \tag{5.1}$$
$$u_y(x,y) = +\frac{\Gamma}{2\pi}\frac{(x-x_c)}{[(x-x_c)^2+(y-y_c)^2]}.$$

Another paradigmatic model of potential flow is the cell flow model whose stream function is given as [72],

$$\psi(x,y) = A\cos(x)\cos(y). \tag{5.2}$$

Streamlines of flow due to these model flows is shown in Fig. 5.1.

5.2 Global stability of inertial particle trajectories within domains of instability

To study the dynamics of inertial particles, we use a Gaussian vortex model which involves a point vortex of the form shown in (5.1) but with a strength that varies smoothly with distance $r = \sqrt{\left(\frac{x^2+y^2}{r_c}\right)}$ away from the center as $\Gamma = \gamma(1 - \exp^{-r^2})$ within a core of radius r_c.

Using the Eulerian criteria (4.19) we can identify the stable and unstable subsets of the gaussian vortex flow. Doing this, we see the the gaussian core of the vortex is part of the stable subset (white) as shown in Fig. 5.2a and so is a region far away from the core of the vortex while there is an unstable subset surrounding this stable core(shown in grey). According to the existing Eulerian criteria, an inertial particle with a certain initial relative velocity can not lose all its relative velocity as long as it stays inside the unstable sub-domain. It was noticed as part of the author's masters degree thesis work [83] that this may not always be the case and that an inertial particle's relative velocity might still decay while the inertial particle never visits the stable subset of the flow domain. It was hypothesized that this could be because every point of H_u that the inertial particle visits might have stable and unstable eigen vectors of the relative velocity subspace slightly more rotated than the previous location of the inertial particle Fig. 5.2d. This would cause the inertial particle's relative velocity to be influenced in a cyclic manner by the stable and unstable eigen vectors with the stable eigen vector's influence being stronger($|-\lambda-\mu| > |\lambda-\mu|$).

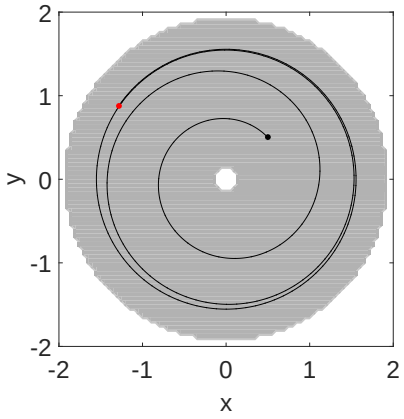

(a) Inertial particle trajectory near a gaussian vortex.

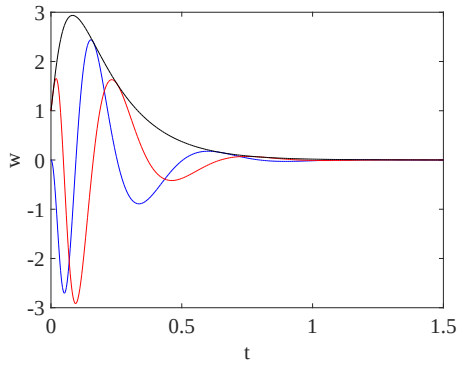

(b) The relative velocity of the inertial particle, w_x(red),w_y(blue) and net magnitude w(black) with time(t)

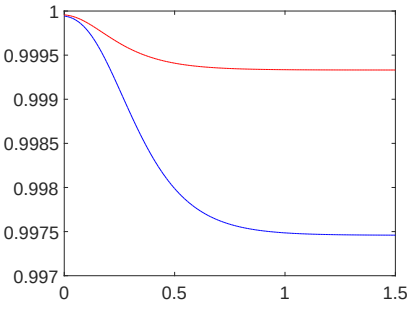

(c) α(red) and β(blue).

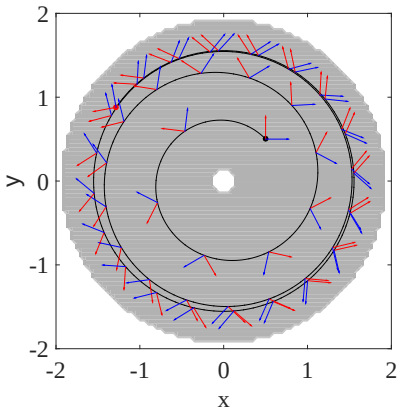

(d) Stable eigen vector w_s in blue and Unstable eigen vector w_u in red

Figure 5.2: (a)The trajectory of an inertial particle(black) inside the unstable subset(H_u) of a gaussian vortex flow(b) The net relative velocity of the inertial particle decaying despite never leaving the unstable region(c) Projections α and β over time (d) Eigen vectors at various positions of the inertial particle.

However, the eigen vectors of the two dimensional system of equations governing dynamics in the relative velocity($w_x - w_y$) subspace might be insufficient to explain the dynamics that unfolds in the full 4 dimensional phase space of the simplified Maxey-Riley equation(4.17). Hence we consider the linearized dynamics of the particle at each point (x, y) in the unstable set $D_u \subseteq H_u$ by calculating the eigen values of the Jacobian ,

$$A = \begin{bmatrix} \frac{\partial u_x}{\partial x} & \frac{\partial u_x}{\partial y} & 1 & 0 \\ \frac{\partial u_y}{\partial x} & \frac{\partial u_y}{\partial y} & 0 & 1 \\ -\frac{\partial^2 u_x}{\partial^2 x}w_x - \frac{\partial^2 u_x}{\partial x \partial y}w_y & -\frac{\partial^2 u_x}{\partial^2 x}w_x - \frac{\partial^2 u_x}{\partial x \partial y}w_y & -\frac{\partial u_x}{\partial x} - \mu & -\frac{\partial u_x}{\partial y} \\ -\frac{\partial^2 u_y}{\partial^2 x}w_x - \frac{\partial^2 u_y}{\partial x \partial y}w_y & -\frac{\partial^2 u_y}{\partial^2 x}w_x - \frac{\partial^2 u_y}{\partial x \partial y}w_y & -\frac{\partial u_y}{\partial x} & -\frac{\partial u_y}{\partial y} - \mu \end{bmatrix}. \tag{5.3}$$

Evaluated about the point $(x, y, 0, 0)$ of the phase space, the jacobian is seen to be a block diagonal matrix of the form,

$$\begin{bmatrix} J & I_{2,2} \\ 0_{2,2} & -(J + \mu I) \end{bmatrix} \tag{5.4}$$

with associated eigen values same as the eigen values of the diagonal blocks, namely, λ,$-\lambda$,$\lambda - \mu$ and $-\lambda - \mu$. If the eigen vectors associated with eigen values λ,$-\lambda$ of J are s_1 and s_2, then the eigen vectors corresponding to the same eigen values in the full system A will be $\eta_1 = \begin{bmatrix} s1 \\ 0 \end{bmatrix}$ and $\eta_2 = \begin{bmatrix} s2 \\ 0 \end{bmatrix}$ respectively. Similarly, if the eigen vectors associated with eigen values $\lambda - \mu$,$-\lambda - \mu$ of $-(J + \mu I)$ are w_s and w_u, then the corresponding eigen vectors in the full system A shall be, $\eta_3 = \begin{bmatrix} P_1 \\ w_s \end{bmatrix}$ and $\eta_4 = \begin{bmatrix} P_2 \\ w_u \end{bmatrix}$. Where simple calculations show that $P_1 = -(J - \lambda_s I)^{-}1 w_s$ and

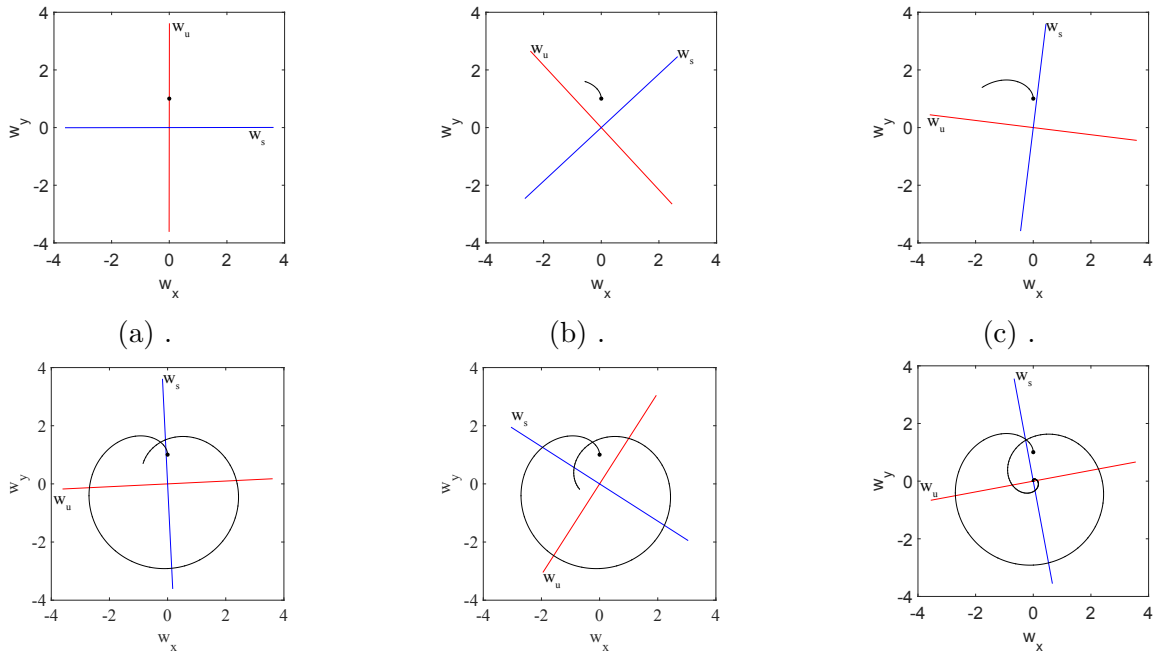

(a) . (b) . (c) .

(d) . (e) . (f) .

Figure 5.3: Various stages in the decay of relative velocity in the unstable subset of Gaussian vortex flow domain.

$P_2 = -(J - \lambda_u I)^{-}1 w_u$.

To compare the eigen vectors η_3 and η_4 with w_s and w_u, we define the projections,

$$\alpha = \frac{\eta_3 \cdot \begin{bmatrix} 0 \\ w_s \end{bmatrix}}{||\eta_3|| ||w_s||} \tag{5.5}$$

and

$$\beta = \frac{\eta_4 \cdot \begin{bmatrix} 0 \\ w_u \end{bmatrix}}{||\eta_4|| ||w_u||}. \tag{5.6}$$

The values of α and β were computed for a stokes number of 0.1 and is plotted

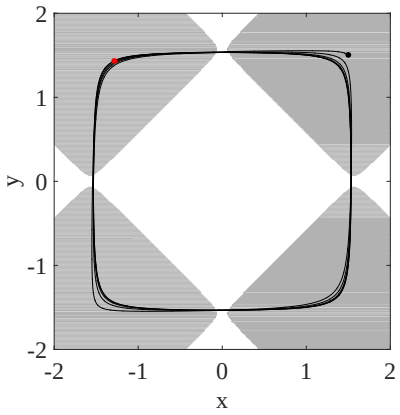

(a) The unstable set D_u is shown in grey and stable set D_s in white.

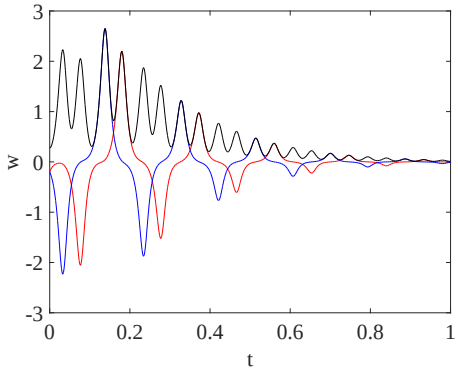

(b) w_x(red),w_y(blue) and net w(black).

Figure 5.4: (a)Inertial particle trajectory in a cell flow(b)Decay of relative velocity w with time.

in Fig. 5.2c, where it can be seen that the values are nearly equal to 1. This has the implication that the eigen vectors w_s and w_u are nearly identical to the corresponding eigen vectors obtained from the full 4 dimensional system. Moreover, this was verified for a large range of stokes numbers ranging form 0.01 to 1 and the values of the projection was always close to unity.

This finding lets us revisit our earlier hypothesis for the mechanism that leads to the decay of an inertial particle relative velocity while never leaving the unstable subset D_u of the flow. Taking a non-zero initial perturbation for an inertial particle which executes tight loops in the unstable domain such as in Fig.5.2d, the perturbation gets influenced alternately by the stable and unstable eigen vector as seen at various time intervals of the trajectory's evolution Fig. 5.3a-Fig. 5.3f causing the relative velocity to grow and wane in each of its two components but with the eventual spiraling in of the perturbation trajectory to the origin ($w_x = 0$,$w_y = 0$) due to the dominant influence of w_s over the relative velocity. Thus the mechanism by which relative velocity decays involves a local unstable manifold at any given point inter-

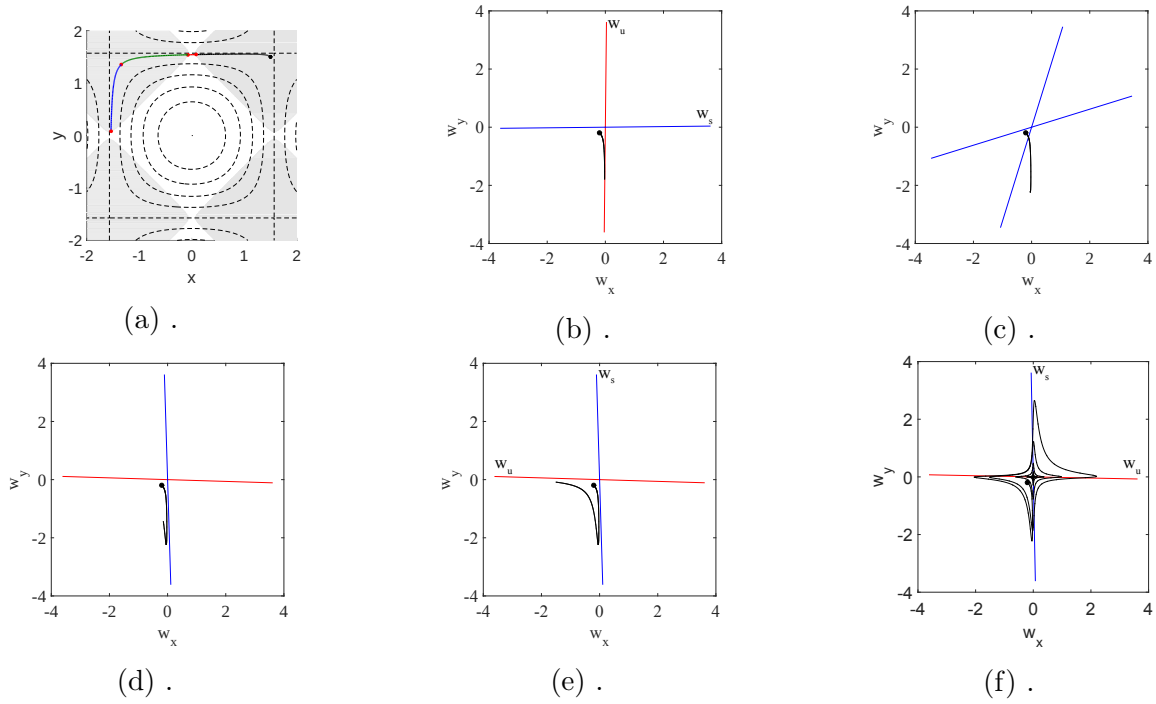

(a) . (b) . (c) .

(d) . (e) . (f) .

Figure 5.5: Various stages in the decay of relative velocity in the unstable subset of cell flow domain.

secting non-transversally with the local stable manifold at another location within the same unstable subset.

This rotation of eigen vectors w_s and w_u need not always be continuous. The rotation of w_s and w_u along the trajectory of the particle can be abrupt and in which case, we can consider them to be switched periodically. A simple example of such a phenomenon occurs in the cell flow model Fig.5.1b. As the inertial particle traverses the edge of a cell, at each corner of the cell, it encounters stable and unstable eigen vectors w_s and w_u which are rotated by an angle of 90 degrees relative to their directions at the previous corner. It is to be noted here that the unstable sets of the cell flow are such that the inertial particle does visit the stable subset D_s during its motion, however the passage through D_s is momentary and of insufficient duration for the relative velocity to decay Fig.5.5a. However, the cyclic growth and decay of

the initial perturbation is apparent as seen in Fig. 5.5b-Fig. 5.5f with the relative velocity once again collapsing into $(w_x = 0, w_y = 0)$ due to the fact that $|w_s| > |w_u|$ always.

The idea of a dynamical system that possesses a manifold that is locally unstable at every point and yet is globally stable due to non-transversal intersections of the local unstable manifold associated with one point on the manifold with the local stable manifold emanating from another point on the manifold is a novel finding. This idea has been generalized to an abstract dynamical system which can exhibit similar locally unstable yet globally stable behavior [84].

5.3 Particle manipulation in viscous flows

The combined framework of singularity models and phase space transport have been seen to yield useful insights into the nonlinear dynamics of inertial particles in potential flows. However, viscosity plays an important role in determining the geometry of fluid flows at the low Reynolds numbers. Hence, to study such fluid flows, the singularities used to model the fluid flows should be singularity solutions of the governing Stokes equations discussed in chapter 2.

The approach to accomplishing this can be broken down into a few steps as shown in Fig.5.6. It is important first, to identify the origin of geometric features in the fluid flows of interest. The nature of forces that give rise to these geometric structures play a key role in the determining the influence these features have on the dynamics of particles in their vicinity. Having determined this, we can then decide on the particular singularity or combination of singularities that best models the fluid flow on interest.

If the particles being manipulated are of finite size, identifying phase space

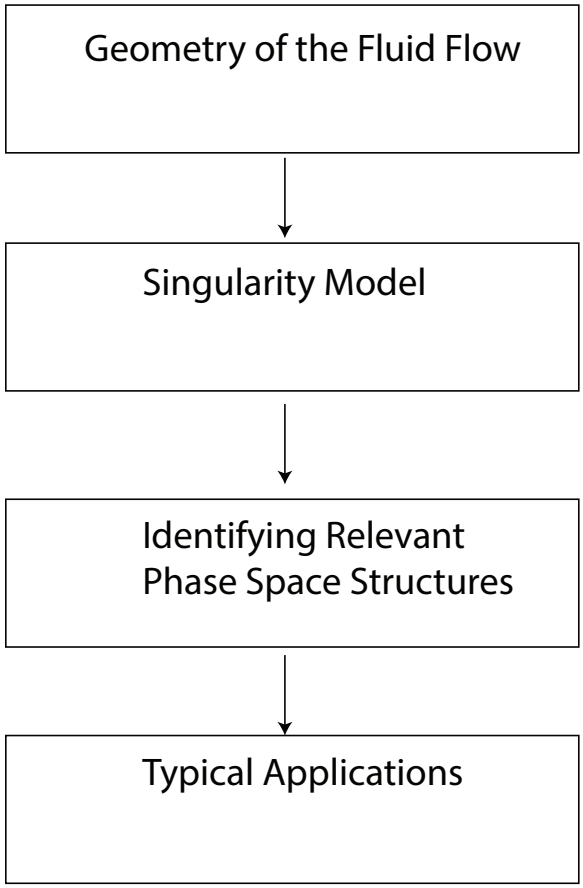

Figure 5.6: A framework to study particle transport in viscous fluid flows.

structures that influence their dynamics enables the identification of behavior such as clustering and size based separation. For fluid tracers, phase space boundaries yield insights into barriers that prevent effective mixing of fluids.

Performing such an analysis could yield useful insights for strategies to improve microfluidic Lab on a chip devices for the purposes of mixing and separation of particles. These techniques could also be used to study models of biological fluid flows.

Chapter 6

Particle Dynamics in Micro-Bubble Streaming Flows

In this chapter, a singularity approximation of the micro-bubble streaming phenomenon in a microfluidic channel is constructed. The fluid flow problem is re-stated as a dynamical system and the stability of the singularity driven flow for inertial particle motion is studied. It is found that this approach to studying the micro-bubble streaming problem is able to re-affirm observations made through experiments and simulations in literature. Having validated this framework, we are able to use the insights gained to make suggestions of possible micro-bubble streaming configurations that can enhance the ability to manipulate micro-particles in such flows.

6.1 Singularity model of micro-bubble streaming flows

Microfluidic devices of the LCAT type discussed in section 4.2 involve bubbles that are closer to being hemispherical than round bubbles. This can be modeled by

placing singularities of stokes flow directly on the wall unlike in in section 4.6 where the singularities were placed at a finite distance above the the wall with images placed at the same distance from the wall on the other side. This would require a suitable modification to the solution shown in Fig. 4.5. While such a singularity model for hemispherical micro-bubble streaming has been presented in [23] where a somewhat more complex method based on the reflection method of Bhattacharya and Blawzdziewicz [85] is used, which enables both the no-slip and no-penetration boundary conditions to be satisfied simultaneously on both walls while improving in accuracy with each reflection, we use a much simpler numerical scheme.

While the classical result of Longuet-Higgins [63] took into account the leading order translational and volumetric modes of oscillation, the side wall trapped bubble oscillations involve higher modes as well [10, 11]. Their contribution to the steady flow can be represented using higher order multipoles of the stokeslet velocity with appropriately chosen strengths [23].

From the forms of (2.12) and (2.13), it can be seen that as the original singularities are moved from their position x_0 above the wall, towards the origin, the image singularity terms with co-efficients having explicit dependence on the height 'h' become smaller and smaller until they disappear at the origin. The original singularity and its identical image may either cancel each other out or get added up depending on the order of the singularity 'n'. A superposition of four surviving higher order singularity solutions [7], namely, a potential dipole, potential quadrupole, stokes quadrupole and a stokes octupole were found to provide a good qualitative agreement to experimental and theoretical flow fields set up by LCAT devices Fig. 6.1a.

$$u_{s_i} = F1_j G^{pd}_{ij} + F2_{jl} G^{pq}_{ijl} + F3_{jlm} G^{sq}_{ijlm} + F4_{jlmk} G^{so}_{ijlmk} \tag{6.1}$$

While this models the flow well, a realistic model of LCAT type flows should take into consideration the presence of the opposite wall. Introducing this parallel wall provides us with the opportunity to impose a parabolic carrier flow that can transport finite sized particle into and out of the microfluidic device in addition to capturing the confinement effects on the streaming flow itself. We do this in two stages, first, we cancel out the velocity normal to a plane U where the second wall is to be introduced, at distance H from the lower wall L to which the bubble is attached. This is done by placing an image of the full bubble flow at distance $2H$ as shown in Fig. 6.1b. This completely cancels out the velocity at the plane U and satisfies the no-penetration condition. However, the introduction of this image violates the no normal velocity and no-slip conditions on the wall L. This is remedied by placing a second set of images at distance $-2H$ from the wall L to cancel out the normal velocity contribution due to the first of images Fig. 6.1c. This procedure can be repeated several times which progressively improves the no-penetration boundary approximation at both walls L and U. As few as 8 reflections gives a qualitative match to analytic micro-bubble streaming flow Fig.6.1d.

6.1.1 Collocation scheme to impose no-slip boundary conditions on channel walls

With the presence of a parallel wall accounted for, we can now impose a parabolic carrier flow such as the plane Poiseuille flow. This has been shown in Fig. 6.2a. It is immediately noticed that there is a re-circulating vortex at the top wall upstream of the bubble. This is to be expected because of the presence of free slip at the channel walls as a result of the image-reflection procedure. To remedy this, we use a collocation scheme akin to the method discussed in section 2.4. We do

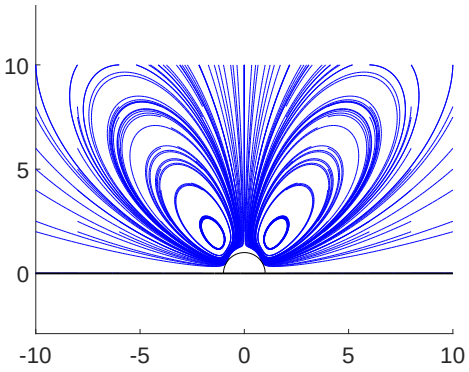

(a) Steady streaming from side wall trapped bubble.

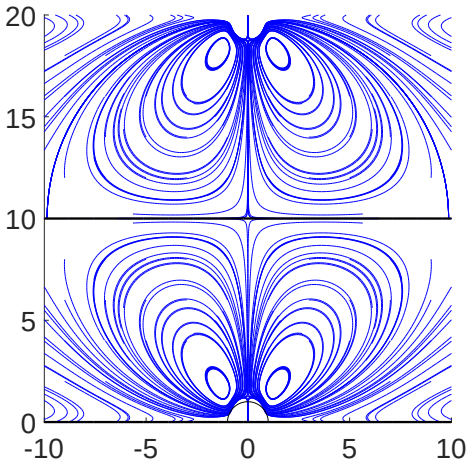

(b) First set of images placed at distance $2H$ from the wall L.

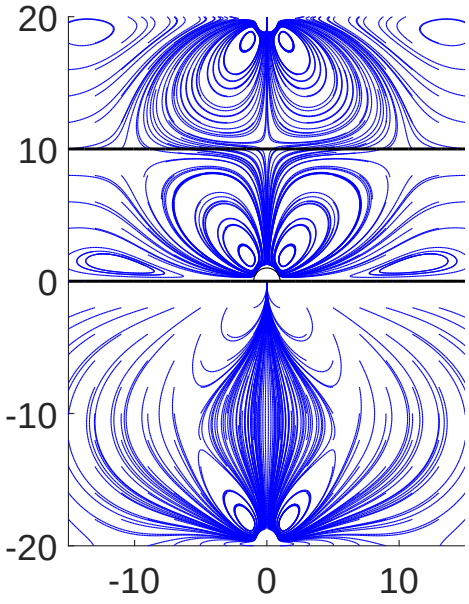

(c) Second set of images placed at distance $-2H$ from the wall L.

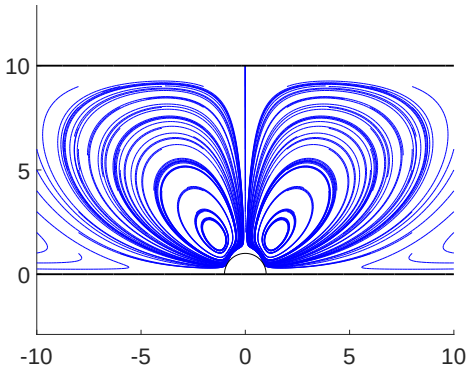

(d) Micro-bubble streaming in a parallel walled channel with no-penetration and free slip.

Figure 6.1: The method of reflections used to model the presence of a parallel wall.

this by placing a series of fundamental solutions of the stokes equation at a small offset from both channel walls outside the domain of the flow so as not to introduce singularities within the flow domain itself. The strengths of these singularities can be chosen numerically such that they cancel out the tangential velocity at several discrete points on the wall while not affecting the flow away from the wall. In other words, these singularities are exponentially decaying solutions that accurately cancel the tangential velocity along the walls in their vicinity. Doing this eliminates the re-circulation vortex and gives a flow with geometry similar to experimentally observed flow patterns in experiments Fig. 6.2b.

6.1.2 Unsteady flow

The velocity field of the flow being modeled can be thought of as the sum of a steady component u_s, the modeling of which has been discussed in the sections above, and an unsteady oscillatory component u_0 [74].

$$u(x, y) = u_0(x, y, t) + u_s(x, y). \tag{6.2}$$

At leading order, the bubble undergoes a volumetric expansion and dilation in a periodic manner. It was suggested in [74] that this mode of oscillation can be effectively captured by an oscillatory potential source monopole and that the leading order oscillatory flow sufficiently captures the unsteady dynamics of inertial particles in the vicinity of the bubble. However, noting the shape modes in experimental images in [74], we use the next higher order potential singularity [23]- the oscillatory

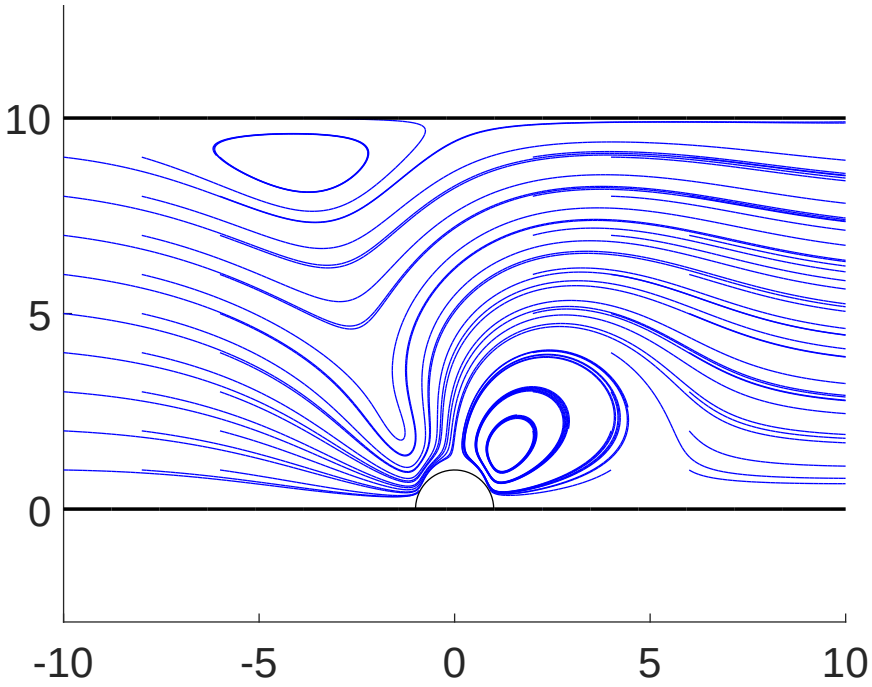

(a) Poiseuille flow imposed in a channel with micro-bubble streaming.

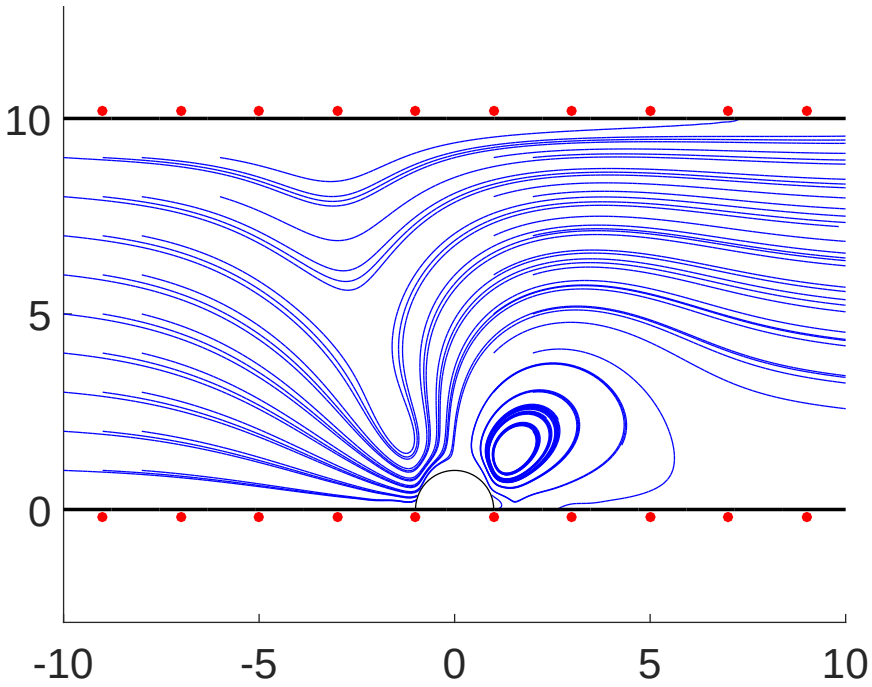

(b) Collocation scheme used to impose no-slip on channel walls.

Figure 6.2: Singularity model of micro-bubble streaming

quadrupole as well in our model.

$$u_{0_i} = -f_s \sin(\omega t+\phi)\big[\frac{\delta_{ij}}{r^2}-\frac{2x_ix_j}{r^4}\big]+f_q \sin(\omega t)\big[-2\frac{\delta_{ij}x_l+\delta_{jl}x_i+\delta_{li}x_j}{r^4}+8\frac{x_ix_jx_l}{r^6}\big] \quad (6.3)$$

6.2 Stability of micro-bubble streaming for inertial particle dynamics

Having studied the interesting properties of inertial particle motion using singularity models of ideal flows in the previous chapter, we turn out attention to the current problem as a natural step forward using more realistic flows where viscous effects are accounted for. To do this, we employ the Maxey Riley equation (4.13) with the lubrication force reviewed in section 4.5.

$$\begin{aligned}\rho_p\frac{d\mathbf{v}}{dt} = \rho_f\frac{D\mathbf{u}}{Dt} + (\rho_p-\rho_f)g - \frac{9\nu\rho_f}{2a_p^2}(\mathbf{v}-\mathbf{u}-\frac{a_p^2\nabla^2\mathbf{u}}{6}) - \frac{\rho_f}{2}(\frac{d\mathbf{v}}{dt}-\frac{D}{Dt}[\mathbf{u}+\frac{\mathbf{a_p}^2}{10}\nabla^2\mathbf{u}])\\ - \frac{9\rho_f}{2a_p}\sqrt{\frac{\nu}{\pi}}\int_0^t \frac{1}{\sqrt{t-\tau}}\frac{d}{d\tau}(\mathbf{v}-\mathbf{u}-\frac{a_p^2\nabla^2\mathbf{u}}{6})\partial\tau - 6\pi\rho\mu a_p^2 e_r\frac{v\cdot e_r - U_b}{4h}. \quad (6.4)\end{aligned}$$

Simplifying this equation using a procedure analogous to the procedure adopted in section 4.4, we arrive at the simplified Maxey Riley equation with a non-dimensional version of the lubrication force F_{lub},

$$\frac{dv}{dt} = \frac{\partial u}{\partial t} + u\cdot\nabla u - \frac{2}{3}St^{-1}(v-u) - \frac{2}{3}St^{-1}a_p\frac{(v\cdot e_r - U_b)}{4h} \quad (6.5)$$
$$\text{where, } St = \frac{2a_p^2U}{9\nu L}.$$

It is important to mention at this juncture that the simplified Maxey Riley equation (4.15) is such that, any relative velocity $w = v - u$ that the inertial particle may possess with respect to the fluid, once lost can not be re-introduced spontaneously without a discontinuous forcing. However, the lubrication force is one such force that provides an external disturbance which periodically perturbs the relative velocity, which in turn would grow larger within unstable subsets H_u of the flow domain. In addition, it is only natural to expect any experiments to possess background noise that could act as perturbations that cause inertial particle to exhibit size based deviation away from the streamlines of flow. Hence, it is a surprising to note that prior experiments [12, 13, 14] and simulation studies [76] find that inertial particles exhibit sized based different behavior only upon approaching very close to the surface of the oscillating bubble. To probe this surprising stability, we study the eigen values of the quantity $-(J+\mu I)$ in the simplified governing equation (6.4). This study allows us to classify the stable and unstable sub-domains of the flow domain. The results of this study is plotted in Figs. 6.3a-6.3d over a range of stokes numbers. These calculations clearly indicate that the micro-bubble streaming flow under study does not contain any significant unstable subsets even for very large sizes of particles. This explains the observed robustness in inertial particle's adherence to the underlying fluid flow. Significantly, even the region of flow adjacent to the oscillating micro-bubble is found to be stable in the associated relative velocity$(w_x - w_y)$ space and the only size based separation is due to the much larger perturbation in the form of lubrication force near the bubble boundary Fig. 6.4. This relatively larger disturbance due to the lubrication effects is also particle size dependent as seen in the simplified governing equations (6.5) causing differential deflection Fig. 6.5a and eventually sized based separation Fig. 6.5b.

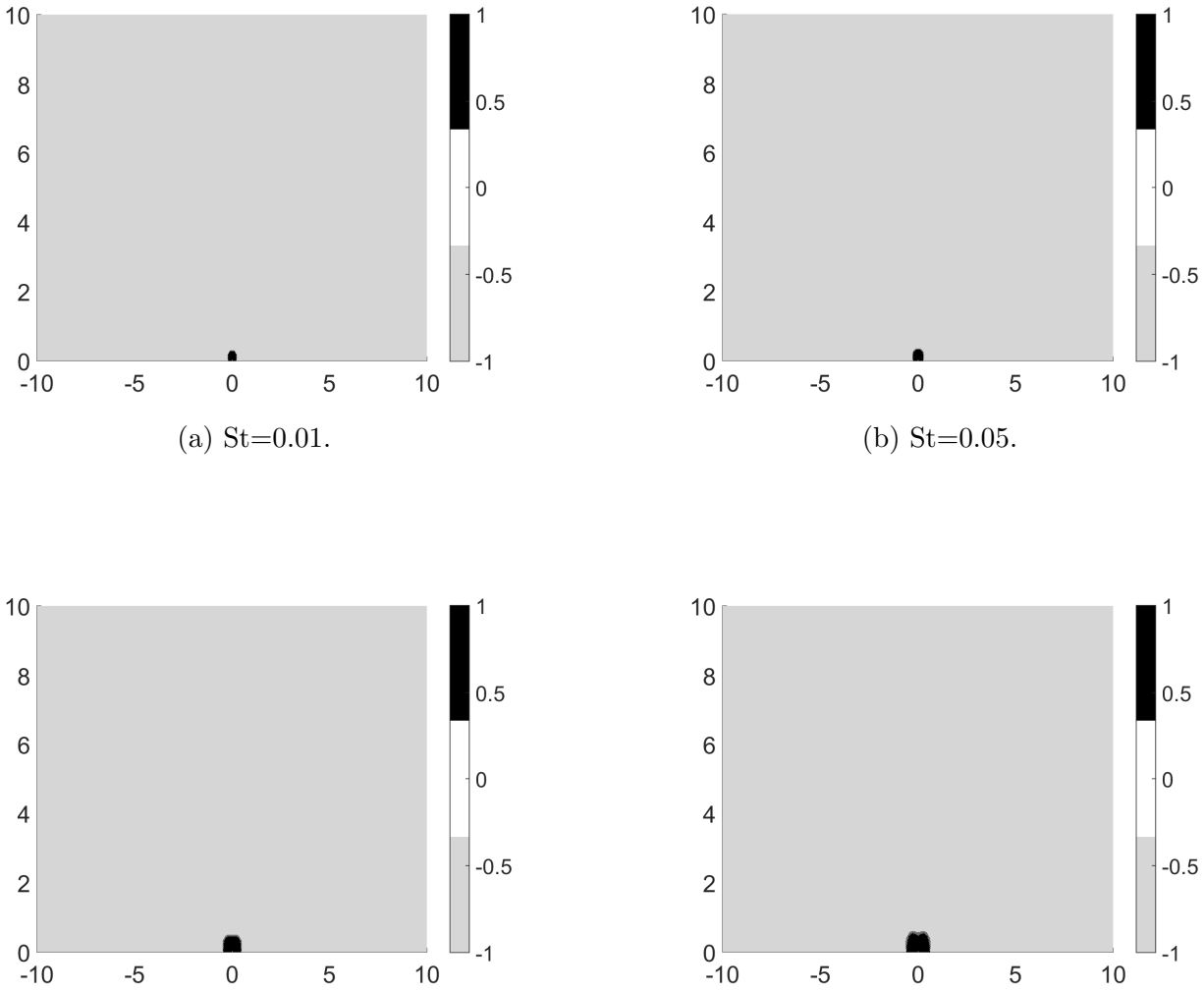

(a) St=0.01.

(b) St=0.05.

(c) St=0.1.

(d) St=1.

Figure 6.3: Binary plots showing the stable(gray) and unstable(black) subsets of the flow domain.

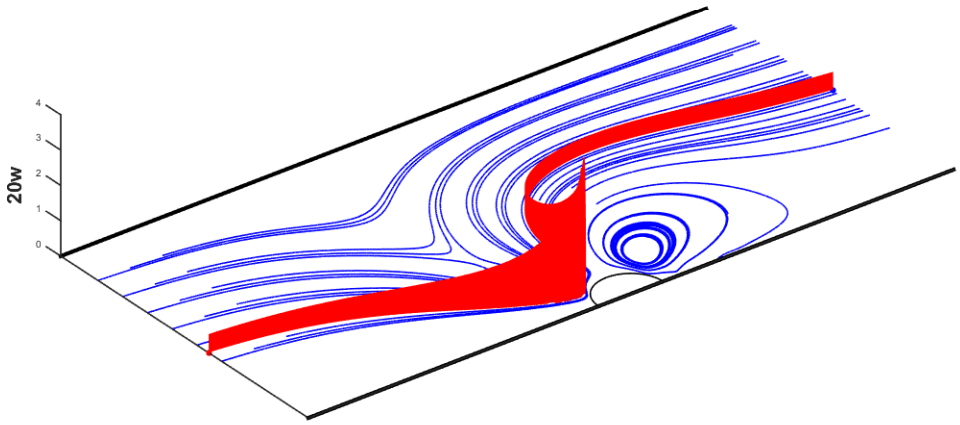

Figure 6.4: Magnitude of relative velocity $|w|$ along the trajectory of a $10\mu m$ inertial particle exaggerated to show the spatial variation.

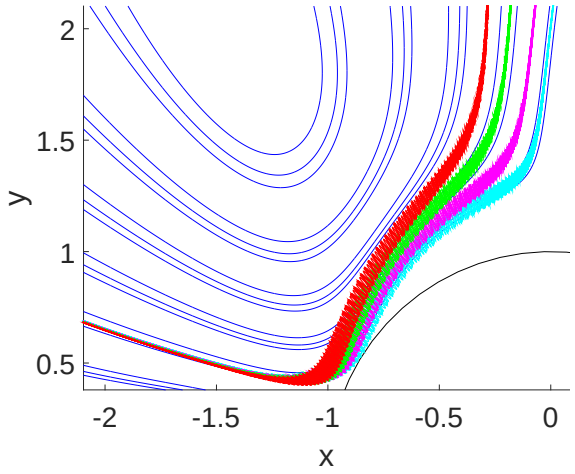

(a) Size based deflection near bubble.

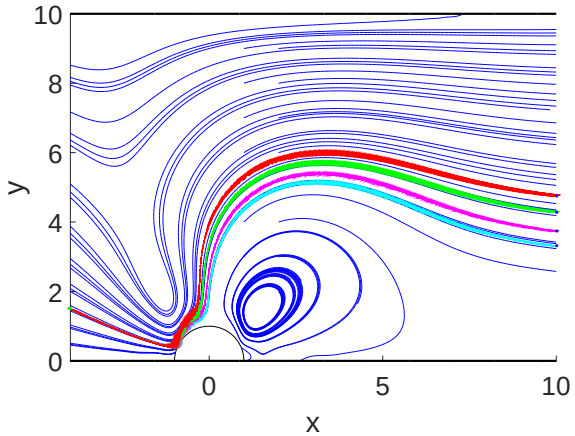

(b) Size based separation away from bubble

Figure 6.5: Sizes $10\mu m$(red),$7.5\mu m$(green),$5\mu m$(magenta) and $2.5\mu m$(cyan)

6.3 Dynamical boundaries in micro-bubble streaming flows

Having seen that the inertial particles even a small distance away from the bubble interface do not retain any relative velocity imparted to them and align with the streamlines of flow exponentially fast, we are now able to accurately consider the separatrices in the two dimensional configuration space (x-y plane) as separatrices for the trajectories of inertial particles as well. More over, noting that steady streaming flow is obtained as an average of the unsteady oscillatory flow, the finite time lyapunov exponent calculation can be performed on fluid tracers advected by the steady streaming flow. The motion of fluid tracers can thus be written as the dynamical system,

$$\begin{aligned} \dot{x} &= u_{s_x} \\ \dot{y} &= u_{s_y}. \end{aligned} \tag{6.6}$$

Identifying Lagrangian coherent structures in this flow helps us identify separatrices in the flow, but more importantly determining the location of repelling LCS allows us to determine regions of the flow that particles which start off close together initially, repelled away in finite time. Conversely, particles which start off far apart initially, approach each other and stay close to each other near attracting LCS. To identify such attracting LCS, we can study the system (6.6) in backward time.

$$\dot{x} = -u_{s_x} \tag{6.7}$$

$$\dot{y} = -u_{s_y}.$$

Such a computation is performed for the one bubble flow configuration being used so far and is shown in Fig.6.6a for forward time FTLE and Fig.6.7a for backward time FTLE.

The fluid LCS can thus tell us something about the geometric structure of the flow and about the fate of particle trajectories in the flow domain. This is more or less equally true for finite sized particles as well as tracers because of the robust stability of the flow domain to any perturbations in inertial particle velocity. However, the one consequence of sized dependent deflection in the vicinity of the micro-bubble is that heavier particles settle down on streamlines further away from the bubble. Naturally, the inertial particles lose the relative velocity quickly, but not before settling down onto a streamline which is closer to the upper attracting LCS in Fig. 6.7a. Thus, the attracting LCS in the top half of the domain has stability properties that are a function of particle size with the larger particles attracted towards it more than lighter particles. To further see this, a large number of finite sized particles are allowed to enter the flow domain from the left, and we see that the largest particles exhibit a larger tendency to cluster close to the upper attracting LCS in Fig.6.8a-Fig.6.8d.

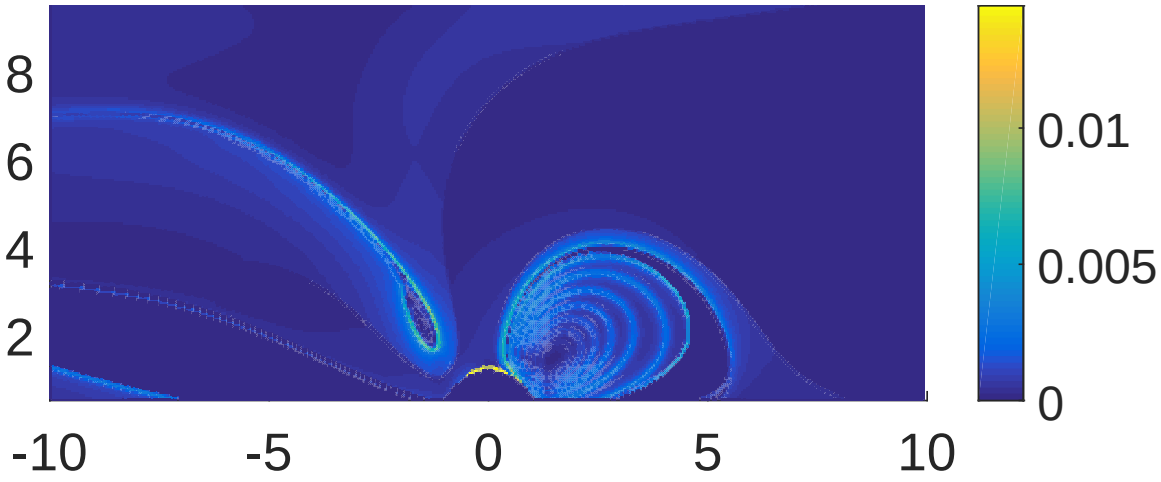

(a) Forward time FTLE of the one bubble steady streaming flow.

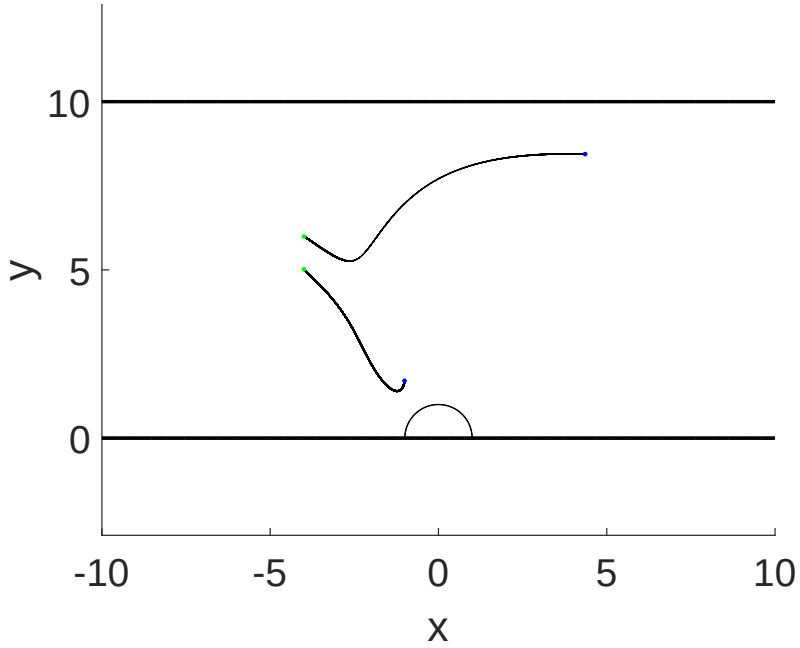

(b) Particles starting on either side of repelling LCS get repelled over finite times.

Figure 6.6: Repelling Lagrangian Coherent Structures in one bubble configuration.

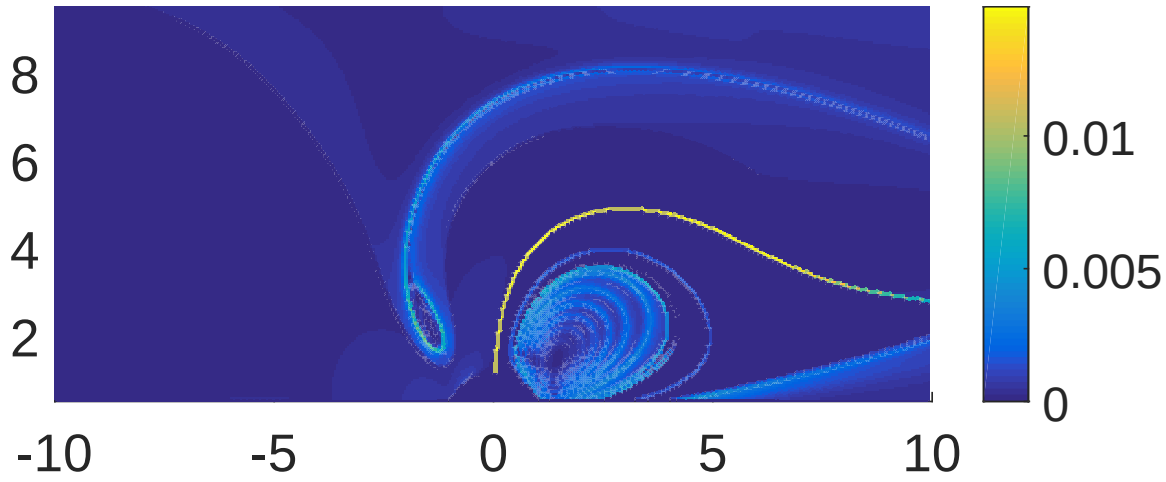

(a) Backward time FTLE of the one bubble steady streaming flow.

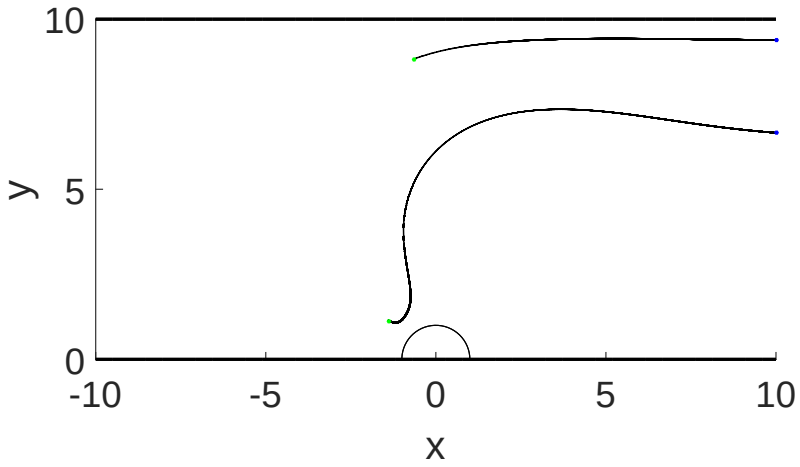

(b) Particles starting far apart on either side of attracting LCS get close to each other over a finite time interval.

Figure 6.7: Attracting Lagrangian Coherent Structures in one bubble configuration.

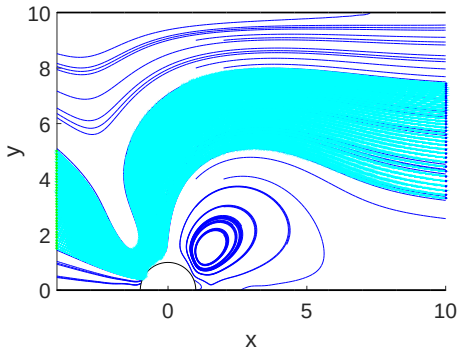

(a) 2.5μm particles behave very similar to tracer particles.

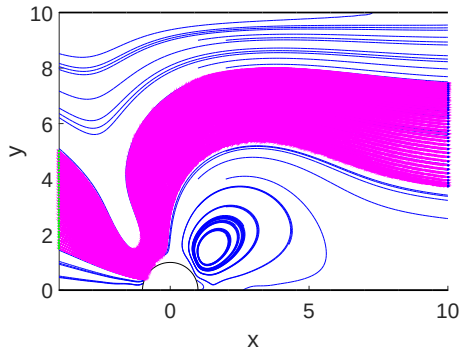

(b) 5μm particles have a large spread about the attracting LCS.

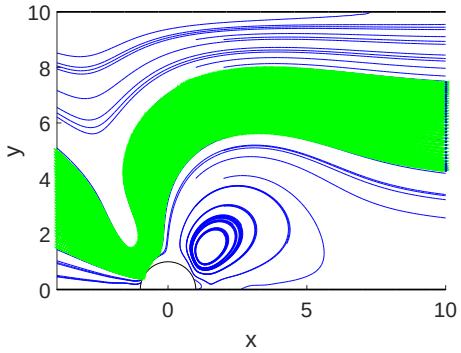

(c) 7.5μm particles begin to focus near the attracting LCS.

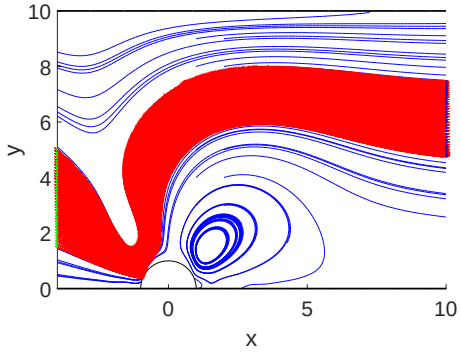

(d) Focused band of 10μm particles.

Figure 6.8: Inertial particle attraction towards attracting fluid LCS.

6.4 Inertial particle manipulation

From the previous section of this chapter and Fig. 6.8, we understand two things about the mechanism which leads to particle separation in micro-bubble particle separators:(1) Repelling LCS in the flow force particles in a portion of the incoming fluid towards the micro-bubble where size dependent deflection takes place (2) Particles of different sizes then get attracted towards the attracting LCS with the larger

particles being attracted more.

Any design of such a micro-bubble separator should hence be designed to effectively use the two mechanisms described above, or in other words, the ideal micro-bubble separator should have repelling LCS that channels a large portion of the incoming particle laden flow towards the bubble and the attracting LCS should be such that it directs the separated particle to a region where further separation could be performed.

One intuitive flow configuration would be one with oscillating micro-bubbles on both sides of the wall with each bubble being offset from the other by a finite distance Fig. 6.9a. This case has been experimentally studied in several cases [13, 67]. The associated backward time FTLE is shown in Fig. 6.9b where it is seen that the attracting LCS emanating from the first bubble near the inlet guides particles towards the second bubble on the opposite wall. The separated particles then get attracted towards the attracting LCS emanating out of the second bubble. Many such configurations of alternating bubbles have been used previously to achieve focused particle bands [13]. This configuration can also be used to achieve enhanced particle separation Fig. 6.9c.

If the horizontal distance by which the bubbles on opposite walls are offset is reduced Fig. 6.10a, the particle focusing is enhanced Fig.6.10b. While this configuration is qualitatively similar to the configuration in Fig.6.9a, the corresponding backward time FTLE Fig. 6.10c shows us that the attracting LCS now create a bottleneck for the flow of inertial particle near the second bubble from the left. This creates a squeezing effect on inertial particles forcing them ever closer to the micro-bubble.

Motivated by this insight, we can choose a configuration of micro-bubbles that

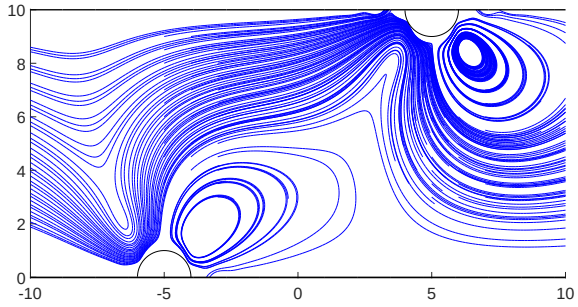

(a) Two bubble flow with bubbles on opposing walls and a large horizontal offset.

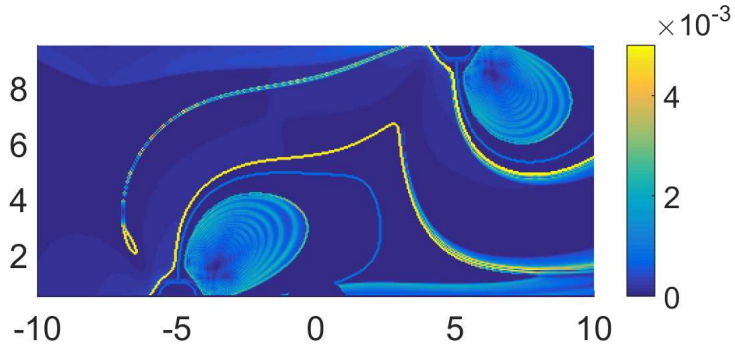

(b) Backward time FTLE and LCS.

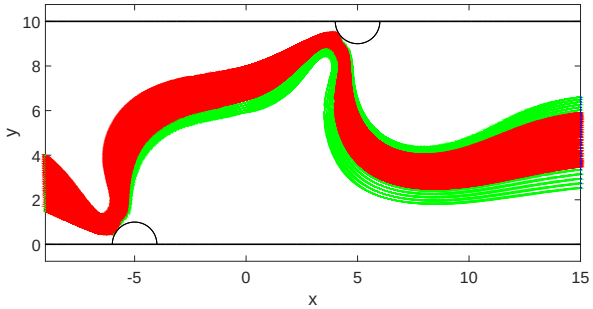

(c) Separation of $5\mu m$ (green)and $10\mu m$ particles.

Figure 6.9: Two bubble flow-Configuration 1

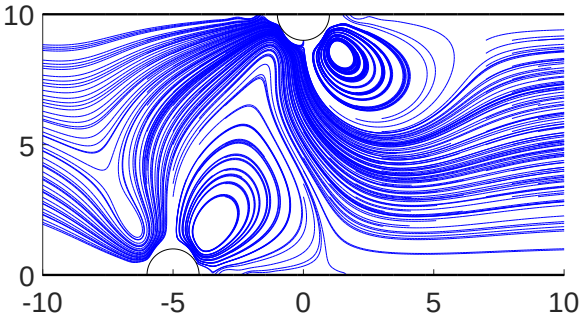

(a) Two bubble flow with bubbles on opposing walls and a small horizontal offset.

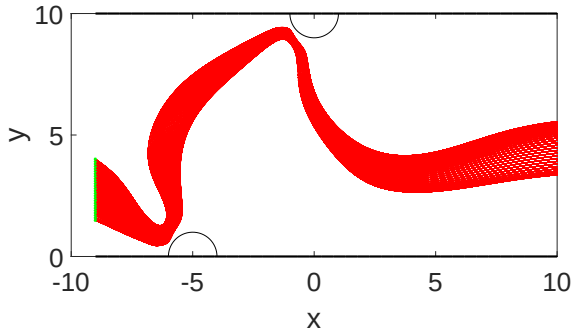

(b) Focused band of $10\mu m$ particles.

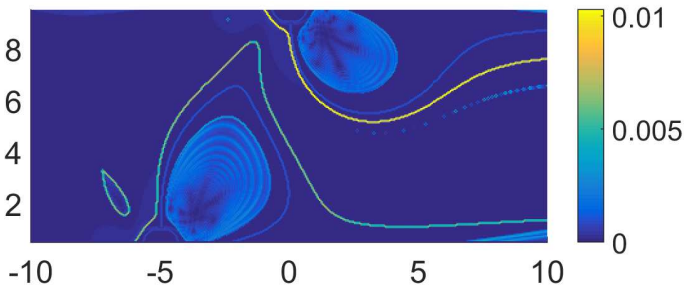

(c) Backward time FTLE and LCS.

Figure 6.10: Two bubble flow-Configuration 2

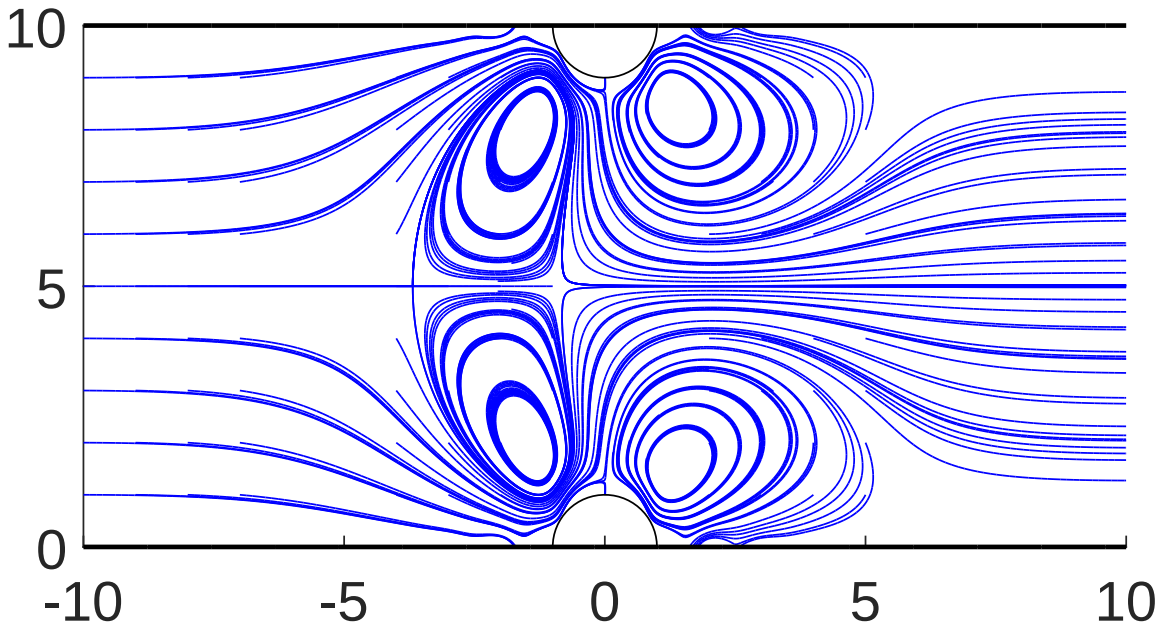

Figure 6.11: Two bubble flow with bubble on opposing walls.

are directly opposite to each other on opposing walls Fig. 6.11. This configuration simultaneously achieves high inertial particle deflection near the micro-bubble and the consequent enhanced focusing near the attracting LCS of the flow Fig.6.12b. As seen for the configuration in Fig. 6.9c, improved size dependent focusing can be harnessed for particle separation as well. This has been demonstrated for the separation of a $5\mu m$ and $10\mu m$ mixture in Fig. 6.13a and the separation of a $2.5\mu m$ and $7.5\mu m$ mixture in Fig. 6.13b.

6.5 Comparison of modeling results to experimental results

The study of inertial particle manipulation using singularity methods and phase space transport yields insights into previously observed experimental results.

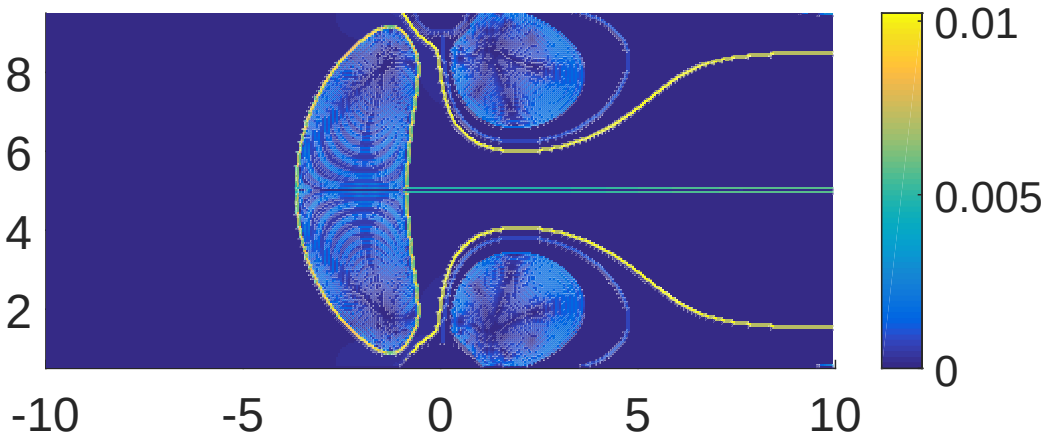

(a) Backward time FTLE and LCS.

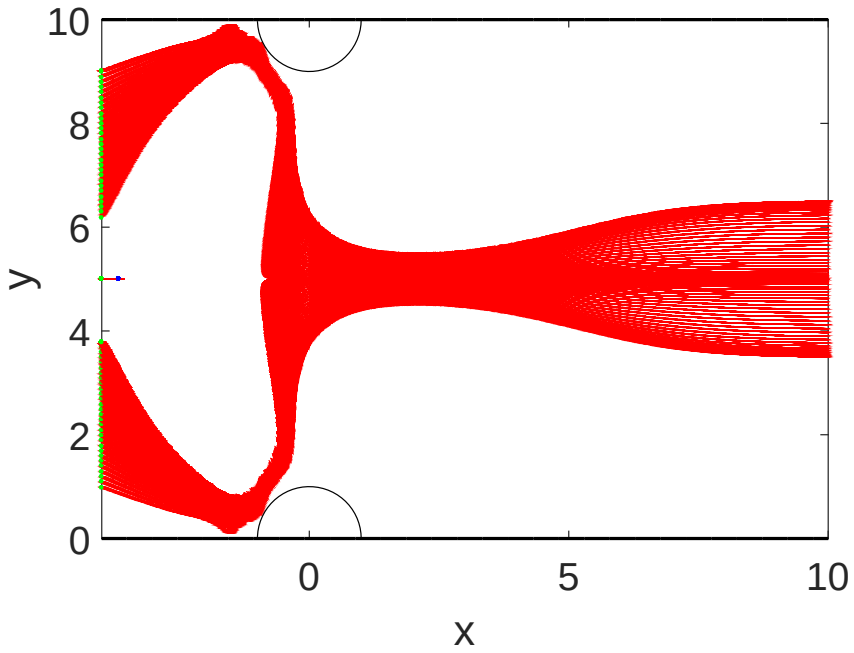

(b) Focused band of $10\mu m$ particles.

Figure 6.12: LCS determines particle focusing behavior

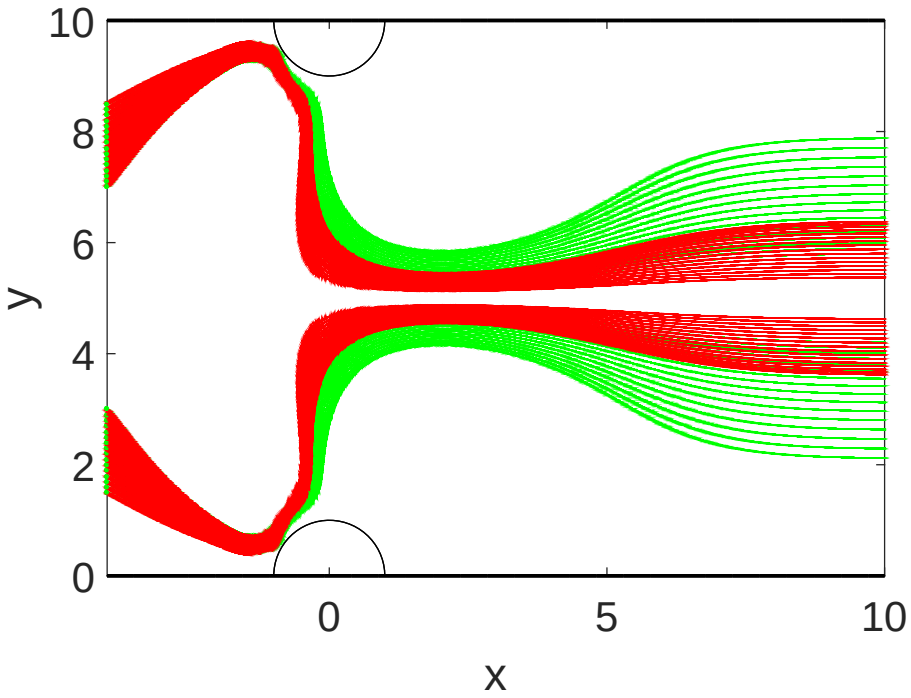

(a) Separation of $5\mu m$(green) and $10\mu m$ (red)particles.

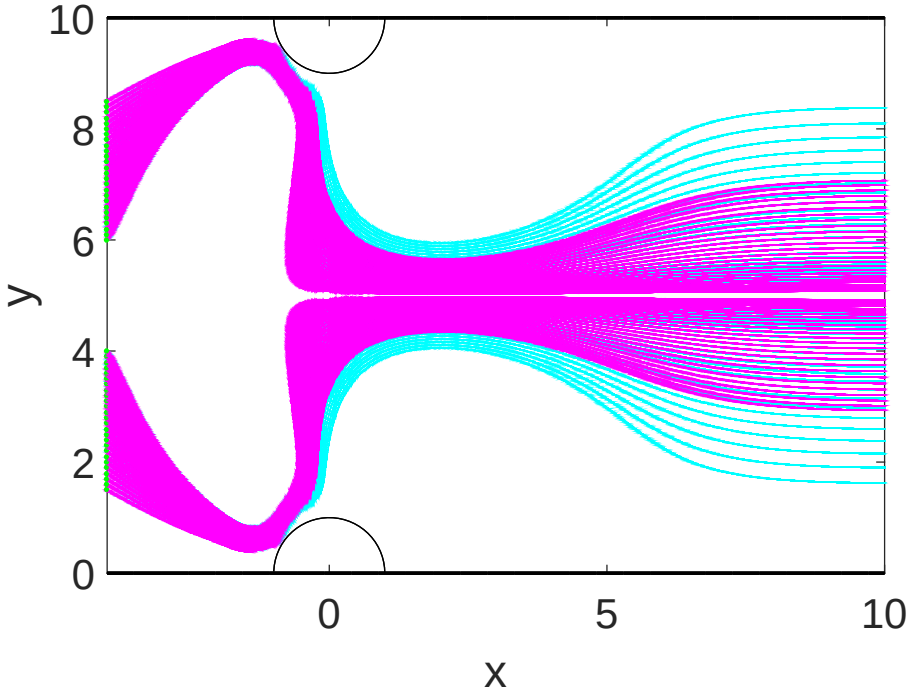

(b) Separation of $2.5\mu m$(cyan) and $7.5\mu m$ (magenta)particles.

Figure 6.13: Focusing behavior harnessed for particle separation

The different amplitudes of deflection experienced by inertial particles near the oscillating bubble surface due to the presence of a lubrication layer has been identified as the reason for sized based particle separation in micro bubble streaming flows [74]. This is in agreement with our computation which shows that the relative velocity subspace of the phase space for inertial particle dynamics does not possess any unstable subsets for particles of realistic sizes. This implies that the LCS identified for the fluid flows also perform the role of transport barriers for the motion of inertial particles when not in the immediate vicinity of the bubble. This agrees with the experimental results on particle focusing using micro bubble streaming flows in [13] where the bottle neck to particle transport caused by the presence of the LCS forces particle trajectories close together. The singularity modeling is able to capture size based particle separation over a particle size difference of about $5\mu m$, however experimental results report the ability to obtain much finer separation accuracy with particles of size differences of up to $2.5\mu m$ being separated [12, 14]. One reason for this could be that the experimental setups in these experiments typically consist of a channel perpendicular to the parallel walled channel containing the oscillating micro bubble. The fluid flow through this channel could modify the flow causing an enhancement in particle separation size ranges.

Chapter 7

Chaotic Transport of Tracer Particles by Micro-rotors

7.1 Review of microfluidic mixing

Mixing of fluids is an essential step in a wide variety of processes in nature and engineering. While the task of fluid mixing is often aided by the presence of turbulence, this may not always be the case and one might encounter flows which are characterized not by the strongly advective nature of turbulent flows and instead are dominated by viscous diffusion. Such low Reynolds number flows where viscous effects dominate over inertial effects are especially prominent at micro scales. With the rise of microfluidic technology for applications ranging from diagnostics and sample preparation to cooling of micro-electronics [86, 87], the problem of mixing small samples of fluid efficiently is gaining importance [88, 89].

Several means for achieving rapid micro-mixing has been proposed over the years. These include active techniques involving the use of external forces of acoustic [90], magnetic [91], electric [92] and other origins to directly influence the flow and

induce large scale advective motion in the flow. Such methods often employ an intermediate mixing element (such as acoustically excited micro-bubbles [93])that serves to focus the externally applied forces. Such techniques can achieve rapid and high quality mixing, especially in the vicinity of the mixing elements. Passive methods of microfluidic mixing on the other hand involve altering the geometry of the flow itself in such a manner as to increase the surface area of contact between portions of the fluid which in turn enhances mixing by viscous diffusion. This can be done by designing innovative channel geometries [94], by incorporating obstacles in the path of the fluid flow [95] and so on. Passive methods have the advantage of not requiring the use of external forces and the mixing is not localized near mixing elements and other sources of the external force. However, they are constrained by a pre-determined channel design and the quality of mixing is directly dependent on the duration the fluid spends within the specially designed geometry thus necessitating longer channels. Microfluidic mixing techniques that can combine rapid mixing characteristic of active techniques along with uniform mixing and uncomplicated methods characteristic of passive methods are needed. One way that has been proposed, is the use of artificial micro-swimmers inspired by naturally occurring micro-organisms which are known to stir up the fluid around them during locomotion [96, 97]. While several different swimmer morphologies have been proposed for the purpose[98, 99], one of the simplest design could be that of a single spinning sphere.

Rotating magnetic discs have been experimentally shown to induce mixing of fluids around them [100]. Ballard etal[101] demonstrated using experiments and Lattice Boltzmann simulations, micro-mixing using magnetic beads. Recently, the flow due to such spinning micro-particles were modeled as a rotlet [102, 103]. The rotlet is a derivative of the fundamental solution to the stokes equation [7].

7.1.1 Chaotic advection in fluid flows

While viscous diffusion can mix fluids, it is a short range phenomenon which occurs primarily at the interface between layers of a fluid/fluids that we need to be mixed [16]. Advective effects in fluid flows cause the fluid to be stretched and folded into thin filaments which reduces coherent blobs or structures that are encountered in unmixed fluids to finer structures which causes the surface area of contact between unmixed regions of the fluid to increase very fast, thus enabling viscous diffusion to homogenize the fluid [104]. However, in the absence of strong advective forces, stretching and folding and the creation of fine scaled structures of the fluid has to be induced artificially. Aref, in his classic 1984 work [15] demonstrated that fluid tracer dynamics when written down as a passive advection system of the form,

$$\begin{aligned} \dot{x} &= u(x, y, t) \\ \dot{y} &= v(x, y, t) \end{aligned} \tag{7.1}$$

where u and v are components of the velocity field in the x and y directions, can be seen to exhibit chaotic behavior characterized by stretching and folding of tracer trajectories even in the simple case of two dimensional laminar flows with periodic time dependence. A consequence of this finding is the realization that tracer trajectories in three dimensional autonomous or two dimensional time periodic laminar flows can also be mixing under certain conditions [24]. This phenomenon has since come to be known as *Chaotic advection* [105].

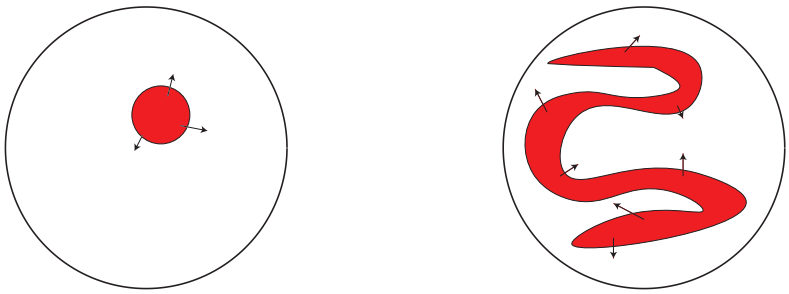

Figure 7.1: Flow has to be stretched and folded into filaments to accelerate viscous diffusion.

7.2 Micro-rotor dynamics and confinement

It was suggested in [106] that the rotlet could effectively model the dynamics of a viscous micro-rotor and small assemblies of rotlets could exhibit qualitatively different behavior depending on their initial positions, their rotation direction and strength relative to each other. Recalling from chapter 2, the expression for velocity due to a single rotlet singularity at position x_0, confined to the horizontal (x-y) plane with it's axis pointing in the direction perpendicular to the plane(z axis-direction) is,

$$u(\mathbf{x}) = \gamma \hat{k} \times \frac{\mathbf{x} - \mathbf{x_0}}{||\mathbf{x} - \mathbf{x_0}||^2}. \tag{7.2}$$

While such an isolated rotlet in an un-bounded domain would simply spin about its own axis and have no net translation, this scenario would change if there is either a boundary in the vicinity or if there are one or more rotlets in its vicinity. In the case of multiple interacting rotlets each of the rotlets get advected by its neighbors and the resulting motion of each rotlet with co-ordinates (x_i, y_i) can then be expressed as,

$$\frac{dx_i}{dt} = \sum_{j=1, j\neq i}^{j=N} \gamma_j \frac{(y_i - y_j)}{R_{ij}^2} \tag{7.3}$$
$$\frac{dy_i}{dt} = \sum_{j=1, j\neq i}^{j=N} -\gamma_j \frac{(x_i - x_j)}{R_{ij}^2}$$

where, the square of distance between the i-th and j-th rotlet is given by $R_{ij}^2 = (x_i - x_j)^2 + (y_i - y_j)^2$. It was shown in [106] that the rotlet motion for the case of two like signed rotlets and three like signed rotlets on the vertices of an equilateral triangle in an infinite domain is as shown in Fig. 7.2.

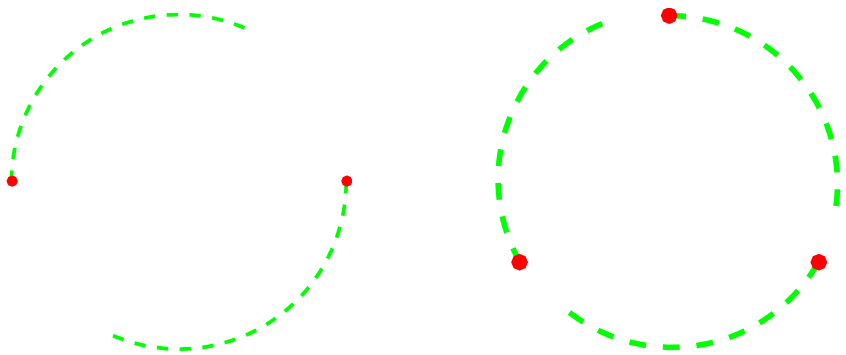

Figure 7.2: Two and three rotlet trajectories in an un-bounded domain

Meleshko and Aref [28] suggested that the "blinking" rotlets under circular confinement will make a good test bed for chaotic mixing studies. Thus, the study of chaotic mixing using free moving rotlets is a natural extension of this idea from time periodic to arbitrary time dependence, while being associated with the important engineering application of micro-mixing using artificial micro-swimmers. The equation (2.15) for a rotlet inside a no-slip circular boundary can be re-written in compact notation as,

$$\psi = \frac{\gamma}{2}\Big[log\frac{A}{B} + \frac{C}{B}\Big] \text{ with, } A = r^2 - 2bx + b^2$$
$$B = a^2 - 2bx + (\frac{b^2r^2}{a^2})$$
$$C = (1 - \frac{r^2}{a^2})(a^2 - \frac{b^2r^2}{a^2}).$$

For multiple rotlets confined inside a circular boundary, the velocity of each i-th rotlet due to the other j=1..(N-1) rotlets in its vicinity, is given by:

$$\frac{dx_i}{dt} = \sum_{j=1,j\neq i}^{j=N} \frac{\gamma_j}{2}[\frac{(\frac{B}{A})(BA_y - AB_y)}{B^2} + \frac{BC_y - CB_y}{B^2}]$$
$$+\frac{\gamma_i}{2}[\frac{(-B_y)}{B} + \frac{BC_y - CB_y}{B^2}] \quad (7.4)$$
$$\frac{dy_i}{dt} = \sum_{j=1,j\neq i}^{j=N} -\frac{\gamma_j}{2}[\frac{(\frac{B}{A})(BA_x - AB_x)}{B^2} + \frac{BC_x - CB_x}{B^2}]$$
$$-\frac{\gamma_i}{2}[\frac{(-B_x)}{B} + \frac{BC_x - CB_x}{B^2}] \quad (7.5)$$

where, the subscript "i" has been dropped on A,B and C. A_x, A_y, B_x, B_y, C_x, C_y etc represent the derivatives of terms A,B and C with respect to spatial variables x and y respectively. Here, the velocity due to the j-th rotlet is computed in a rotated frame of reference such that $\theta_j = 0$ in the rotated coordinates and the computed velocity is then rotated back to the original frame of reference.

The first thing that becomes apparent is, unlike in an un-bounded domain, a single rotlet can now have a net translation in addition to a rotation about its own axis as seen in Fig. 7.3a. While for the un-bounded case the distance between two rotlets R_{ij} is fixed for all time as seen from the simple calculation,

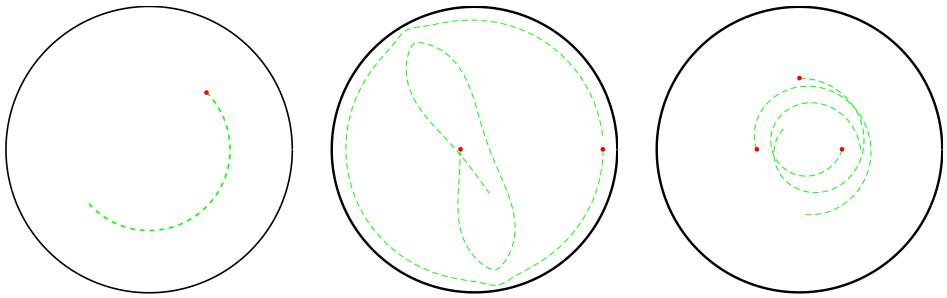

(a) (b) (c)

Figure 7.3: N- rotlet configurations in a circular-bounded domain of unit radius

$$
\begin{aligned}
\frac{dR_{12}^2}{dt} &= \frac{d}{dt}\big((x_1-x_2)^2+(y_1-y_2)^2\big) \\
&= 2(x_1-x_2)(\dot{x_1}-\dot{x_2})+2(y_1-y_2)(\dot{y_1}-\dot{y_2}),\ \text{using (7.3)}, \\
&= \frac{2}{R_{12}^2}(x_1-x_2)\big(\gamma_2(y_1-y_2)-\gamma_1(y_2-y_1)\big) \\
&+ \frac{2}{R_{12}^2}(y_1-y_2)\big(\gamma_2(x_1-x_2)-\gamma_1(x_2-x_1)\big) \\
&= \frac{2}{R_{12}^2}(\gamma_1+\gamma_2)(x_1-x_2)(y_1-y_2) \\
&+ \frac{2}{R_{12}^2}(\gamma_1+\gamma_2)(x_1-x_2)(y_1-y_2) \\
&= 0 \quad (7.6)
\end{aligned}
$$

this need not be the case in a bounded domain as seen in Figs. 7.3b,7.3c.

7.3 Regular and chaotic dynamics of micro-rotors

The simplest case that could be harnessed for the purpose of fluid mixing is that of a single micro-rotor translating and rotating inside the circular domain. However, such a single, bounded rotlet executes circular stirring motion that does not produce significant mixing as seen in Fig. 7.4 where several rotlets started off at different radii from the center

of the domain execute circular trajectories around the center with their distance from the center being invariant. While this by itself does not imply poor mixing, simple dynamics of the rotors are likely to give significant unmixed regions. So, the next simplest case that can be tried is the case of two rotlets inside a circular domain.

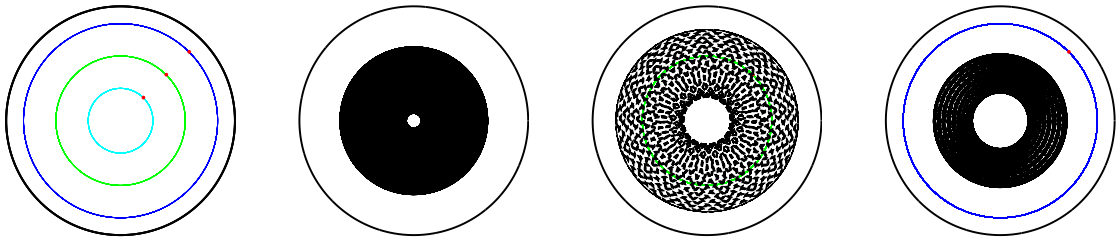

Figure 7.4: (Left most)The trajectories of three rotlets started at different distances $r = 0.2$(cyan),$r = 0.4$(green) and $r = 0.6$(blue) from the center of the domain.(Figures 2-4) Trajectories of a fluid tracer gives rise to significant unmixed regions when stirred using each of the three rotlet configurations.

The two rotlet configuration can exhibit complex dynamics owing to the fact that the boundaries can influence their otherwise regular motion asymmetrically. To probe the boundary effects on their dynamics systematically, we identify the origin as a special point which is farthest from the boundaries where one rotlet is placed, while the second rotlet is moved away from the origin systematically to understand how the boundary effects play a role in determining the dynamics of the two rotlet system.

The various rotlet configurations that have been tried out this way are shown in the first column of Fig. 7.5. Unlike the periodic un-bounded case, the rotlet dynamics are almost periodic with an almost period T. The almost periodic behavior has been captured in set of plots in Fig. 7.5. The first column shows the initial positions of the rotlets, rotlet trajectories after time T are shown in column two, the third column shows the trajectories after time $2T$ while the long time behavior after several almost time periods NT are shown in the final column. Upon reaching the extreme case of one rotlet at the origin and the other very close to the boundary in Fig. 7.5m, we also try out initial configurations where the rotlet at the origin is now moved towards the other end of the domain as seen in Figs. 7.5q-7.5x.

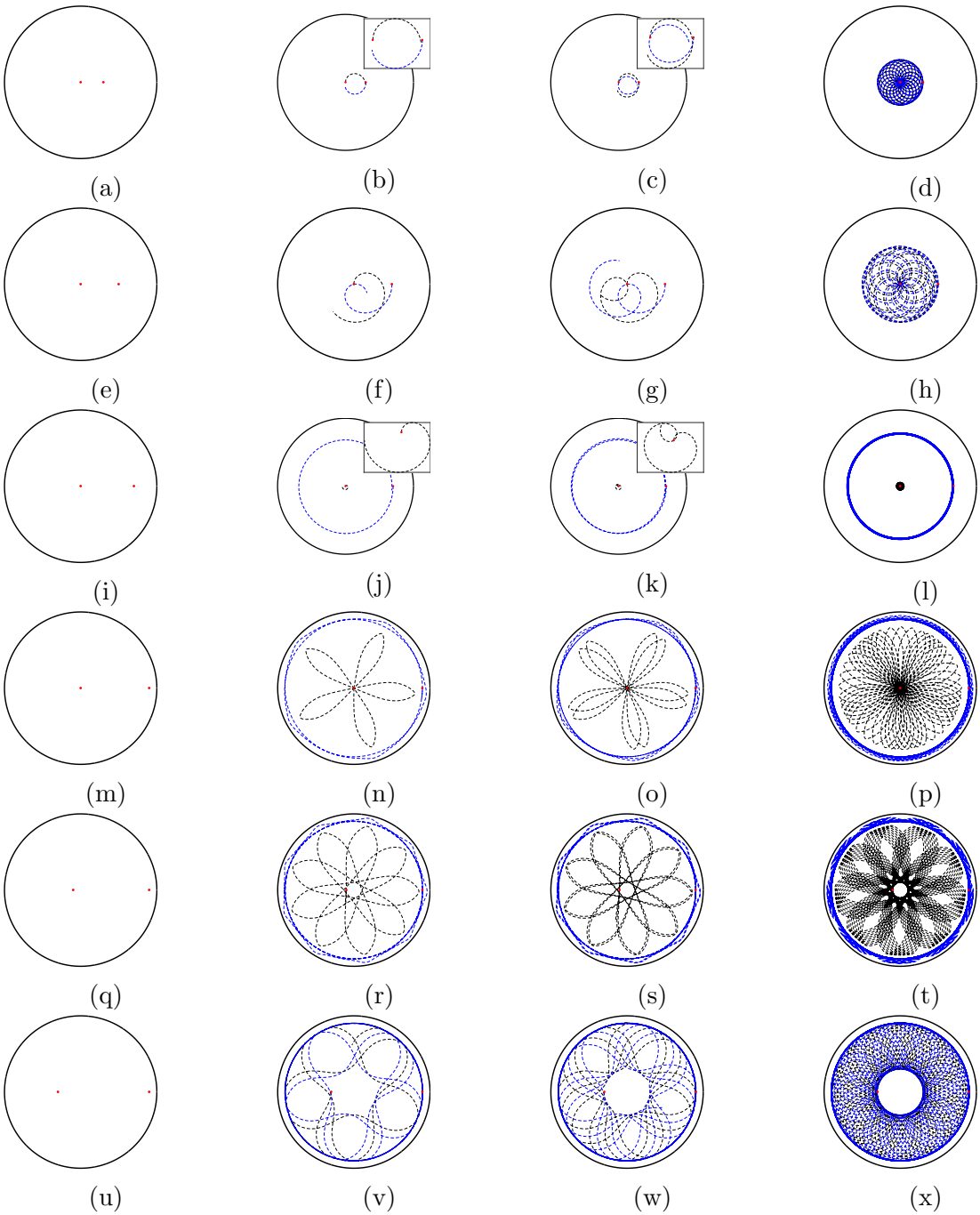

Figure 7.5: Dynamics of the bounded 2 rotlet configuration

Examining the long time trajectories of the 2-rotlet system reveals the existence of two distinct modes of motion. The first mode of motion is seen in configurations on rows 1,2 and 7, where each rotlet exhibits trajectories which are a mirror image of the other and result in a dense overlapping set of trajectories after a long time. The second mode of dynamics is seen in configurations on rows 3,4 and 5, where each rotlet exhibits dynamics which are qualitatively different from that of the other and they end up filling up distinct portions of the domain. It is clear from this numerical experiment that the mode of dynamics exhibited by the two rotlet system depends on the distance of each of the rotlets from the boundary relative to that of the other rotlet. Initial configurations where one rotlet is far from the boundary while the other is heavily influenced by the boundary results in mode 2 dynamics while both rotlets starting close to or away from the boundaries results in mode 1 dynamics.

This observation can be seen to be true even for the case of rotlets not starting collinear with the origin as seen in Fig. 7.6.

7.4 Chaotic advection of tracers: Numerical experiments

The passive advection of fluid tracers in the N rotlet system can be modeled as the $(2N+2)$ dimensional dynamical system,

$$\frac{dx}{dt} = u_x; \;\; \frac{dy}{dt} = u_y \tag{7.7}$$

where u_x, u_y are the components of the velocity at the point, induced by all the micro-rotors that exist in the domain and is obtained using (7.4) and (7.5) with $\sum_{j=1, j\neq i}^{j=N}$

replaced by $\sum_{j=1}^{j=N}$. Hence, for the two rotlet system, we have the 6 dimensional system,

$$\dot{X} = f(x, y, x_1, y_1, x_2, y_2), \;\; X = x, y. \tag{7.8}$$

Despite the configuration space of the dynamics being the Euclidean plane and the orderly nature of streamlines in laminar flows, the higher dimensionality of the dynamical system governing tracer transport enables chaotic advection of fluid tracers.

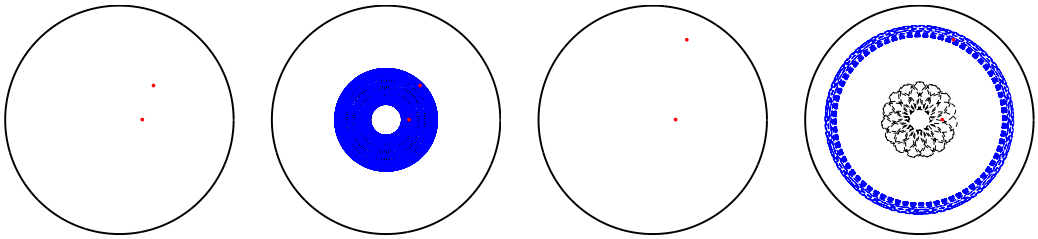

Figure 7.6: Rotlets not initially collinear with the center of the domain

7.4.1 Stirring mechanism

A stirring protocol that produces good mixing should ensure that the stretching and folding of tracer trajectories occurs uniformly over the domain and does not cause the emergence of unmixed islands within a chaotic surrounding region. To identify rotor configurations that are likely to not result in such unmixed islands, we construct Poincaré sections of a reduced, three dimensional time periodic version of the autonomous system (7.8),

$$\dot{X} = f(x, y, \psi(t)) \tag{7.9}$$

which results in two dimensional poincaré maps Fig. 7.7 corresponding to the starting configurations in Fig.7.5.

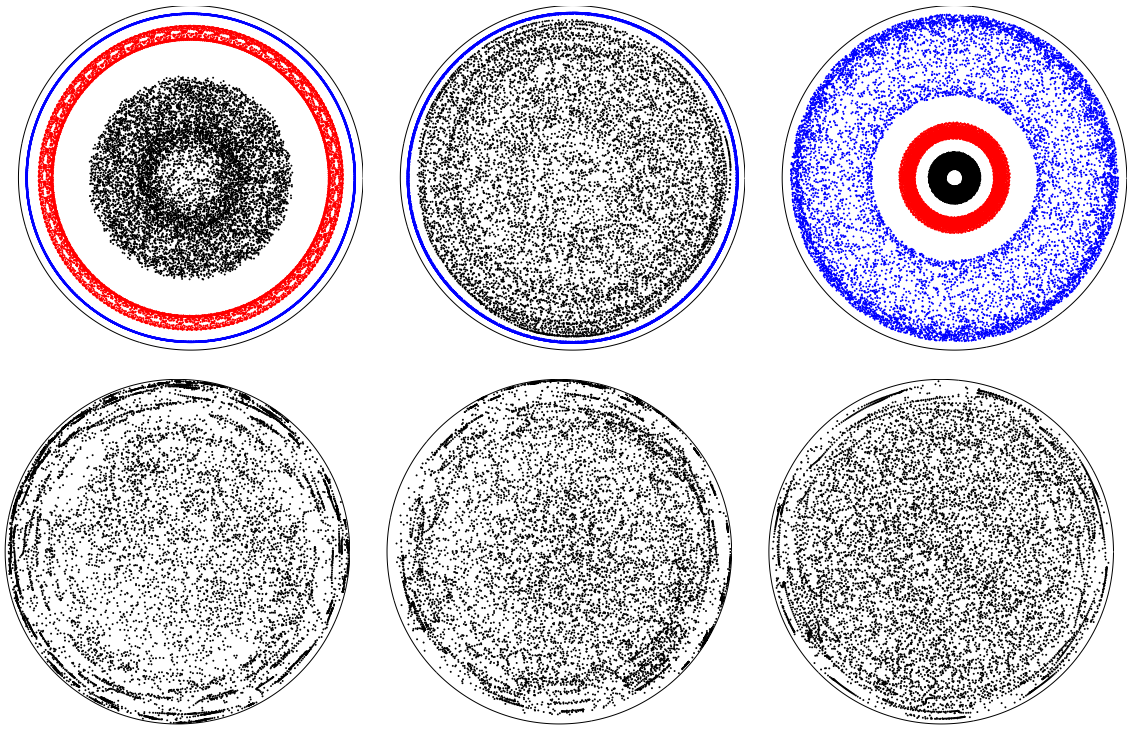

Figure 7.7: Poincaré maps corresponding to the two rotor configurations in Figs. 7.5a-7.5u. Different colored bands are maps of initial conditions started off in different regions that do not mix with each other.

From the Poincaré maps, we realize that like that dynamics of the rotlets themselves, the space filling nature of tracer dynamics is also dependent upon the asymmetry of viscous boundary effects on the rotlets driving the mixing. Rotlets starting close together exhibit poor mixing and the mixing improves with increasing distance between the rotlets and the consequent assymmetry in boundary effects but if the rotlets are too far apart such that the boundary effects become comparable once again, the mixing is poor Fig. 7.8.

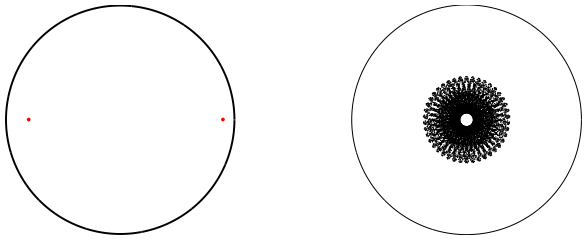

Figure 7.8: Poincaré map for rotors close to the boundaries.

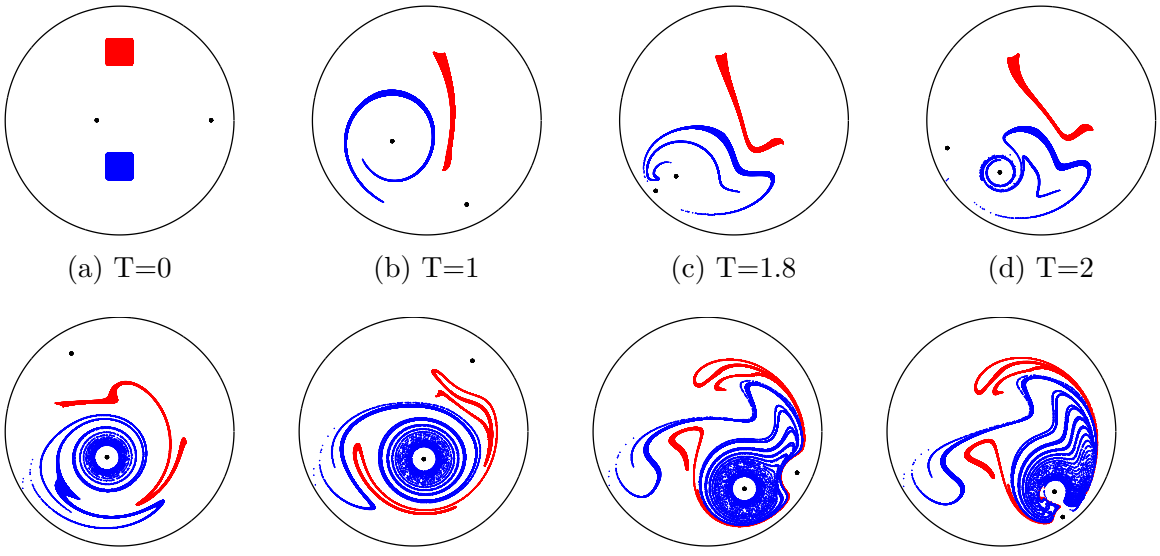

(a) T=0 (b) T=1 (c) T=1.8 (d) T=2

(e) T=4 (f) T=5 (g) T=5.2 (h) T=6

Figure 7.9: Mixing of fluid tracers using the bounded 2 rotor configuration at various intervals of time in the stirring process

Having identified that certain configurations of the bounded 2-rotlet configuration are capable of producing efficient and uniform mixing, we visualize the mixing so produced by following the advection of two differently colored(red and blue) blobs of tracers, with the colors denoting disparate regions where the respective blobs originate. The flow is driven by two rotlets starting out at different positions on the horizontal axis of the circular domain such that the rotlets experience the viscous boundary effects to different extents. After a short time numerical integration of the trajectories, one can visualize the initially square blobs getting stretched and folded onto each other Fig. 7.9. This stretching and folding of coherent blobs of tracers creates thin fluid structures called "striations"[107].

The complex and layered nature of the striations increase the area of contact between the two blobs and hence promote homogenization of the fluid by viscous diffusion into each other. While this numerical experiment provides an insight into the way fluid from two different regions are brought together and mixed into each other, the mechanism which leads to the fluid being stretched and folded warrants further study. To see this and other mechanisms which leads to mixing, we consider an illustrative example. We start with two

sets of initial conditions on either side of the outer rotlet in Fig. 7.10a, where we see that the rotlet rotation about its own axis is the engine which causes blobs of fluid in its vicinity to wrap around each other. This multi-layered combined blob of fluid is then transported by the translation of the rotlet from one point to another in the domain. However, the viscous boundary effects cause the entrained fluid around the rotor to stretch out along the boundary of the domain as seen in Fig. 7.10c,7.10e. A crucial event takes place at this juncture which involves the initially distant rotors reaching the closest point of approach between each other in every time interval T. This event causes the entrained fluid to be de-trained at the boundary while a new blob of fluid is picked up by the rotor Fig. 7.10i and the same process of stretching and detrainment is repeated over and over again Figs. 7.10k-7.10o. Stretching is one crucial half of the effective mixing protocol, the second important step is folding. This is also seen to occur at the same point of time when the two rotlets are at their closest position relative to each other. Any blob of fluid between the two rotlets gets sheared and folded by the relative motion of the rotlets Fig. 7.10g which is seen here as splitting up of tracer blob because of the limitation in the number of tracers being tracked.

7.5 Lagrangian Coherent Structures in micro-rotor induced mixing

The streamlines of flow shown at various instants of the mixing process in Fig. 7.10 are instantaneous separatrices of the flow. However a separatrix at one instant in time ceases to be a separatrix in a different instant in time and this enables fluid tracers to traverse a large portion of the domain and get mixed. Finite Time Lypaunov Exponents(FTLE) on the other hand are not instantaneous and as the name suggests, they enable us to visualize structures of the flow that are persistent over a finite interval of time. The Lagrangian Coherent Structures(LCS) or ridges of the FTLE are also expected to fade away over sufficiently long times for uniform mixing to take place, however, on short time scales the LCSs

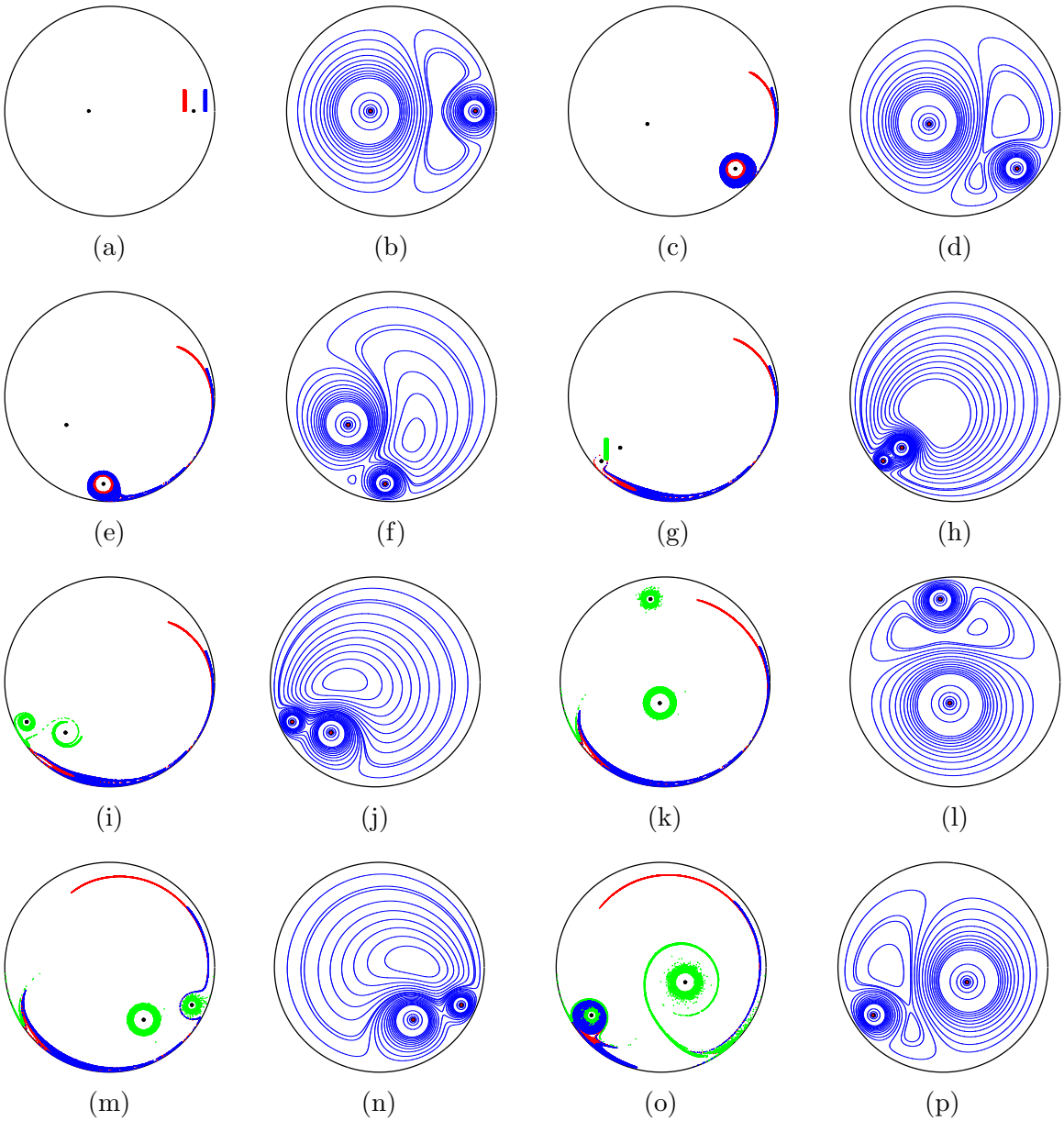

Figure 7.10: Mixing mechanism in the bounded 2 rotor configuration with corresponding streamlines of flow which are imaterial lines of the flow field.

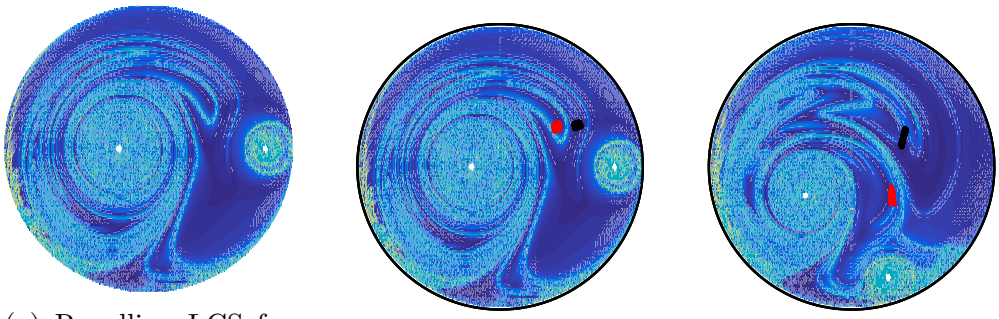

(a) Repelling LCS for the flow at the initial time instant.

(b) Tracers at Time T=0.

(c) Tracers at Time T=1.

Figure 7.11: Repelling LCS induces stretching about itself.

reveal structures that govern the stretching and folding of tracer trajectories.

The LCSs are computed as curves of maximal stretching over a finite time interval and hence, any set of reference trajectories around such a structure could either be repelled away in the normal direction or it could shear in the tangential direction. Thus any set of initial conditions that start overlapping on a repelling LCS gets stretched in opposite directions and deformed Fig.7.11.

The LCS act as transport barriers that "sheperd" the fluid that get trapped within the ridges and transport them from one part of the domain to the other all the while squeezing, stretching and folding the flow around them. This is seen even over short time intervals as seen in Fig.7.12. Thus the role of the LCS as transport barriers which under certain conditions also serve to induce mixing in of the flow is apparent.

7.6 Quantifying mixing

Having already seen that the system describing passive advection of tracers by micro-rotors displays all the qualitative features of a good mixer, the question that remains is that of quantifying mixing rate. One way this can be done is to measure the variance of tracer particle density in the domain of interest [108]. To do this, a discrete measure of variance where the domain of interest is divided into several boxes $b = 1..N$ is used, where each box

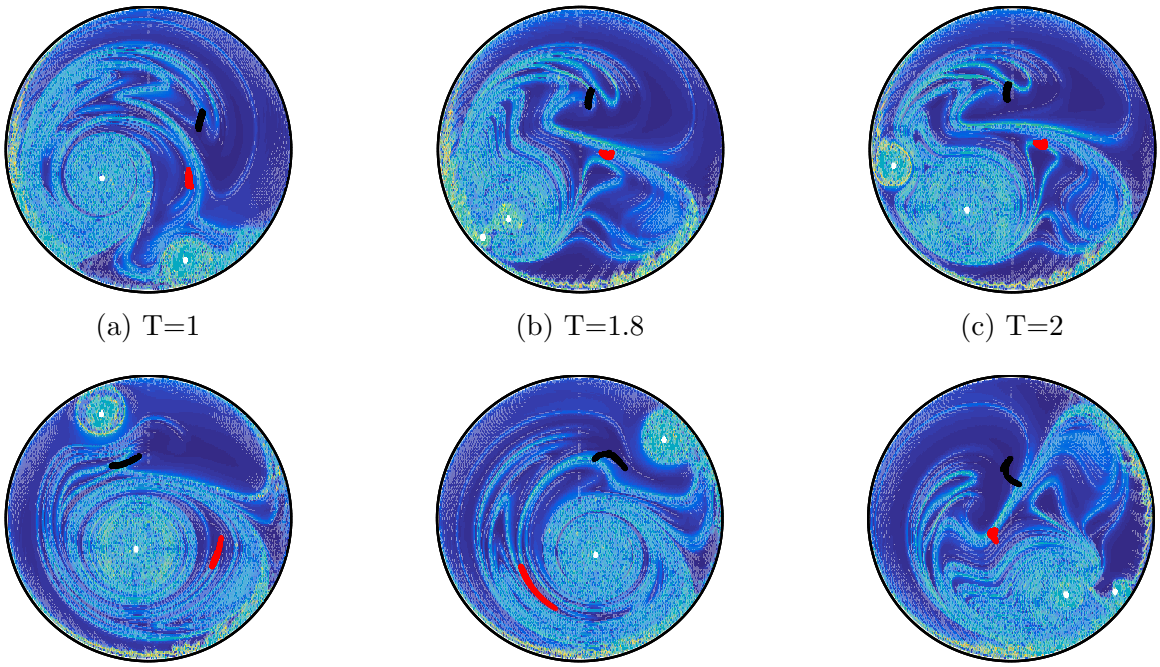

(a) T=1 (b) T=1.8 (c) T=2

(d) T=3 (e) T=4 (f) T=5

Figure 7.12: Forward time FTLE and the associated LCS for micro-rotor mixing.

has a variable area A_b and the number of tracers that end up in each of those boxes are measured as N_b . This lets us calculate the variance in density of tracers within the domain [109].

$$Variance = \sum_{b=1}^{b=N} \Big[\frac{N_b}{A_b}\frac{\sum_b A_b}{\sum_b N_b} - 1\Big]^2 \tag{7.10}$$

The resulting variance as a function of time is plotted in Fig. 7.13 where config 1 to config 6 corresponds to the decay of variance associated with the six configurations of the bounded two rotlet system studied in Fig. 7.5. The variance plots agree well with the Poincaré sections in Fig.7.7 where the configuration 1 performs worst with the variance decaying to smaller values for configurations 3 to 6. Configuration 2 produces better mixing than all but the last configuration because the region around its periphery which remains unmixed with the rest of the domain is thin and does not impede mixing within most of the domain.

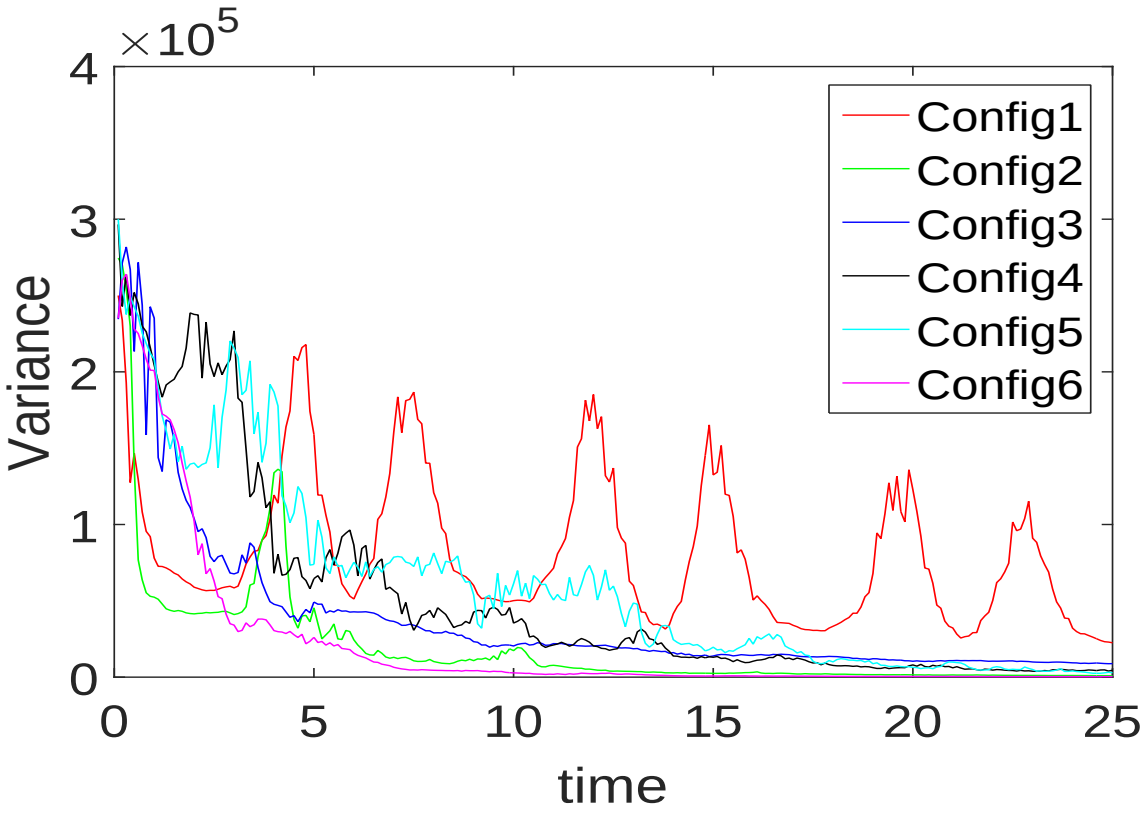

Figure 7.13: Mixing configurations in Fig.7.5 and the associated variance

Chapter 8

Conclusion

8.1 Summary

In summary, we present the combination of singularity methods in fluid dynamics with tools from dynamical systems theory as a framework that can be fruitfully employed in the study of particle dynamics in low Reynolds number fluid flows. After reviewing the necessary background material, we first demonstrate such a framework with the much simpler case of potential flow models. The study of inertial particle dynamics in ideal flows with finite vorticity reveals that previously documented criteria to identify stable and unstable subsets of a flow domain are incomplete and that inertial particle trajectories can exhibit globally stable behavior within domains that are every where locally unstable.

Motivated by the insights gained, we extend the use of this framework to physically realistic viscous flows. An interesting application is the case of steady streaming flows produced by acoustically excited micro-bubbles and their potential to manipulate the dynamics of finite sized particles. We construct a simple approximation of such a flow as a combination of singularity solutions between parallel walls. We explain the robust stability of the flow field for inertial particle motion by conducting a linearized stability analysis of the relative velocity subspace of the governing dynamical system which includes the sim-

plified Maxey Riley equation. The FTLE associated with the flow field reveal Lagrangian Coherent Structures that act as transport barriers for motion of inertial particles as well. Micro-bubble placement such that the influence of attracting LCS is maximized has been suggested as a criteria in the design of micro-bubble particle manipulation devices.

The interesting problem of chaotic micro-mixing has been studied in the context of employing viscous micro-rotors as non-localized mixing elements. The rotlet model under circular confinement has been used to conduct numerical experiments of passive tracer advection. The asymmetry in viscous boundary effects has been identified as a reason for the rotlets and by association, micro-rotors, to exhibit complex dynamics which stirs the surrounding fluid efficiently and uniformly.

8.2 Closing remarks

This work attempts to review in one place the essential analytical and computational tools required for a framework that is well suited for studies of particle manipulation in viscous fluid flows. While a few applications of this combination of techniques have been demonstrated, we expect that many more interesting problems in particle manipulation can be tackled using similar techniques.

Bibliography

[1] Maria Del Carmen Jaramillo, Eduard Torrents, Rodrigo Martínez-Duarte, Marc J. Madou, and Antonio Juárez. On-line separation of bacterial cells by carbon-electrode dielectrophoresis. *Electrophoresis*, 31(17):2921–2928, 2010.

[2] Katarina Kolostova, Daniela Pinterova, Robert M. Hoffman, and Vladimir Bobek. Circulating human prostate cancer cells from an orthotopic mouse model rapidly captured by immunomagnetic beads and imaged by GFP expression. *Anticancer Research*, 31(5):1535–1539, 2011.

[3] Evelien W. M. Kemna, Rogier M. Schoeman, Floor Wolbers, Istvan Vermes, David A. Weitz, and Albert van den Berg. High-yield cell ordering and deterministic cell-in-droplet encapsulation using Dean flow in a curved microchannel. *Lab on a Chip*, 12(16):2881, 2012.

[4] Meltem Elitas, Rodrigo Martinez-Duarte, Neeraj Dhar, John D. McKinney, and Philippe Renaud. Dielectrophoresis-based purification of antibiotic-treated bacterial subpopulations. *Lab on a Chip*, 14(11):1850–1857, 2014.

[5] Khashayar Khoshmanesh, Sara Baratchi, Francisco J. Tovar-Lopez, Saeid Nahavandi, Donald Wlodkowic, Arnan Mitchell, and Kourosh Kalantar-Zadeh. On-chip separation of Lactobacillus bacteria from yeasts using dielectrophoresis. *Microfluidics and Nanofluidics*, 12(1-4):597–606, 2012.

[6] Robin Hui Liu, Jianing Yang, Ralf Lenigk, Justin Bonanno, and Piotr Grodzinski. Self-Contained , Fully Integrated Biochip for Sample Preparation , Polymerase Chain Reaction Amplification , and DNA Microarray Detection. *Analytical Chemistry*, 76(7):1824–1831, 2004.

[7] C. Pozrikidis. *Boundary integral and singularity methods for linearized viscous flow*. Cambridge University Press, 1992.

[8] Stephen Wiggins. *Chaotic Transport in Dynamical Systems*. Springer Science & Business Media, New York, 1 edition, 1992.

[9] C. Eugene Wayne. Vortices and two-dimensional fluid motion. *Notices of the AMS*, 58(1):10–19, 2011.

[10] Cheng Wang, Bhargav Rallabandi, and Sascha Hilgenfeldt. Frequency dependence and frequency control of microbubble streaming flows. *Physics of Fluids*, 25(2), 2013.

[11] Bhargav Rallabandi, Cheng Wang, and Sascha Hilgenfeldt. Two-dimensional streaming flows driven by sessile semicylindrical microbubbles. *Journal of Fluid Mechanics*, 739:57–71, 2014.

[12] Cheng Wang, Shreyas V. Jalikop, and Sascha Hilgenfeldt. Size-sensitive sorting of microparticles through control of flow geometry. *Applied Physics Letters*, 99(3):3–6, 2011.

[13] Cheng Wang, Shreyas V. Jalikop, and Sascha Hilgenfeldt. Efficient manipulation of microparticles in bubble streaming flows. *Biomicrofluidics*, 6(1):1–11, 2012.

[14] Raqeeb Thameem, Bhargav Rallabandi, and Sascha Hilgenfeldt. Particle migration and sorting in microbubble streaming flows. *Biomicrofluidics*, 014124:15–17, 2016.

[15] Hassan Aref. Stirring by chaotic advection. *Journal of Fluid Mechanics*, 143:1–21, 1984.

[16] S. Wiggins and J. M. Ottino. Foundations of chaotic mixing. *Philosophical Transactions of the Royal Society A: Mathematical, Physical and Engineering Sciences*, 362(1818):937–970, 2004.

[17] Imre M. Jánosi, Tamás Tél, Dietrich E. Wolf, and Jason A.C. Gallas. Chaotic particle dynamics in viscous flows: The three-particle Stokeslet problem. *Physical Review E - Statistical Physics, Plasmas, Fluids, and Related Interdisciplinary Topics*, 56(3):2858–2868, 1997.

[18] S R Otto, A N Yannacopoulos, and J R Blake. Transport and mixing in Stokes flow: the effect of chaotic dynamics on the blinking stokeslet. *Journal of Fluid Mechanics*, 430(2001):1–26, 2001.

[19] Allen T. Chwang and T. Yao Tsu Wu. Hydromechanics of low-Reynolds-number flow. Part 2. Singularity method for Stokes flows. *Journal of Fluid Mechanics*, 67(4):787–815, 1975.

[20] Sangtae Kim and Seppo J.Karilla. *Microhydrodynamics. Principles and Selected Applications*. Dover Publications, Boston, dover edition, 2005.

[21] J. R. Blake. A note on the image system for a stokeslet in a no-slip boundary. *Mathematical Proceedings of the Cambridge Philosophical Society*, 70(2):303–310, 1971.

[22] J. R. Blake and a. T. Chwang. Fundamental singularities of viscous flow. *Journal of Engineering Mathematics*, 8(1):23–29, 1974.

[23] David Gordon Hansen. *Axisymmetric Stokes Flow Solutions and Bubble Microstreaming*. PhD thesis, Northwestern University, 2009.

[24] H. Aref and S. Balachandar. Chaotic advection in a Stokes flow. *Phys. Fluids*, 29(11):3515–3521, 1986.

[25] G B Jeffery. The rotation of two circular cylinders in a viscous fluid. *Proceedings of the Royal Society A: Mathematical, Physical and Engineering Science*, 101(709):169–174, 1922.

[26] K B Ranger. Eddies in two dimensional stokes flow. *International Journal of Engineering Science*, 18(1):181–190, 1980.

[27] S H Smith. Low Reynolds number flow resulting from an array of rotlets. *Physics of Fluids*, 30(12), 1987.

[28] V V Meleshko and H Aref. A blinking rotlet model for chaotic advection. *Physics of Fluids*, 8(12):3215–3217, 1996.

[29] P Daripa and D Palaniappan. Singularity induced exterior and interior Stokes flows. *Physics of Fluids*, 13(11):3134–3154, 2001.

[30] D Palaniappan and Prabir Daripa. Interior Stokes ows with stick-slip boundary conditions. *Physica A*, 297:37–63, 2001.

[31] D. Palaniappan and P. Daripa. Exterior Stokes flows with stick-slip boundary conditions. *Zeitschrift fur Angewandte Mathematik und Physik*, 53(2):281–307, 2002.

[32] Pijush k. Kundu and Ira m. Cohen. *Fluid Mechanics*. Academic Press, second edition, 2002.

[33] N Liron and S Mochon. Stokes flow for a stokeslet between two parallel flat plates. *Journal of Engineering Mathematics*, 10(4):287–303, 1976.

[34] D. L. Young, S. J. Jane, C. M. Fan, K. Murugesan, and C. C. Tsai. The method of fundamental solutions for 2D and 3D Stokes problems. *Journal of Computational Physics*, 211(1):1–8, 2006.

[35] Edward N. Lorenz. Deterministic Nonperiodic Flow. *Journal of the Atmospheric Sciences*, 20(2):130–141, 1963.

[36] Wang Sang Koon, Martin W. Lo, Jerrold E. Marsden, and Shane D. Ross. *Dynamical systems, the three-body problem and space mission design*. Free online Copy: Marsden Books, 2008.

[37] P. Tallapragada, S. D. Ross, and D. G. Schmale. Lagrangian coherent structures are associated with fluctuations in airborne microbial populations. *Chaos*, 21(3):1–16, 2011.

[38] G. Haller and G. Yuan. Lagrangian coherent structures and mixing in two-dimensional turbulence. *Physica D: Nonlinear Phenomena*, 147(3-4):352–370, 2000.

[39] Emmanuelle Gouillart, Jean Luc Thiffeault, and Matthew D. Finn. Topological mixing with ghost rods. *Physical Review E - Statistical, Nonlinear, and Soft Matter Physics*, 73(3):1–8, 2006.

[40] Steven H. Strogatz. *Nonlinear Dynamics and Chaos: With Applications to Physics,Biology,Chemistry and Engineering*. CRC Press, 1 edition, 1994.

[41] Stephen Wiggins. *Introduction to Applied Nonlinear Dynamical Systems and Chaos*. Springer-Verlag, 1990.

[42] Santo Banerjee, Lamberto Rondoni, and Mala Mitra, editors. *Applications of Chaos and Nonlinear Dynamics in Science and Engineering - Vol. 2*, volume 2. Springer-Verlag, 2012.

[43] V Rom-kedar, A Leonard, and Stephen Wiggins. An analytical study of transport, mixing and chaos in an unsteady vortical flow. *Journal of Fluid Mechanics*, 214:347–394, 1990.

[44] G. Haller. Lagrangian structures and the rate of strain in a partition of two-dimensional turbulence. *Physics of Fluids*, 13(11):3365–3385, 2001.

[45] Shawn C. Shadden, Francois Lekien, and Jerrold E. Marsden. Definition and properties of Lagrangian coherent structures from finite-time Lyapunov exponents in two-dimensional aperiodic flows. *Physica D: Nonlinear Phenomena*, 212(3-4):271–304, 2005.

[46] Hiroshi Teramoto, George Haller, and Tamiki Komatsuzaki. Detecting invariant manifolds as stationary Lagrangian coherent structures in autonomous dynamical systems. *Chaos*, 23(4), 2013.

[47] N Riley. Steady streaming. *Annual Review of Fluid Mechanics*, 33:43–65, 2001.

[48] M.Faraday. On a Peculiar Class of Acoustical Figures ; and on Certain Forms Assumed by Groups of Particles upon Vibrating Elastic Surfaces. *Philosophical Transactions of the Royal Society A: Mathematical, Physical and Engineering Sciences*, 121(1831):299–340, 1831.

[49] E. N. da C. Andrade. On the Circulations Caused by the Vibration of Air in a Tube. *Proceedings of the Royal Society A: Mathematical, Physical and Engineering Sciences*, 134(824):445–470, 1931.

[50] C. N. Davies. Viscous Flow Transverse to a Circular Cylinder. *Proceedings of the Physical Society. Section B*, 63(4):288–296, 1950.

[51] Lord-Rayleigh. On the circulation of air observed in Kundt's tubes, and on some allied acoustical problems. *Philosophical Transactions of the Royal Society of London*, LXXV, pt.(January):1–21, 1884.

[52] Wesley L. Nyborg. Acoustic Streaming due to Attenuated Plane Waves. *The Journal of the Acoustical Society of America*, 25(1):68–75, 1953.

[53] P J Westervelt. The theory of steady rotational flow generated by a sound field. *Journal of the Acoustical Society of America*, 25(1):60–67, 1953.

[54] Sir James Lighthill. Acoustic streaming. *Journal of Sound and Vibration*, 61(3):391–418, 1978.

[55] J. Holtsmark, I. Johnsen, T. Sikkeland, and S. Skavle. Boundary Layer Flow Near a Cylindrical Obstacle in an Oscillating, Incompressible Fluid. *The Journal of the Acoustical Society of America*, 26(1):26–39, 1954.

[56] J. T. Stuart. Double boundary layers in oscillatory viscous flow. *Journal of Fluid Mechanics*, 24(4):673–687, 1966.

[57] Chang-Yi Wang. On high-frequency oscillatory viscous flows. *Journal of Fluid Mechanics*, 32(1):55–68, 1968.

[58] Barry R Lutz, Jian Chen, and Daniel T Schwartz. Hydrodynamic Tweezers : 1 . Noncontact Trapping of Single Cells Using Steady Streaming Microeddies ability to gently position cells for repeated measurements. *Analytical Chemistry*, 78(15):5429–5435, 2006.

[59] Valerie H Lieu, Tyler A House, and Daniel T Schwartz. Hydrodynamic Tweezers: Impact of Design Geometry on Flow and Microparticle Trapping. *Analytical Chemistry*, 84:1963–1968, 2012.

[60] Kwitae Chong, Scott D Kelly, Stuart Smith, and Jeff D Eldredge. Inertial particle trapping in viscous streaming Inertial particle trapping in viscous streaming. *Physics of Fluids*, 033602(25), 2013.

[61] B. J. Davidson and N. Riley. Cavitation microstreaming. *Journal of Sound and Vibration*, 15(2):217–233, 1971.

[62] Milton S. Plesset and Andrea Prosperetti. Bubble Dynamics and Cavitation. *Annual Review of Fluid Mechanics*, 9:145–85, 1977.

[63] M. S. Longuet-Higgins. Viscous streaming from an oscillating spherical bubble. *Proceedings of the Royal Society A: Mathematical, Physical and Engineering Sciences*, 454(1970):725–742, 1998.

[64] Philippe Marmottant and Sascha Hilgenfeldt. Controlled vesicle deformation and lysis by single oscillating bubbles. *Nature*, 423(6936):153–156, 2003.

[65] P. Marmottant and S. Hilgenfeldt. A bubble-driven microfluidic transport element for bioengineering. *Proceedings of the National Academy of Sciences*, 101(26):9523–9527, 2004.

[66] P. Marmottant, J. P. Raven, H. Gardeniers, J. G. Bomer, and S. Hilgenfeldt. Microfluidics with ultrasound-driven bubbles. *Journal of Fluid Mechanics*, 568:109–118, 2006.

[67] Cheng Wang. *Microbubble Streaming Flows for Non-Invasive Particle Manipulation and Liquid Mixing*. Phd dissertation, University of Illinois at Urbana-Champaign, 2013.

[68] Venkatarama Bhargav Rallabandi. *Quantifying Microbubbe Streaming and its Applications*. Phd dissertation, University of Illinois at Urbana-Champaign, 2015.

[69] Maulik V. Patel, Armando R. Tovar, and Abraham P. Lee. Lateral cavity acoustic transducer as an on-chip cell/particle microfluidic switch. *Lab Chip*, 12:139–145, 2012.

[70] Martin R. Maxey and James J. Riley. Equation of motion for a small rigid sphere in a nonuniform flow. *Physics of Fluids*, 26(4):883–889, 1983.

[71] E Michaelidis. Review - the transient equation of motion for particles, bubbles, and droplets. *AMSE Journal of Fluids Engineering*, 119(June 1997), 1997.

[72] Armando Babiano, Julyan H.E. Cartwright, Oreste Piro, and Antonello Provenzale. Dynamics of a small neutrally buoyant sphere in a fluid and targeting in Hamiltonian systems. *Physical Review Letters*, 84(25):5764–5767, 2000.

[73] Themistoklis Sapsis and George Haller. Instabilities in the dynamics of neutrally buoyant particles. *Physics of Fluids*, 20(1):1–7, 2008.

[74] Raqeeb Thameem, Bhargav Rallabandi, and Sascha Hilgenfeldt. Fast inertial particle manipulation in oscillating flows. *Physical Review Fluids*, 052001:1–8, 2017.

[75] P. G. Saffman. The lift on a small sphere in a slow shear flow. *Journal of Fluid Mechanics*, 22(2):385–400, 1965.

[76] Raqeeb Thameem. *Quantifying Particle Sorting in Microbubble Streaming Flows*. Ms thesis, University Of Illinois at Urbana-Champaign, 2015.

[77] Senbagaraman Sudarsanam and Phanindra Tallapragada. Global stability of trajectories of inertial particles within domains of instability. *Communications in Nonlinear Science and Numerical Simulation*, 42:313–323, 2017.

[78] Dino Di Carlo. Inertial microfluidics. *Lab on a Chip*, 9(21):3038, 2009.

[79] H. Helmholtz. Über Integrale der hydrodynamischen Gleichungen, welche den Wirbelbewegungen entsprechen. *J.Reine Angew. Math.*, 55:25–55, 1858.

[80] Paul K Newton. *The N-Vortex Problem:Analytical Techniques*. Springer-Verlag New York, New York, 1 edition, 2001.

[81] A. T. Conlisk and D. Rockwell. Modeling of vortex-corner interaction using point vortices. *Physics of Fluids*, 24(12):2133–2142, 1981.

[82] Hassan Aref. Point vortex dynamics: A classical mathematics playground. *Journal of Mathematical Physics*, 48(6):1–23, 2007.

[83] Senbagaraman Sudarsanam. *Inertial Particle Dynamics in Simple Vortex Flow Configurations*. Ms thesis, Clemson University, 2015.

[84] Phanindra Tallapragada and Senbagaraman Sudarsanam. A globally stable attractor that is locally unstable everywhere. *AIP Advances*, 7(12), 2017.

[85] S. Bhattacharya and Jerzy Bławzdziewicz. Image system for Stokes-flow singularity between two parallel planar walls. *Journal of Mathematical Physics*, 43(11):5720–5731, 2002.

[86] Daniel Mark, Stefan Haeberle, Günter Roth, Felix von Stetten, and Roland Zengerle. From microfluidic application to nanofluidic phenomena issue. *Chemical Society reviews*, 39(3):1153–82, 2010.

[87] Kevin Ward and Z. Hugh Fan. Mixing in microfluidic devices and enhancement methods. *Journal of Micromechanics and Microengineering*, 25(9), 2015.

[88] J. M. Ottino and S. Wiggins. Introduction: mixing in microfluidics. *Philosophical Transactions of the Royal Society A: Mathematical, Physical and Engineering Sciences*, 362(1818):923–935, 2004.

[89] M A Stremler, F R Haselton, and H Aref. Designing for chaos: applications of chaotic advection at the microscale. *Philosophical Transactions of the Royal Society A: Mathematical, Physical and Engineering Sciences*, 362(1818):1019–1036, 2004.

[90] Goksen G. Yaralioglu, Ira O. Wygant, Theodore C. Marentis, and Butrus T. Khuri-Yakub. Ultrasonic mixing in microfluidic channels using integrated transducers. *Analytical Chemistry*, 76(13):3694–3698, 2004.

[91] Hiroaki Suzuki and Chih Ming Ho. A magnetic force driven chaotic micro-mixer. *Proceedings of the IEEE Micro Electro Mechanical Systems (MEMS)*, pages 40–43, 2002.

[92] Martin Z. Bazant and Todd M. Squires. Induced-Charge Electrokinetic Phenomena: Theory and Microfluidic Applications. *Physical Review Letters*, 92(6):1–4, 2004.

[93] S. S. Wang, Z. J. Jiao, X. Y. Huang, C. Yang, and N. T. Nguyen. Acoustically induced bubbles in a microfluidic channel for mixing enhancement. *Microfluidics and Nanofluidics*, 6(6):847–852, 2009.

[94] P. Garg, J. R. Picardo, and S. Pushpavanam. Chaotic mixing in a planar, curved channel using periodic slip. *Physics of Fluids*, 27(3), 2015.

[95] A D Stroock. Chaotic Mixer for Microchannels. *Science*, 295(5555):647–651, 2002.

[96] H. Kurtuldu, J. S. Guasto, K. A. Johnson, and J. P. Gollub. Enhancement of biomixing by swimming algal cells in two-dimensional films. *Proceedings of the National Academy of Sciences*, 108(26):10391–10395, 2011.

[97] Andrey Sokolov, Raymond E. Goldstein, Felix I. Feldchtein, and Igor S. Aranson. Enhanced mixing and spatial instability in concentrated bacterial suspensions. *Physical Review E - Statistical, Nonlinear, and Soft Matter Physics*, 80(3):1–8, 2009.

[98] Mir Abbas Jalali, Atefeh Khoshnood, and Mohammad Reza Alam. Microswimmer-induced chaotic mixing. *Journal of Fluid Mechanics*, 779:669–683, 2015.

[99] Peter Mueller and Jean Luc Thiffeault. Fluid transport and mixing by an unsteady microswimmer. *Physical Review Fluids*, 2(1):1–22, 2017.

[100] C. J. Campbell and B. A. Grzybowski. Microfluidic mixers: from microfabricated to self-assembling devices. *Philosophical Transactions of the Royal Society A: Mathematical, Physical and Engineering Sciences*, 362(1818):1069–1086, 2004.

[101] Matthew Ballard, Drew Owen, Zachary Grant Mills, Peter J. Hesketh, and Alexander Alexeev. Orbiting magnetic microbeads enable rapid microfluidic mixing. *Microfluidics and Nanofluidics*, 20(6):1–13, 2016.

[102] Enkeleida Lushi and Petia M. Vlahovska. Periodic and Chaotic Orbits of Plane-Confined Micro-rotors in Creeping Flows. *Journal of Nonlinear Science*, 25(5):1111–1123, 2015.

[103] Kyongmin Yeo, Enkeleida Lushi, and Petia M. Vlahovska. Collective dynamics in a binary mixture of hydrodynamically coupled microrotors. *Physical Review Letters*, 114(18):1–5, 2015.

[104] Hassan Aref, John R. Blake, Marko Budišić, Silvana S.S. Cardoso, Julyan H.E. Cartwright, Herman J.H. Clercx, Kamal El Omari, Ulrike Feudel, Ramin Golestanian, Emmanuelle Gouillart, Gertjan F. Van Heijst, Tatyana S. Krasnopolskaya, Yves Le Guer, Robert S. MacKay, Vyacheslav V. Meleshko, Guy Metcalfe, Igor Mezić, Alessandro P.S. De Moura, Oreste Piro, Michel F.M. Speetjens, Rob Sturman, Jean Luc Thiffeault, and Idan Tuval. Frontiers of chaotic advection. *Reviews of Modern Physics*, 89(2):1–66, 2017.

[105] Hassan Aref. The development of chaotic advection. *Physics of Fluids*, 14(4):1315–1325, 2002.

[106] Enkeleida Lushi and Petia M Vlahovska. Periodic and Chaotic Orbits of Plane-Confined Micro-rotors in Creeping Flows. *Journal of Nonlinear Science*, 25(5):1111–1123, 2015.

[107] M. A. Stremler, F. R. Haselton, and H. Aref. Designing for chaos: applications of chaotic advection at the microscale. *Philosophical Transactions of the Royal Society A: Mathematical, Physical and Engineering Sciences*, 362(1818):1019–1036, 2004.

[108] Sanjeeva Balasuriya. Dynamical systems techniques for enhancing microfluidic mixing. *Journal of Micromechanics and Microengineering*, 25(9), 2015.

[109] Jean Luc Thiffeault. Using multiscale norms to quantify mixing and transport. *Nonlinearity*, 25(2), 2012.